Spring 5-1-2015

Cure Kinetics, Morphologies, and Mechanical Properties of Thermoplastic/MWCNT Modified Multifunctional Glassy Epoxies Prepared via Continuous Reaction Methods

Xiaole Cheng
University of Southern Mississippi

The University of Southern Mississippi

CURE KINETICS, MORPHOLOGIES, AND MECHANICAL PROPERTIES OF THERMOPLASTIC/MWCNT MODIFIED MULTIFUNCTIONAL GLASSY EPOXIES PREPARED VIA CONTINUOUS REACTION METHODS

by

Xiaole Cheng

Abstract of a Dissertation
Submitted to the Graduate School
of The University of Southern Mississippi
in Partial Fulfillment of the Requirements
for the Degree of Doctor of Philosophy

May 2015

ABSTRACT

CURE KINETICS, MORPHOLOGIES, AND MECHANICAL PROPERTIES OF THERMOPLASTIC/MWCNT MODIFIED MULTIFUNCTIONAL GLASSY EPOXIES PREPARED VIA CONTINUOUS REACTION METHODS

by Xiaole Cheng

May 2015

The primary goal of this dissertation is to develop a novel continuous reactor method to prepare partially cured epoxy prepolymers for aerospace prepreg applications with the aim of replacing traditional batch reactors. Compared to batch reactors, the continuous reactor is capable of solubilizing and dispersing a broad range of additives including thermoplastic tougheners, stabilizers, nanoparticles and curatives and advancing epoxy molecular weights and viscosities while reducing energy consumption.

In order to prove this concept, polyethersulfone (PES) modified 4, 4'-diaminodiphenylsulfone (44DDS)/tetraglycidyl-4, 4'-diaminodiphenylmethane (TGDDM) epoxy prepolymers were firstly prepared using both continuous reactor and batch reactor methods. Kinetic studies confirmed the chain extension reaction in the continuous reactor is similar to the batch reactor, and the molecular weights and viscosities of prepolymers were readily controlled through reaction kinetics. Atomic force microscopy (AFM) confirmed similar cured network morphologies for formulations prepared from batch and continuous reactors. Additionally tensile strength, tensile modulus and fracture toughness analyses concluded mechanical properties of cured epoxy matrices produced from both reactors were equivalent.

Effects of multifunctional epoxy compositions on thermoplastics phase-separated morphologies were systematically studied using a combination of AFM with nanomechanical mapping, spectroscopic and calorimetric techniques to provide new insights to tailor cured reaction induced phase separation (CRIPS) in multifunctional epoxy blend networks. Furthermore, how resultant crosslinked glassy polymer network and phase-separated morphologies correlated with mechanical properties are discussed in detail.

Multiwall carbon nanotube (MWCNT)/TGDDM epoxy prepolymers were further prepared by combining the successful strategies for advancing epoxy chemistries and dispersing nanotubes using the continuous reactor. Optical microscopy (OM) and scanning electron microscopy (SEM) were used to characterize the MWCNT dispersion states and stabilization in epoxy prepolymer matrix after continuous process and during curing cycles. Additionally, electrical conductivities and mechanical properties of final cured MWCNT/TGDDM composites were measured and discussed in view of their corresponding MWCNT dispersion states.

Ternary blends of MWCNT reinforced thermoplastic/epoxy prepolymers were prepared by the continuous reactor. Influence of MWCNT on the CRIPS mechanism and the cured morphologies were systematically investigated using SEM and rheological analysis. Incorporation of MWCNT in thermoplastic/epoxy matrices can lead to a morphological transformation from phase inverted, to co-continuous, and to droplet dispersed morphology. In additional, dynamic mechanical analysis revealed the heterogeneity of MWCNT dispersion in thermoplastic/thermosets systems.

The University of Southern Mississippi

CURE KINETICS, MORPHOLOGIES, AND MECHANICAL PROPERTIES OF THERMOPLASTIC/MWCNT MODIFIED MULTIFUNCTIONAL GLASSY EPOXIES PREPARED VIA CONTINUOUS REACTION METHODS

by

Xiaole Cheng

A Dissertation
Submitted to the Graduate School
of The University of Southern Mississippi
in Partial Fulfillment of the Requirements
for the Degree of Doctor of Philosophy

Approved:

Dr. Jeffrey Wiggins_____
Committee Chair

Dr. Sarah Morgan_____

Dr. Joshua Otaigbe_____

Dr. Sergei Nazarenko_____

Dr. Robson Storey_____

Dr. Karen Coats_____
Dean of the Graduate School

May 2015

DEDICATION

This dissertation is dedicated to my wonderful fiancé Yanan for her endless support and encouragement, and to my parents for their patience and understanding.

ACKNOWLEDGMENTS

I would like to gratefully and sincerely thank my advisor, Dr. Jeffrey S. Wiggins, for his guidance, understanding, patience, and most importantly, his friendship during my graduate studies at USM. His mentorship was paramount in providing a well rounded experience consistent my long-term career goals. I would also like to acknowledge my committee members: Dr. Sarah Morgan, Dr. Sergei Nazarenko, Dr. Joshua Otaigbe, Dr. Robson Storey and Dr. Dan Savin for their excellent guidance and insight on my research.

I would also like to thank those persons whom I have collaborated with over the years for their contribution to my dissertation and graduate research. Specifically, I would like to acknowledge Dr. Qi Wu (AFM-QNM), Dr. David Kingsley and Dr. Jinhai Yang (Continuous Reactor Design).

Finally I would like to thank all the current and former members of the Wiggins Research Group, especially Dr. Katherine Frank, Alex Hamilton, Brian Greenhoe, Joya Cerutti for their support in my research work.

TABLE OF CONTENTS

ABSTRACT ii

DEDICATION iv

ACKNOWLEDGMENTS v

LIST OF TABLES viii

LIST OF ILLUSTRATIONS ix

CHAPTER

I. INTRODUCTION 1

Preface
Epoxy-Based Prepregs and Prepolymers
Thermoplastic-Toughened Epoxies
MWCNT-Reinforced Epoxy Nanocomposites
Fully Intermeshing Co-rotating Twin Screw Extrusion
Research Overview

II. EXPERIMENTAL 27

Materials
Sample Preparation
Characterization

III. DEVELOPMENT OF CONTINUOUS REACTOR FOR THERMOPLASTIC MODIFIED EPOXY-AMINE PREPOLYMERS .. 41

Abstract
Results and Discussion
Conclusion

IV. EFFECTS OF MULTIFUNCTIONAL EPOXY COMPOSITION ON MORPHOLOGIES AND MECHANICAL PROPERTIES OF PES MODIFIED EPOXY BLENDS 62

Abstract
Results and Discussion
Conclusion

V. DISPERSION AND STABILIZATION OF MWCNT IN EPOXY PREPOLYMER MATRIX USING CONTINUOUS REACTOR 86

Abstract
Results and Discussion
Conclusion

VI. EFFECTS OF MWCNT ON REACTION INDUCED PHASE SEPERATION AND PROPERTIES OF EPOXY/PEI BLENDS 109

Abstract
Results and Discussion
Conclusion

REFERENCES 125

LIST OF TABLES

Table

1. Compositions of Prepolymer Batch and Continuous Reactions 30

2. PES Modified TGDDM/TGAP/44DDS Blends Nomenclatures and Compositions 31

3. TGDDM/MWCNT Prepolymer Nomenclatures and Processing Conditions 33

4 . MWCNT Reinforced Epoxy Prepolymer/PEI Blends Nomenclatures and Compositions 34

5. Kinetic and Diffusion Control Parameters for TGDDM/44DDS/PES Batch Reaction 45

6. Predicted and Experimental Results for TGDDM/44DDS/PES Prepolymer Continuous Reaction 51

7. Process Conditions and Properties of TGDDM/44DDS/PES Prepolymers 53

8. Mechanical Properties of Cured TGDDM/44DDS/PES Matrices 60

9. Imaging Analysis of PES Modified TGDDM/TGAP/44DDS Blends 74

10. Dispersion Indices and Processing Viscosities of TGDDM/MWCNT Prepolymers at Different Dispersing Temperatures 90

11. Critical Time and Viscosities of MWCNT Re-agglomeration in TGDDM Prepolymer Matrix at Various Cure Temperatures 100

LIST OF ILLUSTRATIONS

Figure

1. Schematic free energy curve as a function of volume fraction at different temperature (top) and phase diagram (bottom). 7

2. Schematic dependence of phase behavior on molecular weight of polymer. 8

3. Schematic process of (A) SD and (B) NG mechanism in a binary system..... 10

4. Schematic viscosity changes of neat epoxy resin cure, SD, and NG phase separation process. 13

5. Schematic peak-Force Tapping evaluation from the AFM force-distance curves. The software calculates the sample's peak force F_{peak}, the adhesion force F_{adh} and the peak deformation d_{def}. 14

6. Electron microscopy image of entangles MWCNT agglomerates (Baytube CP150). Provided by Bayer Corporation. 15

7. Optical images recorded on MWCNT dispersion in Bis-F (a) after mixing, and (b) after cured at 120 °C for 5 h. 18

8. Flexural properties of epoxy composites with different MWCNT functional groups..... 19

9. Electrical conductivities of epoxy composites with different MWCNT functional groups. 20

10. Screw elements used for co-rotating twin screw extruder.. 22

11. Co-rotating TSE continuous reactor based on ZSK 26MC Compounder..... 23

12. Schematic dispersive mixing and distributive mixing mechanism. 24

13. (a) 44DDS, (b) TGDDM, (c) TGAP, (d) PES, and (e) PEI. 28

14. Screw configuration of the continuous reactor based on Prism 16 mm TSE. 29

15. Screw configuration of the continuous reactor based on ZSK 26 Mega Compounder..... 32

16. Calibration curve for ion viscosity as a function of tracer concentration. 37

17. Optical images recorded on batch reactor dissolution states at 120 °C. 43

18. Cure conversions vs. reaction time at different curing temperatures..... 44

19. Arrhenius plot of the rate constants for the cure reaction. 45

20. Calculated vs. experimental TGDDM/44DDS/PES conversion at 120 °C. 46

21. Conversion and 80 °C Brookfield viscosity of TGDDM/44DDS/PES prepolymers..... 47

22. Continuous reactor RTD (solid line is best fit). 48

23. Optical images recorded on continuous reactor dissolution states at various temperatures. 49

24. Comparison of simulation vs. experimental cure conversion in continuous reactor. 52

25. Optical images recorded on continuous reactor dissolution states at various screw speeds..... 54

26. Changes of RTD at different screw speeds of continuous reactor. 54

27. Changes of RTD at various throughputs of continuous reactor..... 56

28. Optical images recorded on continuous reactor dissolution states at various throughputs. 56

29. Peak-Force Tapping images of cured TGDDM/44DDS/PES systems: (a) batch reaction (b) continuous reaction (c) batch imaging (d) continuous imaging. 58

30. PES phase diameter histograms of (a) batch reaction and (b) continuous reaction..... 59

31. ^{1}H NMR of TGDDM/PES mixtures before (a) and after (b) 1 h at 125 °C..... 65

32. NIR spectra of TGDDM/44DDS cure reaction at 125 °C. 66

33. NIR plots tracking conversion for TGDDM/44DDS/PES system..... 67

34. ^{1}H NMR spectra of TGAP/PES mixtures before (a) and after (b) 1 h of curing at 125 °C. 68

35. NIR spectra of TGAP/44DDS cure reaction at 125 °C. 69

36. Schematic network formation of PES modified TGDDM/TGAP/44DDS blends. 70

37. SEM micrographs of the fracture surface for 0TM/100TP. 72

38. Peak-Force Tapping images of PES modified TGDDM/TGAP/44DDS blends. . 73

39. DMA of PES modified TGDDM/TGAP/44DDS blends. 75

40. Gel times of PES modified TGDDM/TGAP/44DDS blends. 77

41. Complex viscosity traces of PES modified TGDDM/TGAP/44DDS blends. 78

42. Tensile modulus of TGDDM/TGAP/44DDS blends. 79

43. Fracture toughness of TGDDM/TGAP/44DDS blends. 80

44. Schematic phase-separated domain sizes of epoxy/thermoplastics blends and techniques limitations. 82

45. Viscosity changes of TGDDM/PES and DGEBA/PES mixtures at 125 °C. 83

46. Optical micrographs of MWCNT dispersion states in TGDDM/MWCNT prepolymers at different dispersing temperatures. 88

47. Dispersion index changes of TGDDM/MWCNT prepolymers vs. dispersing zone temperatures. 89

48. Optical micrographs of MWCNT dispersion states in TGDDM/MWCNT prepolymers at different screw speeds. 91

49. Dispersion indices of TGDDM/MWCNT prepolymers vs. screw speeds. 92

50. Optical micrographs of MWCNT/TGDDM prepolymers curing at 120 °C. 94

51. Optical micrographs of MWCNT/TGDDM prepolymers curing at 140 °C. 94

52. Optical micrographs of MWCNT/TGDDM prepolymers curing at 160 °C. 95

53. Optical micrographs of MWCNT/TGDDM prepolymers curing at 180 °C. 95

54. SEM images of fully cured MWCNT/TGDDM nanocomposites. 96

55. Dispersion index vs. curing time at different isothermal temperatures. 99

56. Viscosity profiles of MWCNT/TGDDM prepolymers at various cure temperatures. 100

57. OM (a) and SEM (b) images of TGDDM containing 0.5 wt% MWCNT during and after cured at 80 °C for 24 h and 120 °C for 5 h. 102

58. Viscosity profiles during cured at 80 °C for 24 h and 120 °C for 5 h. 103

59. Electrical conductivities vs. MWCNT contents of TGDDM/MWCNT nanocomposites. 105

60. Storage modulus and tan δ of MWCNT/TGDDM composites containing 0.5 wt% MWCNT. 106

61. Tensile modulus vs. MWCNT contents of MWCNT/TGDDM nanocomposites. 107

62. SEM images of TGDDM/TGAP/PEI phase morphologies cured at 180 °C. 111

63. Complex viscosities of TGDDM/TGAP/PEI prepolymers cured at 180 °C. 112

64. Tan delta curves of TGDDM/TGAP/PEI blends cured at 180 °C. 113

65. SEM images of 6.4 PEI morphologies with different MWCNT weight contents. 116

66. SEM images of 9.6 PEI morphologies with different MWCNT weight contents. 118

67. SEM images of 12.8 PEI morphologies with different MWCNT weight contents. 120

68. Complex viscosity of 9.6 PEI with different MWCNT weight contents cured at 180 °C. 121

69. Tan delta curves of 9.6 PEI blends with different MWCNT contents cured at 180 °C. 122

CHAPTER I

INTRODUCTION

Preface

The uses of "green" processing technologies and chemistries are continuing to become an important area of research in the world today. Raw materials derived from renewable resources such as the production of commercial polymers from sustainable feedstock will be economically, socially, and environmentally favorable.[1] In addition, new chemical manufacturing technologies which are solvent free, and reduce energy consumption are desirable.[2] As a result, governments, universities, materials science based corporations have displayed an increased commitment to adopt, develop and implement green technologies in products and manufacturing.

Polymerization reactors and processes are energy intensive. An example of energy demanding polymerization reactions is the synthesis of epoxy prepolymers used as structural matrices in aerospace carbon fiber reinforced prepreg materials. In this case, epoxides, curatives and modifiers are mixed and reacted in low-shear batch reactors which may exceed 1000 L volume through slow heating over 24 h. Once advanced to prescribed molecular weights, epoxy prepolymers are discharged from the batch reactors and stored at low temperature for indefinite periods of time to retard cure and preserve viscosity. Subsequently, prepolymers are removed from cold storage, heated above their glass transition temperatures and converted into thin films when use in prepreg filming. The total energy consumed throughout this entire process is substantial. Furthermore, epoxy prepolymers are reactive intermediates and their viscosities are constantly changing during heating and cold storage leading to potential inconsistencies in prepreg quality.[3, 4]

Next generation epoxy prepolymer reactors need to disperse a broad range of additives including thermoplastic toughеners, stabilizers, nanoparticles, solubilize curatives, and advance prescribed molecular weights and viscosities while reduce total energy consumption. One possible solution for reducing energy and improving quality is to develop high-shear continuous reactors based on twin-screw extruder (TSE). The potential advantages of high-shear continuous reactors compared to low-shear batch reactors are low cost, improved efficiencies and excellent control of processing parameters. TSE have been proven beneficial for controlling shear energies, heat transfer, feeding, mixing, devolatilization, and changes in viscosity.

We believe continuous reactors based on TSE can be incorporated in-line of prepreg filming operations to provide a monomer-to-prepreg process, thus eliminating substantial energy while improving quality. The advancement of continuous reactors in this field will lead to new avenues for mixing and blending a broad array of co-reactants, blends, nanoparticles and etc. in epoxy prepolymer matrices. The specific aim of this dissertation is to demonstrate the feasibility of continuous reactor methods for epoxy prepolymers preparation and to present the findings regarding the process-structure-property relationships in the thermoplastics and/or nanoparticles modified epoxy prepolymers and crosslinked glassy epoxy networks.

Epoxy-Based Prepregs and Prepolymers

Prepreg materials are becoming increasingly common in the manufacturing of advanced high-performance composite products due to their ease of use, consistent properties and high quality surface finish. The term “prepreg” is shorthand for “preimpregnated”, referring to fiber-based reinforcing materials preimpregnated with matrix resin prior to the part layup and cured by the application of heat. Prepregs

differentiate themselves from other composite materials in that they contain a pre-determined ratio of fiber reinforcement and matrix resin. The foremost example is the epoxy-based prepregs used in aerospace industries. It typically consists of 67 wt% unidirectional carbon fibers pre-impregnated with 33 wt% epoxy prepolymer resins.[5] The reinforcing carbon fibers can provide strength and stiffness, while epoxy resins can give the desired shape or structure to the composites and distribute the stress between the reinforced fibers.

Epoxy prepolymers used as prepreg matrix resin are typically formulated from multifunctional epoxide resins with difunctional amine hardeners and partially reacted as an initial stage before being applied onto prepreg filming.[6, 7] It is also called "B-stage" epoxy, different from the typical "A-stage" uncured epoxy and "C-stage" fully cured epoxy. The primary characteristics of partially cured epoxy prepolymers are the controlled flow and self-adhesion. Controlled flow requires that the resin maintain a target viscosity during prepregging and laminating. As a result, consistent resin content and thickness are produced in the final cured composites. Self-adhesion allows the layers of carbon fibers and prepregs can be stacked and bonded easily during layup process. Epoxy prepolymer resins with such properties usually remain tacky but not sticky.

In the traditional batch reaction process for preparing epoxy prepolymers, epoxides are firstly heated at appropriate temperature to dissolve amines and initiate epoxy-amine cure reaction. Reaction continues at relatively low temperature over long periods of time to prevent exotherm. Once epoxy prepolymers are advanced to a prescribed molecular weight with desired viscosity, they are discharged from batch reactors, quenched, and stored in freezers for indefinite periods of time to slow kinetics, minimize continued cure reaction, and maintain the target viscosity. When use in prepreg,

epoxy prepolymers are reheated above their glass transition temperature, discharged to film lines, and processed into thin films. One drawback of this batch reactor process is that the total energy consumed in the batch heating, sub-ambient storage, re-heating, and filming processes is substantial. Furthermore, since epoxy prepolymers are reactive intermediates, the extent of reaction and viscosity are constantly changing during heating and sub-ambient storage. This behavior counts for the inherent inconsistencies in quality and leads to variation in the prepreg and final cured composite structures. Therefore, there is an increasing demand from composite manufacturers to reduce the energy consumption required to produce epoxy prepolymers and to minimize the variation in quality. This is the main driving force for this dissertation to develop a continuous reaction method for preparing epoxy prepolymers with reduced energy consumption and improved quality consistence.

Thermoplastic-Toughened Epoxies

In the area of aerospace-grade composites, epoxy resins are generally formulated from a selection of materials including multifunctional epoxides and diamine hardeners. Composite matrices based on multifunctional epoxies tend to have higher strengths, stiffnesses, and glass transition temperatures than difunctional epoxies due to their higher crosslink densities.[8] However, the highly crosslinked structures result in inherent brittleness which limits their applications. Thus, many efforts have been devoted to improve the toughness of multifunctional epoxy resins over the last decades.

Elastomers such as carboxyl terminated butadiene acrylonitrile rubbers (CTBN)[9,10] and amine terminated butadiene-acrylonitrile rubbers (ATBN)[11] have traditionally been used to improve epoxies toughness. However, elastomer toughenens are known to reduce thermal and mechanical properties of the glassy polymer networks,

which is undesirable for advanced aerospace composite materials.[12, 13] More recently, linear high molecular weight thermoplastics have been used as the modifiers for epoxies with an advantage for preservation of thermal and mechanical properties. The first two toughening studies using thermoplastic additives were reported by Bucknall[14] and Partridge[15] in 1980s. Commercial polyethersulphone (PES, Victrex 100P) was used in their studies to toughen epoxy resins and effective enhancement was obtained when thermoplastic phase separated from epoxy matrix combined with good interfacial adhesion. Since then, various types of high performance linear thermoplastics including polysulfone (PSF),[16] polyetherimide (PEI),[17] polyetherketone (PEK),[18] and etc. have been intensively explored in literatures. The main research areas are focused on the phase separation mechanism, final phase separated morphologies, and phase separation detection.

Thermodynamic Theory of Phase Separation

From thermodynamic point of view, the stability of a system is described by the free energy of mixing (ΔG_m) which is related to the enthalpy (ΔH_m) and entropy (ΔS_m) changes in terms of $\Delta G_m = \Delta H_m - T\Delta S_m$. ΔG_m is dependent on temperature and pressure. Phase separation may occurs when ΔG_m is changed upon the changes on temperature and pressure, leading a transition from single phase to two or more distinct phases. For a binary system to be considered as fully miscible at any given composition (ϕ), the following two requirements need be satisfied:

$$\Delta G_m\,(\phi) < 0 \quad \text{(Eq. 1)}$$

$$\frac{\partial^2 \Delta G_m}{\partial \phi^2} > 0 \quad \text{(Eq. 2)}$$

According to Flory-Huggins theory,[19] the free energy can be further expressed in terms of the volume fraction of each component in a binary system, ϕ_1 and ϕ_2 as:

$$\frac{\Delta G_m}{kT} = \phi_1 \ln \phi_1 + \phi_2 \ln \phi_2 + \phi_1 \phi_2 \chi \text{ (Eq. 3)}$$

The first two terms in Eq. 3 represent the entropy whereas the last term reflects the enthalpy which is related to the interaction parameter (χ). Figure 1(a) shows the schematic free energy curves as a function of polymer volume fraction at different temperatures. Compositions that correspond to the inflection points ($\frac{\partial^2 \Delta G_m}{\partial \phi^2} > 0$) for each free energy curve are called as spinodal points.

In order for a binary system presenting two stable phases, both phases must be at their corresponding equilibrium states. The criteria are the temperature and pressure must be identical in those two phases and the chemical potential of component 1 is the same in both phases and the chemical potential of component 2 is equal in both phases:

$$\mu_1(\phi_1') = \mu_1(\phi_1^{"});\ \mu_2(\phi_2') = \mu_2(\phi_2^{"}) \text{ (Eq. 4)}$$

There is only one mathematical solution ($\phi_1', \phi_2^{"}$) for both equations at a particular temperature and pressure, which refers to common tangent construction (binodal point).

Phase diagram is obtained by combining the binodal and spinodal points in the fraction volume and temperature space, showing in Figure 1(b). System located inside the spinodal curve is considered as miscible and homogenous. System entered the outside the binodal curve is phase-separated and heterogeneous. Regions between spinodal and binodal curve are called meta-stable region. The critical point is defined as the common tangent of spinodal curve and binodal curve. For instance, system is fully miscible and stable above the critical point for a binary mixture with an upper critical solution temperature. Changes of temperature, pressure, and composition may result in phase

separation from a homogenous single phase to binary phases depending on which one is more stable.

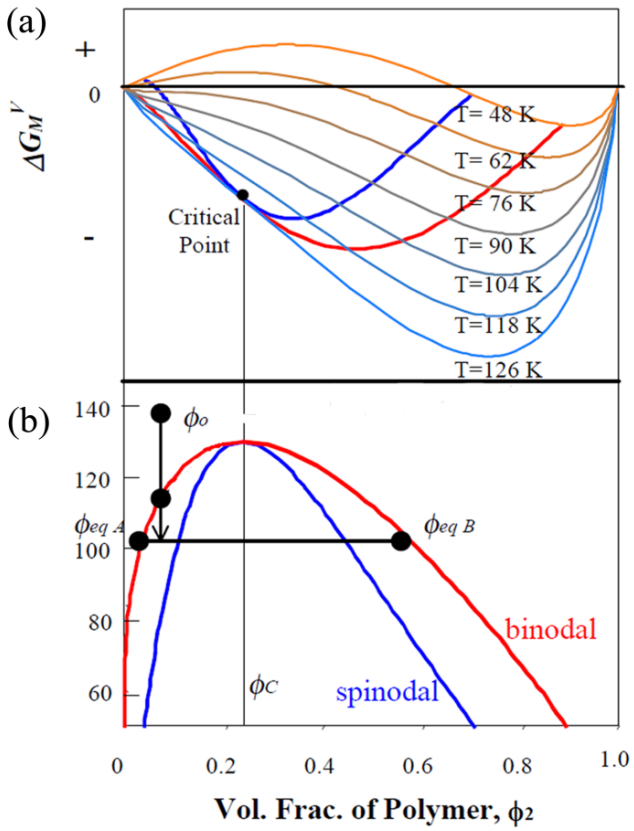

Figure 1. Schematic free energy curve as a function of volume fraction at different temperature (top) and phase diagram (bottom). Reproduced from reference with permission.[19]

Interaction parameter (χ) is related to the ratio of size of a polymer molecule to that of a solvent. Change of polymer molecular weight or solvent will alter the interaction parameter, resulting in a shift of phase diagram. The effect of polymer molecular weight on the phase behavior is illustrated in Figure 2. As the differences between polymer and solvent molecular weights increases, system with a particular composition may move from stable region into unstable region and initiate phase separation. This accounts for

the occurrence of phase separation in thermoplastic/thermosets binary systems, which will be discussed later in details.

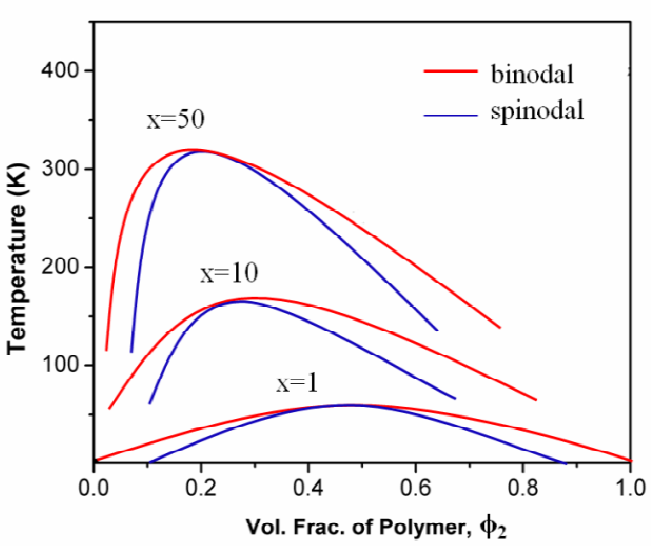

Figure 2. Schematic dependence of phase behavior on molecular weight of polymer. Reproduced from reference with permission.[19]

Kinetics of Phase Separation

Thermodynamic theory describes only where the most stable state lies and whether the system is stable or not at current status, but does not describe the pathways of phase separation. Phase separation is a kinetic process and can be distinguished into two types of kinetic mechanism: spinodal decomposition (SD) and nucleation and growth (NG).

For SD mechanism, a new phase is spontaneously generated from the parent phase at a thermodynamically unstable state. The new phase and parent phase form an interconnected co-continuous structure and can continue growing until reach their equilibrium states. If the viscosity of the system were sufficiently low, density differences of both phases may lead to dynamic asymmetry between the two components and cause

the phase transition from a co-continuous structure to spheres structure with a lower interfacial energy. SD occurs when the system enters the spinodal region of the phase diagram. A fast transition such as quench is typically required to allow the system moving from the stable region through the meta-stable region and into the unstable spinodal region.

For NG mechanism, a series of new nuclei are generated from the parent phase so that the parent phase reduces its composition with a decreased free energy. Once the nuclei are formed, they can grow spherically and may coalesce with each other. In order for nuclei formation, it is required that the system maintain at the meta-stable state and composition fluctuations is large enough. NG differs from SD in that phase separation only occurs at nucleation sites instead of throughout the parent phase. However, both mechanisms may give the same phase separated morphology at the end of phase separation if matrix viscosity is sufficient low. Figure 3 depicts the schematic phase separation processes in the binary system followed by SD mechanism and NG mechanism.

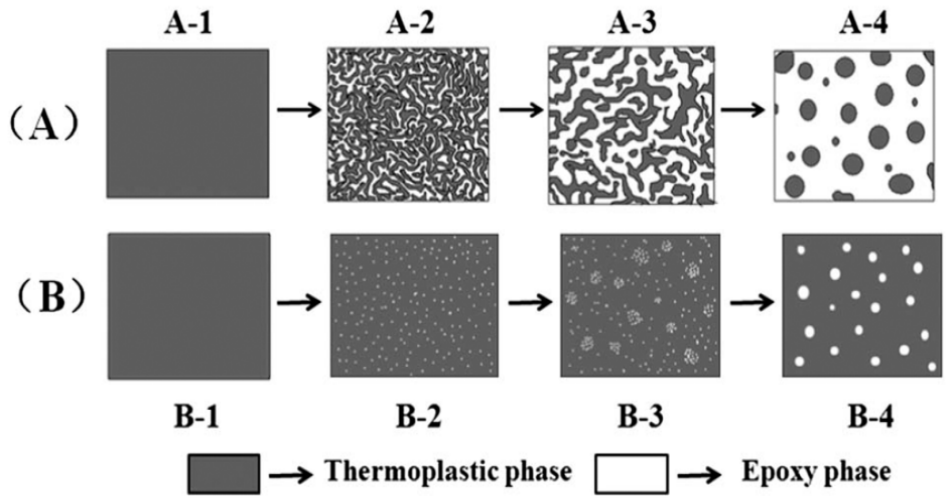

Figure 3. Schematic process of (A) SD and (B) NG mechanism in a binary system. Reproduced from reference with permission.[20]

Cure Reaction Induced Phase Separation

In thermoplastic/thermosets binary systems, thermoplastic is usually fully miscible in epoxies before curing. Once cure reaction is initiated by heat, the molecular weight of epoxies increases and causes the shift of phase diagram. At a certain extent of cure, system can cross the thermodynamic phase boundaries and enter the unstable regions, resulting in a transition from homogeneous state into phase-separated state. This phase separation process induced by cure reaction of thermosets is called cure-reaction induced phase separation (CRIPS). Furthermore, since phase separation is highly viscosity-dependent, the increased molecular weight and viscosity of epoxy matrices upon cure reaction could reduce the phase separation rate and completely suppress when system vitrified. As a consequence, the final cured morphology of epoxy-thermoplastic binary system is affected by the competition between phase separation kinetics and cure reaction rate. Three types of phase morphologies are often observed at micro-scale

including droplets dispersed morphology, co-continuous structure and phase inverted morphology.[21]

Knowledge of phase separation mechanism and crosslinked reaction kinetics comprise the basis of morphology design for thermoplastic/thermosets systems. There are extensive literatures focused on parameters that could use to control CRIPS morphologies in epoxy-thermoplastic systems. It has been known morphologies can be modified in multiple ways including changing thermoplastic weight fraction and molecular weight,[22] altering thermoplastic end group reactivity,[23] and varying epoxy cure chemistry such as cure rate, cure temperature, and epoxy-amine stoichiometric ratio.[24, 25] General trends have been found that decreasing miscibility of thermoplastic in epoxy before curing or reducing cure rate of epoxy crosslinking chemical reaction could facilitate phase separation process.

It is our opinion that despite the prevalence of scientific reports in CRIPS mechanism and morphology control in epoxy-thermoplastic system, the relationship between cross-linked glassy polymer network structures, cured network morphologies and their influence on ultimate mechanical properties is still not fully understood. One of the goals of this dissertation is to investigate effects of multifunctional epoxy compositions on thermoplastics phase-separated morphology domain sizes and their final mechanical properties.

Detection of Phase Morphology

Scanning electron microscopy (SEM) and transmission electron microscopy (TEM) are the two most commonly used techniques to observe phase morphologies. They offer a directly visual evidence of phase separation on sample surfaces through solvent etching and staining techniques. Optical microscopy (OM) equipped with a

temperature-controlled heating chamber is able to detect the onset of phase separation in thermoplastic modified epoxy systems.[26] It allows focusing on the description of phase separation time-temperature dependency which is of great interests in the composites industry.

Rheological analysis is another useful technique for studying CRIPS. It can measure the abrupt viscoelastic changes associated with phase separation. Depending on the kinetics of phase separation mechanism (spinodal decomposition, and nucleation and growth) there are two typical viscosity profiles during curing as presented in Figure 4. Compared with the complex viscosity (η^*) changes of neat epoxy system during cure, both thermoplastic modified epoxy systems exhibited a fluctuation at early stage of cure reaction that is related to the onset of phase separation. For nucleation and growth mechanism, the complex viscosity shows a rapid decrease owing to the demixing of high viscous thermoplastic from continuous epoxy matrix and forming nuclei. While for spinodal decomposition, the abrupt increase in complex viscosity is corresponding to the formation of bi-continuous structures which continuous thermoplastic phase starts to dominate the matrix viscosity.

Several other techniques have also been reported to monitor reaction induced phase separation process, such as dynamic mechanical analysis[27] and small angle light scattering.[28] Each of the techniques measures different variables that are expected to change throughout phase separation evolution. They can be used alone or combined together to develop a deeper understanding of reaction induced phase separation process, and through that understanding, a prediction of final cured morphology.

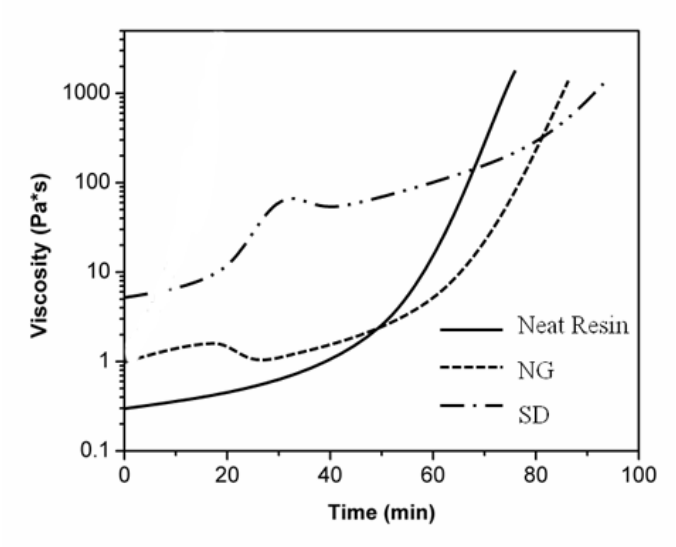

Figure 4. Schematic viscosity changes of neat epoxy resin cure, SD, and NG phase separation process.

In this research besides all the techniques mentioned above, atomic force microscopy with quantitative nanomechanical mapping (AFM-QNM) will be used for the first time to study reaction induced phase separation morphology in epoxy-thermoplastic systems. AFM-QNM maps and distinguishes between nanomechanical properties, including modulus and adhesion, while simultaneously images topographical information at a nanometer scale on sample surface. After calibrating by comparing to a reference sample (relative method) and by measuring the tip end radius and spring constant (absolute method), AFM can provide quantitative elastic modulus over a broader detectable range. The modulus is determined by fitting the force-distance curves to a Derjaguin-Muller-Toporov (DMT) model.[29] Figure 5 elucidates how mechanical modulus and adhesion property are extracted from force-separation curves. This powerful technique allows detecting phase-separated morphology in a nanostructure level through quantifying two phases modulus difference.

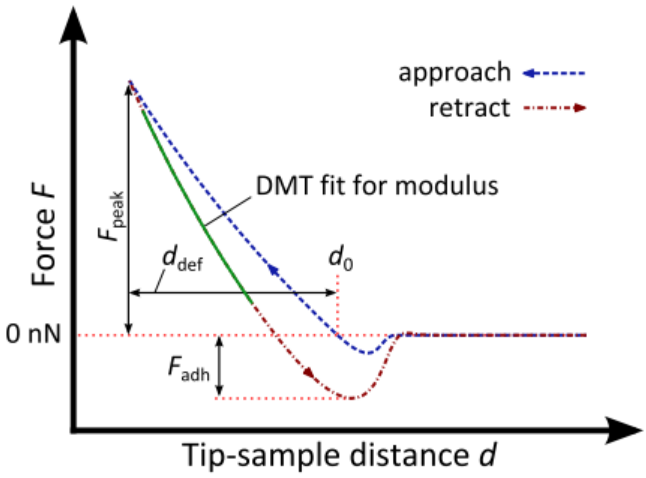

Figure 5. Schematic peak-Force Tapping evaluation from the AFM force-distance curves. The software calculates the sample's peak force F_{peak}, the adhesion force F_{adh} and the peak deformation d_{def}. Reproduced from reference with permission.[30]

MWCNT-Reinforced Epoxy Nanocomposites

Multiwall carbon nanotubes (MWCNT) have drawn a lot of interest as the reinforced nanoparticles for epoxy matrix composites owing to its unique structural, electrical, and mechanical properties.[31, 32] They have been intensively explored in the view of their potential applications in the electronics, automotive, and aerospace industries. However, the experimentally observed reinforcing effects strongly depend on the dispersion state of nanotubes. High quality dispersion of MWCNT is difficult to obtain due to the high amount of energy required to overcome the van der Waals interactions between neighboring tubes. In addition, commercialized MWCNT are generally supplied in the form of heavily entangled bundles (Figure 6), resulting in inherent difficulties in dispersion. Those difficulties associated with the poor interfacial interaction between MWCNT and epoxy matrix could lead to cured network with diminished material properties.[33, 34]

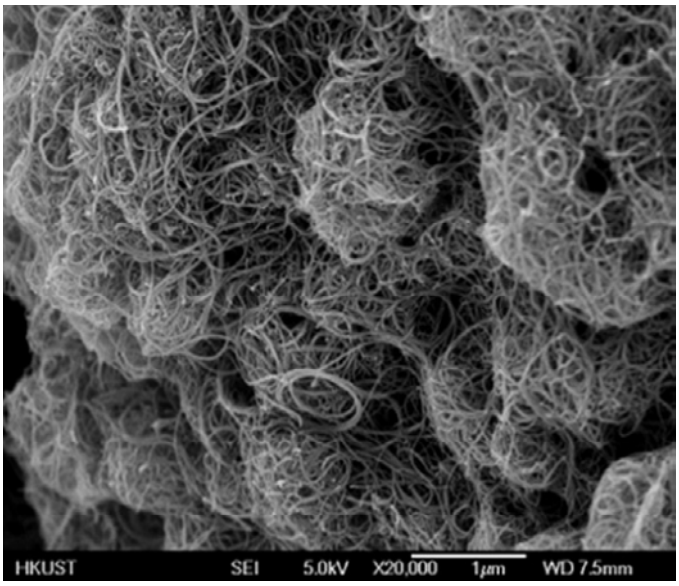

Figure 6. Electron microscopy image of entangles MWCNT agglomerates (Baytube CP150). Provided by Bayer Corporation.

Dispersion of MWCNT in Epoxy Matrices

Several approaches have been developed to improve MWCNT dispersion in epoxy matrices over last decades. These approaches include mixing techniques such as sonication[35], and chemical techniques such as surface functionalization[36] and use of dispersive agents or surfactants.[37, 38]

The most successful MWCNT dispersion technique probably is sonication, which was first used in 1999[39] and has been optimized over the years. Sonication is effective at dispersing MWCNT owing to its high shear force generated from the shear rates exceeding 10^7 per second. A typical procedure for dispersion MWCNT in epoxy begins with suspension of MWCNT in a solvent or a solvent-epoxy mixture (usually acetone, ethanol, or DMF) using either bath or tip ultrasonic mixing. Following dispersion, cure agents are added and subsequently cured by heat. Unfortunately sonication techniques are often limited to lab-scale reactions as larger scale equipment is neither available nor

practical due to the large amounts of heat generated by the high localized shear force. The high shear rates have also been shown to cause nanotube size reduction and degrade epoxy components.[40]

Lower shear techniques such as extrusion and calendaring are very promising techniques to achieve relatively good MWCNT dispersion in polymer matrices. Calendaring was first used as dispersion approach in 2004, and is particularly useful for dispersing MWCNT in low viscous epoxy matrices.[41, 42, 43] One major advantage of calendaring method is the gap between rollers can be mechanically adjusted within micro length so that the nanotubes size distribution is controllable. However, the rollers have gap limitation which is typically much larger than the diameter of individual nanotube, suggesting the calendaring method can only disperse large agglomerates into small ones at micro level. Twin screw extrusion is a popular technique to disperse MWCNTs into solid polymer matrices like most thermoplastic and has been investigated as a method for dispersing nanotubes in epoxy. In those studies, the amine curative was mixed with epoxy-MWCNT mixture after extrusion which brings manufacturing difficulties owing to the high viscous epoxy matrices.[44, 45] To our best knowledge, single-step reactive extrusion of epoxy resin, curative, and nanotubes has not yet been reported.

Chemical dispersing methods such as using dispersion agents and nanotube surface functionalization are able to enhance the interfacial interactions between MWCNT and epoxies through covalent or hydrogen bonds. These methods greatly improve the dispersion of MWCNT in epoxy matrices, but they have the potential to decrease material physical properties by acting as plasticizers and reduce electrical conductivity by preventing the formation of interconnected MWCNT conducting network.[46,47]

Re-agglomeration and Stabilization of MWCNT in Epoxy Matrices

The existing research on MWCNT dispersion mentioned above has mainly focused on the nanotubes themselves, either making them more dispersible in epoxy matrices or using high-shear mixing techniques to break up aggregates. The effects of growing epoxy network on nanotube dispersion have been somewhat ignored. Within epoxy resins, the issue of MWCNT dispersion is complicated by its differences from thermoplastics as most epoxy resins have two components, a resin and a hardener, and typically require elevated temperature with long-time heating for curing. Factors such as matrix viscosity, curing temperature, and curing time are going to influence the MWCNT stabilization during curing process and may lead to re-agglomeration in the final cured glassy epoxy composites.[48]

Re-agglomeration of MWCNT in epoxy matrices during cure reaction can be directly observed in real-time using optical microscopy. K.C Amit[49] recently studied MWCNT re-agglomeration evolution during cure cycles and found that a good MWCNT dispersion at initial stage of curing was completely lost as the cure reaction progressed at elevated temperature. Large cluster-like MWCNT structures were formed after cure reaction completed as depicted in Figure 7. R. Hollertz[50] investigated the effects of cure temperature on MWCNT stabilization in epoxy matrices. Similar trends were observed for samples cured at different temperature while larger extent of re-agglomeration was obtained at higher temperature. As consequences, good nanotube dispersion is only retained in the epoxies before curing other than final cured composites.

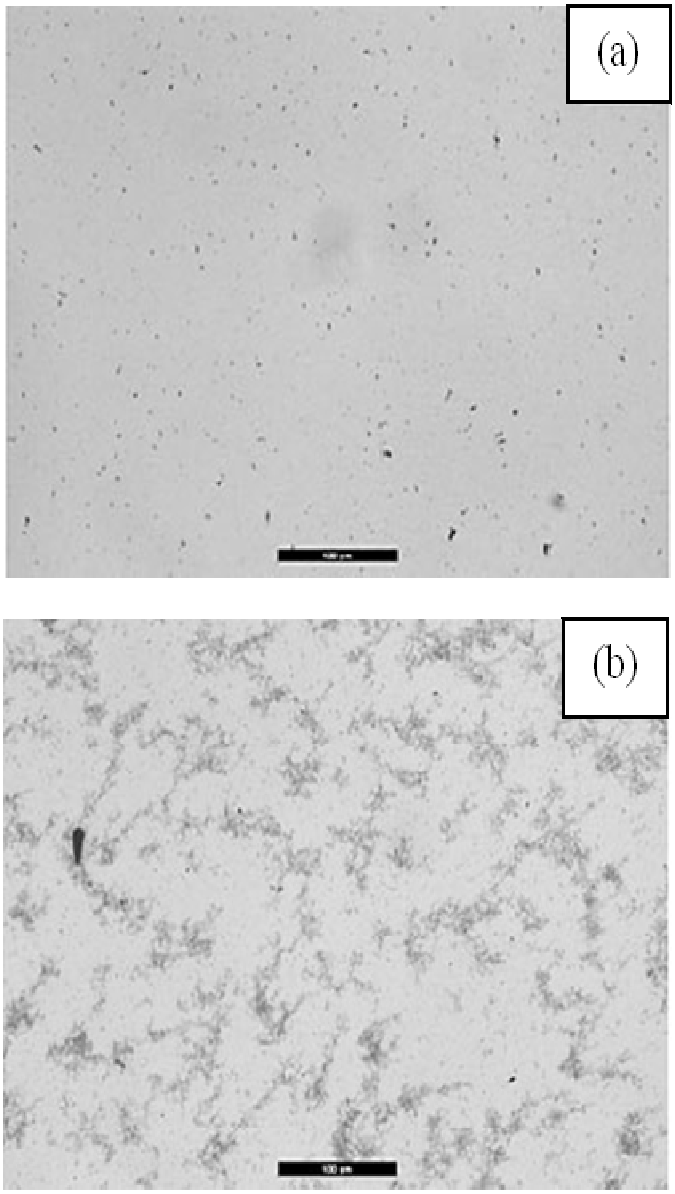

Figure 7. Optical images recorded on MWCNT dispersion in Bis-F (a) after mixing, and (b) after cured at 120 °C for 5 h. Reproduced from reference with permission.[50]

Increasing interfacial interaction between MWCNT and epoxy matrices through chemical functionalization is an effective method to prevent MWCNT re-agglomeration during cure reaction. Commonly-used functional groups are amino groups[51] and acid groups.[52] Other dispersion strategies such as using surfactant wrapping MWCNT also reported to avoid re-agglomeration by steric hindrance.[53] Epoxy matrices reinforced by

functionalized MWCNT generally exhibited increased mechanical strengths and moduli compared to those modified by pristine MWCNT, as showed in Figure 8.[54] This enhancement in mechanical property is attributed to the well-dispersed MWCNT in final cured composites, facilitating the loading transfer between matrices and fillers.

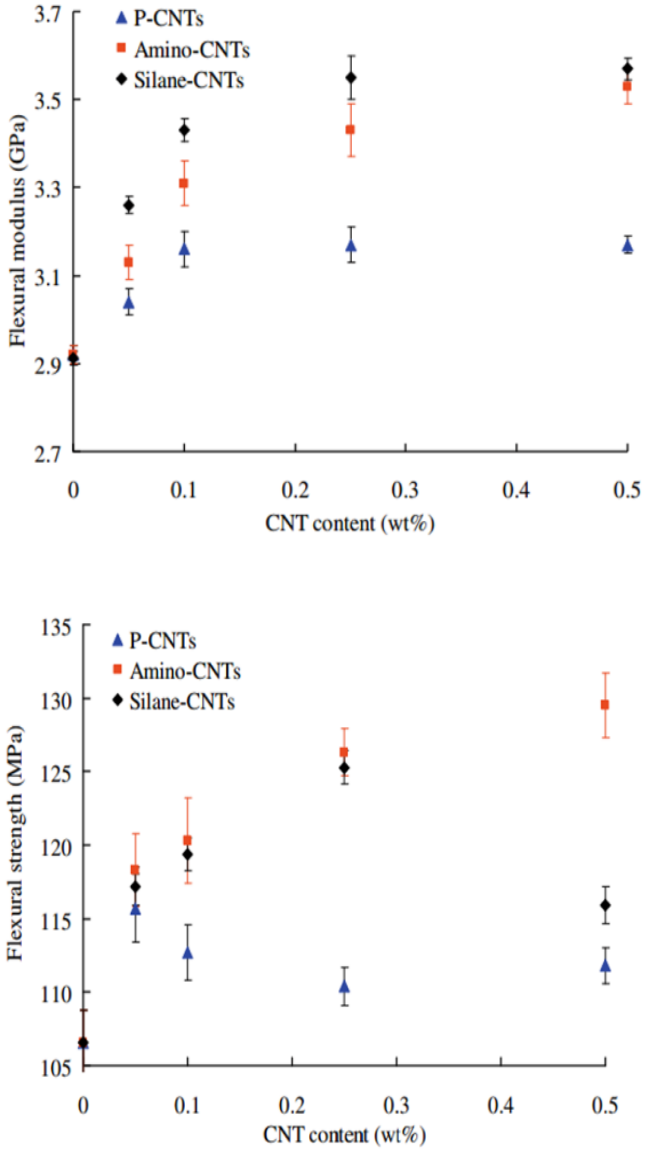

Figure 8. Flexural properties of epoxy composites with different MWCNT functional groups. Reproduced from reference with permission.[54]

However, electrical conductivity of functionalized MWCNT-epoxy composites is decreased in orders of magnitude compared to untreated MWCNT-epoxy composites with the same loading level (Figure 9). Two major reasons are responsible for the reduced electrical conductivity. Improved interfacial interaction between MWCNT and epoxy matrix results the wrapping of MWCNT by epoxy after curing. The wrapped polymer chain perturbs the π electron system of the MWCNT wall.[55] Additionally, the improved interfacial interaction between MWCNT and epoxy is known to be detrimental to the formation of continuous MWCNT conducting networks.

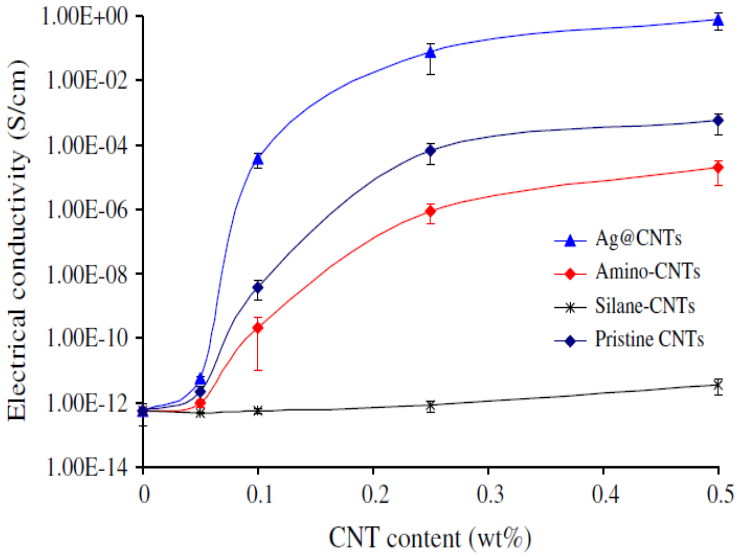

Figure 9. Electrical conductivities of epoxy composites with different MWCNT functional groups. Reproduced from reference with permission.[55]

Stabilization and re-agglomeration of pristine MWCNT in epoxy matrices is mainly governed by its mobility which is predominately affected by epoxy matrices viscosity. Since epoxy matrices viscosity is continually changing during cure cycle, MWCNT dispersion states are therefore directly depend on the curing time and curing

temperature. To our best knowledge, the time-temperature dependent MWCNT dispersion in epoxies has not been fully understood. Within this work we will investigate epoxy network growing kinetics and rheological progresses during cure reaction in the presence of MWCNT to gain a better understanding of time-temperature dependent MWCNT re-agglomeration and stabilization in epoxy matrices, allowing for the development of optimized glassy network chemistry and final properties.

Fully Intermeshing Co-rotating Twin Screw Extruder

Co-rotating twin screw extruder (TSE) has draw much attention in both academia and industry as it is a continuous and economic method for industrial scale manufacturing. Since 1980s, it has been reported to use as polymer continuous reactors,[56] bulk polymerization reactors,[57] polymer grafting reactors,[58] and polymer blend compatibilization reactors.[59] Literature reviews about TSE process have been published by Brown and Orlando,[60] and Xanthos.[61] The primary advantages of TSE compared to other polymerization reactors, such as batch reactors, is the capability of transporting materials over a broad range of viscosities. Additionally, the absence of solvent combined with simultaneous transport of low molecular weight monomers and high molecular weight polymers improves energy consumption making the reactor environmentally favorable. TSE also provides controlled shear energy, excellent heat transfer, precision feeding, mixing, devolatilization and insensitivity to viscosity changes.[62]

Fully intermeshing co-rotating twin screw extruders offer the highest level of mixing, dispersion and shear control among all types of TSE, making them the primary technology used as continuous chemical reactors.[63, 64, 65] It offers a broad array of screw elements design which are the core technology of extruders and provide necessary transport, mixing and shear abilities. Typically, three types of screw elements are used for

TSE including conveying elements, kneading elements and reversing elements. Examples of intermeshing co-rotating modular screw elements are illustrated in Figure 10. Reactor screws are precisely fit within a series of barrel sections equipped with independent temperature control by adjusting heating and cooling. Barrel sections along the extruder are the points where various liquid, solid reactants, catalysts, modifiers, and vacuum etc. are introduced. Figure 11 shows a typical TSE continuous reactor based on ZSK 26MC Compounder from Coperion Incorporation.

Figure 10. Screw elements used for co-rotating twin screw extruder.

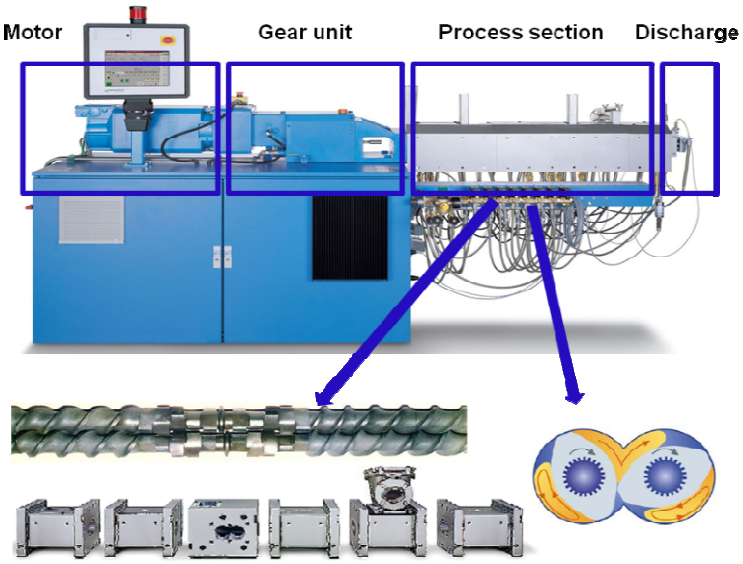

Figure 11. Co-rotating TSE continuous reactor based on ZSK 26MC Compounder.

During co-rotating continuous reaction, mixing mechanism is generally categorized into dispersive mixing and distributive mixing. For dispersive mixing, a critical stress is applied to the dispersant through laminar shear stress generated along the screw elements which overcomes cohesive forces of particulates so phase sizes are reduced. High shear rates are a requirement for successful dispersive mixing. In contrast, distributive mixing is more effectively carried out by shear stress that generates large strains as there is no critical stress threshold. Distributive mixing is facilitated by splitting and reorienting the flow streams. Figure 12 illustrates good or poor dispersive and distributive mixing in a particle/liquid system. When considering screw element geometries, wide kneading blocks with reverse pitch facilitate dispersive mixing while narrower kneading blocks with forward pitch, gear and tooth elements (ZME) provide distributive mixing. Continuous reactor modular screws are designed by placing appropriate screw elements in their proper positions according to the type of action

favorable to accomplish specific reactions or activities within specified regions of the reactor.

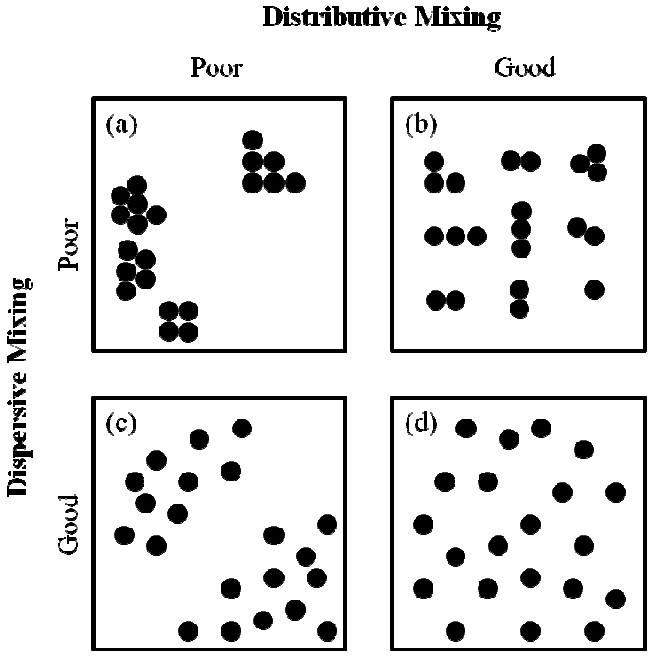

Figure 12. Schematic dispersive mixing and distributive mixing mechanism. Reproduced from reference with permission.[66]

Within numerous applications for polymer process and polymer reaction, TSE are mainly used for high molecular weight linear thermoplastic. They are non-traditional when preparing glassy epoxy network due to the possibility of gelation and crosslink resulting from the exothermic cure reactions. In addition, since epoxies are formulated in low viscous state when mixing with additives and cure agents, the applied shear force is greatly reduced at a constant shear rate and therefore limits its application for epoxy matrices. Previous research reported by Titier[67, 68] described a continuous reactor method for linear epoxy-amine chain extension reactions, but this research was limited to mono-epoxides as termination agents which was used to avoid gelation. In this dissertation, we want to develop a continuous reactor for crosslinkable epoxy-amine prepolymers through

a systematic analysis of reaction kinetics, reactor design and process conditions with the aim of replacing traditional epoxy batch reactors.

Research Overview

The goal of this dissertation is to develop a continuous reactor method for preparing crosslinkable epoxy prepolymers and to investigate the fundamental process-structure-property relationship between continuous prepolymer reaction, phase morphologies and mechanical properties in glass epoxy matrices. This research is motivated by the growing scientific and industrial interest in "green" processing technologies. Next-generation epoxy prepolymer reactors should be able to solubilize and disperse a broad range of additives including thermoplastic toughenners, stabilizers, nanoparticles and curatives and achieve prescribed molecular weights and viscosities while reducing energy consumption. Continuous reaction based on twin screw extruder presents unique advantages for energy saving and cost reduction. We believe continuous reactors could be incorporated in-line of prepreg filming operations to provide a monomer-to-prepreg process, thus eliminating substantial energy while improving quality of epoxy based prepregs and composites.

In Chapter III, the continuous reaction method to prepare thermoplastic modified epoxy prepolymers will be developed through fundamental understanding the epoxy-amine chemistry, reactor design and process conditions. A direct comparison of traditional batch and continuous reactors will be performed to demonstrate the feasibility.

Followed by the successful preparation of thermoplastic modified epoxy prepolymers, their phase separation mechanism and final cure morphologies will be investigated using SEM and AFM-QNM in Chapter IV. Effects of multifunctional epoxy

compositions on phase-separated morphologies and mechanical properties of final cured matrices will be symmetrically discussed.

MWCNT reinforced epoxy nanocomposites will be introduced in Chapter V. Our intention will be to combine the successful strategies for advancing epoxy chemistries as discussed in Chapter III with our approaches to achieving good levels of nanotubes dispersion and stabilization in epoxy matrices using the continuous reactor. Additionally electrical conductivities and mechanical properties of MWCNT-epoxy composites will be measured and discussed in view of their corresponding MWCNT dispersion states.

In Chapter VI, MWCNT will be incorporated into epoxy-thermoplastic binary systems and its impact on the phase separated morphologies and physical properties will be examined.

CHAPTER II

EXPERIMENTAL

Materials

The following materials were used as received: tetraglycidyl-4,4'-diaminodiphenylmethane (TGDDM) (Huntsman, UT, USA, M_n = 422.5 g/mol); triglycidyl p-amino phenol (TGAP) (Huntsman, UT, USA, M_n = 277.3 g/mol); 4,4'-diaminodiphenylsulfone (44DDS) (Royce Chemical Corp, PA, USA, M_n = 248.3 g/mol, particle size 4 μm); polyethersulfone (PES) (Virantage® VW-10700 RFP, Solvay, NJ, USA, M_n = 22,000 g/mol, particle size 75 μm); polyetherimide (PEI) (Ultem® 1000P, SABIC Plastics, MA, USA, M_n = 39000 g/mol, particle size 350 μm); multi-walled carbon nanotube (MWCNT) (Bay tube® C150P, Bayer Corp, PA, USA, length>1 μm, diameter 4~13 nm). The density of MWCNT after incorporation into epoxy matrices is approximately 1.75 g/cm^3.[69] Their chemical structures are presented in Figure 13.

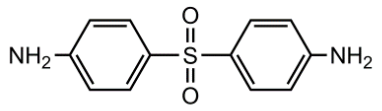

(a)

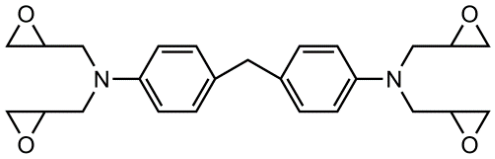

(b)

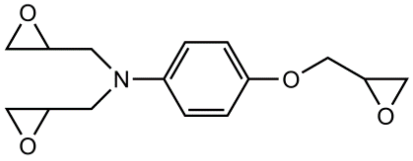

(c)

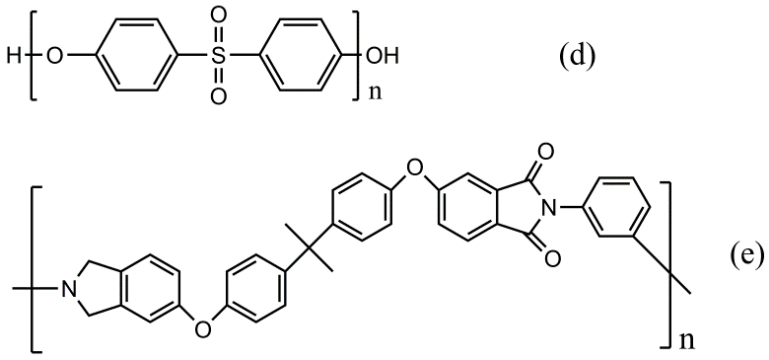

Figure 13. (a) 44DDS, (b) TGDDM, (c) TGAP, (d) PES, and (e) PEI.

Sample Preparation

Thermoplastic Modified Epoxy Prepolymer Batch Reaction

Epoxy prepolymers were formulated at 1:1 stoichiometric equivalents of epoxide to active amine hydrogen for all reactions throughout this dissertation. Thermoplastic modified epoxy prepolymers were generally prepared in batch reactors in two steps. First, thermoplastics were dissolved into epoxides at 120 °C to 150 °C over a relatively long period of time until fully dissolved. Once dissolved, temperature was adjusted for amine dissolution and prepolymer was advanced to prescribed molecular weights and viscosities. Herein, we reported 120 °C for dissolution of PES and 44DDS to simplify our analysis.

Epoxy prepolymer batch reactions were used to set benchmarks. In a typical prepolymer batch reaction, 100.0 g of TGDDM and 8.4 g of PES were charged into a 250 mL two neck round-bottom flask equipped with mechanical stirring. The reactor was immersed into a 120 °C pre-heated oil bath and stirred until visible dissolution (~30 min) when 58.8 g of 44DDS was charged, mixed, dissolved and reacted to a chain-extended

prepolymer with a target Brookfield viscosity of approximately 20 Pa·s at 80 °C. The prepolymers were removed from the oil bath and placed into a freezer.

Thermoplastic Modified Epoxy Prepolymer Continuous Reaction

Laboratory-scale continuous reaction was accomplished using a Thermo Prism 16mm co-rotating intermeshing twin-screw extruder (L/D = 25). The reactor consists of a feed zone, five electrical heated and liquid cooled zones, and an electrically heated die zone. The screw configuration shown in Figure 14 was designed to balance shear mixing and residence time with a combination of various conveying, kneading and reverse elements. The reaction screws were optimized using three sections of kneading blocks to provide adequate shear mixing. Reverse elements were incorporated in Zone 3 to optimize the residence time, generate back-pressure and promote the chain-extension reactions.

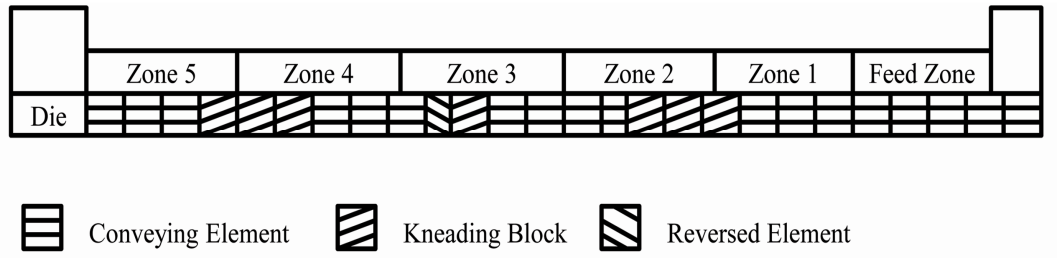

Figure 14. Screw configuration of the continuous reactor based on Prism 16 mm TSE.

In a typical thermoplastic modified epoxy prepolymer continuous reaction, approximately 1 L of TGDDM was charged into a 2 L glass vessel reactor fitted with a heating mantle and rubber stopper which contained the pump inlet tube immersed into the epoxide liquid. Epoxide was pre-heated to 80 °C and delivered into the continuous reactor through a liquid feeding port using a peristaltic pump calibrated to convey

TGDDM at a rate of 22.5 g/min. 500 g of 44DDS and 72 g of PES were dry blended and charged into a volumetric solids feeder calibrated to deliver a rate of 15.1 g/min providing 13.2 g/min of 44DDS and 1.9 g/min of PES. Continuous reactions were conducted at 120 °C, 140 °C, 160 °C, 180 °C and 200 °C (constant across all zones) and a constant screw speed for all reactions of 300 rpm. Prepolymers were collected and placed into a freezer to prevent further cure reaction. Compositions of prepolymer batch and continuous reactions in this work are summarized in Table 1.

Table 1

Compositions of Prepolymer Batch and Continuous Reactions (Discussed in Chapter III)

Samples	TGDDM	44DDS	PES	TGDDM/44DDS/PES (wt %)
Batch Reaction	100 g	58.8 g	8.4 g	60/35/5
Continuous Reaction	22.5 g/min	13.2 g/min	1.9 g/min	60/35/5

Thermoplastic Modified Multifunctional Epoxy Prepolymer Blends

Thermoplastic modified multifunctional epoxy blends with different epoxy compositions were prepared using the continuous reaction method mentioned above. Mixtures of TGDDM and TGAP were pre-heated to 80 °C in a 2 L glass vessel reactor fitted with a heating mantle and delivered into the continuous reactor through a liquid feed port using a peristaltic pump at a rate of 20.0 g/min. 44DDS and PES were dry blended and charged into a volumetric solid feeders calibrated to deliver at 1:1 stoichiometric equivalents of epoxy to amine hydrogen with 15 wt% PES content of total polymer weight. Continuous reactions described in this section were conducted at 180 °C across all reactor zones at a constant screw speed of 300 rpm. Table 2 describes the

nomenclature employed within this chapter for thermoplastic modified multifunctional epoxy systems.

Table 2

PES Modified TGDDM/TGAP/44DDS Blends Nomenclatures and Compositions (discussed in Chapter IV)

Sample	Epoxide blend (*w/w*)	Epoxide feeding rate (g/min)	Amine feeding rate (g/min)	PES feeding rate (g/min)
100TM/0TP	100% TGDDM	20	11.75	5.60
75TM/25TP	75%TGDDM/25%TGAP	20	12.17	5.68
50TM/50TP	50%TGDDM/50%TGAP	20	12.58	5.75
25TM/75TP	25%TGDDM/75%TGAP	20	13.01	5.82
0TM/100TP	100% TGAP	20	13.43	5.90

MWCNT Reinforced Epoxy Prepolymer Blends

MWCNT reinforced epoxy prepolymers continuous reaction were scaled up using Coperion ZSK 26 MC Compounder (L/D = 40). The reactor was modular and specific designed for advancing epoxy-amine chemistry and dispersing MWCNT in epoxy prepolymer matrix. Its screw profile, as shown in Figure 15, consists of a liquid feed zone (Zone 1), a solid feed zone connected with a side screw feeder (Zone 2), eight electrical heated and liquid cooled zones (Zone 3-10), and a melt pumping zone. Screw configuration was designed to balance shear mixing and residence time with a combination of various conveying, kneading, gear and reverse elements. The reaction screws were optimized using two sections of kneading blocks to provide adequate shear

mixing. Gear and reverse elements were incorporated in Zone 8 to optimize the residence time, generate back-pressure and enhance MWCNT dispersion.

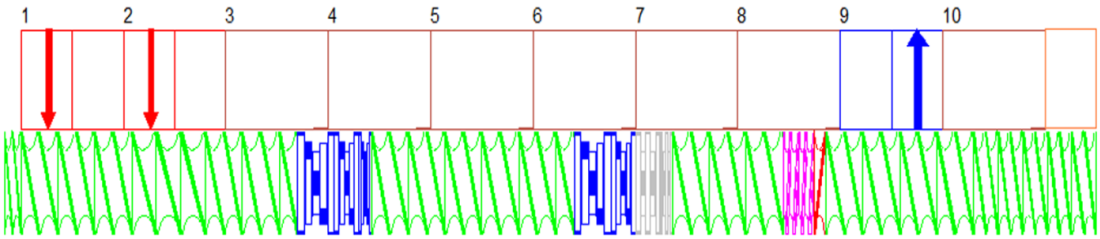

Figure 15. Screw configuration of the continuous reactor based on ZSK 26 Mega Compounder.

Reaction temperatures through the processing barrel profiles were designed for two purposes. The pre-curing zones (Zone 2 to 6) were kept at the same temperature of 180 °C which is an ideal temperature for solubilizing 44DDS in TGDDM and advancing molecular weight and viscosity as addressed in Chapter III. The dispersing zones (Zone 7~10) were maintained at low temperatures ranged from 40 to 100 °C for MWCNT dispersion. Besides different temperature profiles, various screw speeds were chosen under constant processing temperature profile to study its effects on MWCNT dispersion. Table 3 describes the nomenclature and process conditions of MWCNT reinforced TGDDM prepolymers employed within this dissertation. Additionally, a series of TGDDM/44DDS prepolymers with different MWCNT loading levels between 0 wt% and 10 wt% were produced under the evaluated best processing conditions (180 °C, 60 °C, and 600 rpm).

For a typical continuous reaction, TGDDM were pre-heated to 80 °C in a 50 L vessel reactor fitted with a heating mantle and delivered into the continuous reactor through the liquid feeding port at zone 1 at a rate of 47.7 g/min under pressure. 44DDS

was charged into a gravimetric solid feeder to deliver at a rate of 28.0 g/min which will give 1:1 stoichiometric equivalents of epoxy to amine hydrogen. MWCNT was fed by using a laboratory vibratory feeder with a constant feeding rate as low as 0.5 g/min. Both 44DDS and MWCNT were added through a side feeder at Zone 2. Samples were collected after melting pump and placed into a freezer.

Table 3

TGDDM/MWCNT Prepolymer Nomenclatures and Processing Conditions (discussed in Chapter V)

Sample name	CNT (wt%)	Pre-curing temperature (°C)	Dispersing temperature (°C)	Screw speed (rpm)	Throughput (kg/h)
Epoxy/MWCNT prepolymers with different temperatures					
EMT01	1.0	180	40	400	4.5
EMT02	1.0	180	60	400	4.5
EMT03	1.0	180	80	400	4.5
EMT04	1.0	180	100	400	4.5
Epoxy/MWCNT prepolymers with different screw speeds					
EMS01	1.0	180	80	200	4.5
EMS02	1.0	180	80	400	4.5
EMS03	1.0	180	80	600	4.5
EMS04	1.0	180	80	800	4.5

MWCNT Reinforced Epoxy Prepolymer/PEI Blends

MWCNT reinforced epoxy/PEI blends were prepared using the continuous reactor designed based on Prism 16 mm TSE method mentioned in Chapter III. Epoxies were pre-heated to 80 °C and delivered into the continuous reactor through a liquid

feeding port using a peristaltic pump calibrated to convey at a rate of 20.0 g/min. 44DDS, PEI, and MWCNT were dry blended and charged into a volumetric solid feeders calibrated to deliver at 1:1 stoichiometric equivalents of epoxy to amine hydrogen with different PEI and MWCNT contents. Continuous reactions described in this section were conducted at 180 °C across all five zones with a constant screw speed of 300 rpm. Prepolymer blends were collected and placed into a freezer. Compositions and nomenclatures of MWCNT reinforced TGDDM/PEI blends were listed in Table 4.

Table 4

MWCNT Reinforced Epoxy Prepolymer/PEI Blends Nomenclatures and Compositions (discussed in Chapter VI)

Samples	TGDDM (g)	TGAP (g)	44DDS (g)	PEI (g)	MWCNT (g)
3.2 PEI	30	30	40	3.2	0
6.4 PEI	30	30	40	6.4	0
9.6 PEI	30	30	40	9.6	0
12.8 PEI	30	30	40	12.8	0
0.5 MWCNT	30	30	40		0.5
1.0 MWCNT	30	30	40	6.4/9.6/12.8	1.0
1.5 MWCNT	30	30	40		1.5

Characterization

^{1}H Nuclear Magnetic Resonance (^{1}H NMR)

^{1}H NMR spectroscopy was conducted on a Bruker ascend 600 spectrometer at 600 MHz. Standard ^{1}H pulse sequences were used. All ^{1}H chemical shifts were referenced to TMS (0 ppm). Samples were prepared by dissolving in DMSO (20-50 mg/mL) and charging this solution to a 5 mm NMR tube.

Near-infrared Spectroscopy (NIR)

NIR spectra in transmission mode were recorded using a Thermo Scientific Nicolet 6700 FT-IR in the range of 4000-8000 cm^{-1}. A white light source was used in conjunction with a KBr beam splitter and a DTGS KBr detector. Samples were prepared by placing between glass slides separated by a 0.8 mm Teflon spacer. The reaction progressed according to varying curing prescriptions in a Simplex Scientific Heating Cell.

The total absorbance of the peak integral was related to concentration using the following form of the Beer-Lambert law:

$$A = \varepsilon c l \quad (\text{Eq. } 5)$$

where A is the total absorbance, ε is the molar absorptivity of the functional group in mol/(kg·cm), c is the concentration of the functional group in kg/mol, and l is the path length (sample thickness) in cm. Prior to analysis, spectra were normalized using the aromatic region at 4600-4640 cm^{-1}. In an effort to normalize conversion measurements, all calculations assumed zero conversion at the start of each test. Secondary amine absorptivity was calculated from the absorbance at 6550-6760 cm^{-1} with the assumption that no 2° amine converted to 3° amine at the onset of the reaction.

Differential Scanning Calorimetry (DSC)

DSC was performed on a TA Instruments DSC Q200 to study cure kinetics. Total heat of cure reaction (ΔH_T) was established from batch reaction prepolymer aliquots removed 5min after 44DDS dissolution and measured at a ramp rate of 5 °C/min from 25 to 300 °C. Isothermal DSC measurements were used to calculate the extent of cure (x) for prepolymers as $x = \Delta H_t/\Delta H_T$, where ΔH_t is heat of enthalpy at reaction time (t).

DSC was used to determine glass transition temperature (T_g) of epoxy prepolymers. Heating rate was 5 °C/min in the temperature range of -50 °C to 100 °C under nitrogen. The midpoints of the slopes from heat capacity plots are reported as T_g for the prepolymers.

Brookfield Viscometry

A Brookfield CAP 2000+ Viscometer was used to measure epoxy prepolymer viscosities at a frequency of 1 Hz at 80 °C.

Dynamic Rheological Analysis

Rheological analysis was conducted on ATS Rheosystems rheometer with disposable 25 mm parallel plates to measure the complex viscosity change as a function of time during isothermal cure. The experiments were performed at a strain of 5 % and a frequency of 1 Hz. The rheological gel point was taken as the point at which storage modulus (*G'*) equaled the loss modulus (*G"*).

Residence Time Distribution

Residence time distribution of continuous reaction was determined by doping the solids feed with 0.5 g of montmorillonite as a dielectric tracer. An in-line Netzsch 230/1 dielectric analyzer fitted with two planar inter-digitized comb electrode sensors was used to measure the real-time changes in ion viscosity of the mixtures at a frequency of 1 kHz.[13] The tracer concentration at time *t* (C_t) was acquired according to a calibration curve generated by measuring the ion viscosity changes with known tracer concentration in TGDDM (Figure 16). The residence time distribution (E_t) and the number average residence time ($\overline{t_m}$) were calculated using Eq.6 and Eq.7, respectively.

$$E_t = \frac{C_t}{\sum_0^\infty C_t \cdot \Delta t} \quad \text{(Eq. 6)}$$

$$\overline{t_m} = \sum_{0}^{\infty} t \cdot E(t) \cdot \Delta t \quad \text{(Eq. 7)}$$

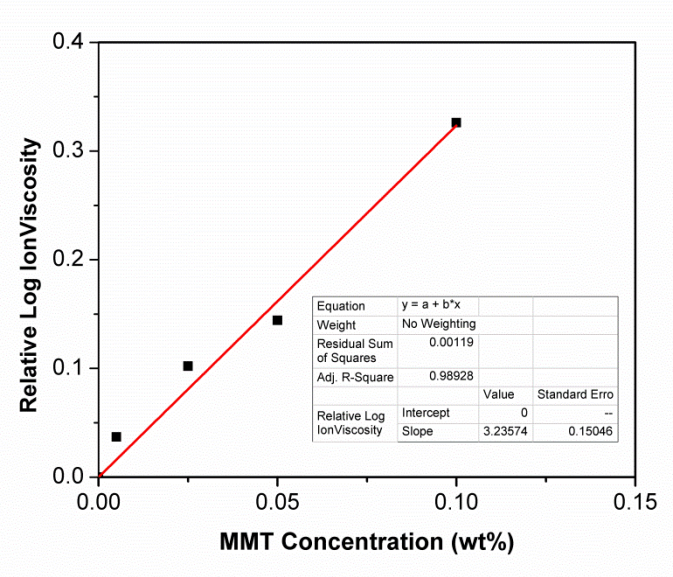

Figure 16. Calibration curve for ion viscosity as a function of tracer concentration.

Optical Microscopy

Olympus GX51 metallurgical microscope with a reflection light source was used to examine the dissolution states of PES and dispersion states of MWCNT in epoxy prepolymer matrices and during cure cycles. Samples were prepared by pressing materials between two pieces of cover glass with a Teflon film, as a spacer, to form specimens with a thickness about 0.2 mm. The dissolution states of PES in epoxy matrices were quantified in terms of Percentages of undissolved PES area (*P*) in the observed area using Olympus Stream Image Analysis software. In this dissertation PES was considered to be fully dissolved when < 1 % PES in TGDDM was observed at 20X magnifications.

The dispersion states of MWCNT in epoxy matrices were also quantified by Olympus Stream Image Analysis software by neglecting those agglomerates with

diameters smaller than 1μm. Dispersion index (*D*) which reflects the normalized agglomeration area was calculated using Eq.8:[70]

$$D = \left(1 - f\frac{A_{CNT}/A_0}{\emptyset_{vol}}\right) \times 100\% \ \text{(Eq. 8)}$$

The area occupied by MWCNT agglomerates A_{CNT} and the total investigated area A_0 were obtained from image analysis. The parameter $\emptyset_{vol}$ is the CNT volume fraction and *f* is a factor related to the density of CNT agglomerates and was estimated to be 0.25. According to Eq.8, a *D* value of 100% corresponds to a perfect macro dispersion of MWCNT containing no agglomerates with sizes above 1 μm. A decreasing dispersion state is reflected in a decreasing *D* value.

Scanning Electron Microscopy (SEM)

FEI Quanta 200 SEM was employed to examine fracture surface morphologies of samples. Samples were fully cured according to a two-step cure prescription (5 h at 125 °C, 1 h at 200 °C) unless otherwise specified and fractured in liquid nitrogen and sputter-coated with silver prior to observation. Images were collected in high vacuum mode with an accelerating voltage of 20 kV.

Atomic Forced Microscopy (AFM)

Phase morphologies of cured samples were observed using a Bruker Dimension ICON Scanning Probe AFM. Plane surfaces were prepared by cutting with microtome. Nanomechanical mapping images were acquired with a silicon probe from Bruker (RTESP) with a nominal spring constant of 20-80 N/m. The calibration process followed the absolute method and checked through the relative method. Evaluation of the Derajaguin-Mueller-Toporov (DMT) modulus was carried out using the Nanoscope Analysis 1.40 software. All the processes were performed in the peakforce QNM air

mode in Nanoscope 8 software. After calibration of the AFM tip, the DMT modulus provides the elastic modulus of the surface from the contact lines of force-displacement curves.[71]

Dynamic Mechanical Analysis (DMA)

Dynamic mechanical properties were measured using a Thermal Analysis Q800 DMA. Specimens were cast into silicone molds with dimensions of 1 mm x 5 mm x 15 mm and then cured at 125 °C for 5 h and post cured at 200 °C for 2 h unless otherwise specified. Tests were conducted in tensile mode with strain amplitude of 0.05 % and frequency of 1 Hz. Temperature was ramped from 50 °C to 300 °C at a rate of 5 °C/min.

Tensile and Fracture Toughness

Tensile tests followed ASTM Standard D638-10. Type IV dog bone shaped tensile bars were prepared by casting prepolymers into a silicone mold and cured at 125 °C for 5 h and post cured at 200 °C for 2 h unless otherwise specified. The tensile bars were strained at a displacement controlled test rate of 1.27 mm/min on an MTS Insight electromechanical universal test frame equipped with mechanical wedge grips. Displacement was measured by linear variable differential transformer, and load was measured using a MTS 10 kN load cell.

Fracture toughness was determined from the critical value of stress intensity factor (K_{1C}), which was measured by the single notched three-point bending method according to ASTM D5045-99. Dimensions of specimens (L x W x B) were 75 mm x 15 mm x 6 mm. A sharp pre-crack was formed by carefully sliding a fresh razor blade in a sawing motion across a notch that was machined according to the Standard. Specimens were loaded at a constant cross-head speed of 10 mm/min. K_{IC} was calculated using Eq.9:

$$K_{IC} = \frac{PY}{BW^{1/2}} \quad (\text{Eq. } 9)$$

where *P* is the maximum load obtained from the fracture load- deflection curve, and *Y* Parameter calculated from the length of the crack using Eq.10:

$$Y = f(R) = \frac{(2+R)(-0.886 + 4.64R - 13.32R^2 + 14.72R^3 - 5.6R^4)}{(1-R)^{3/2}} \quad (\text{Eq. } 10)$$

where *R=a/W* and *a* is the crack length. The average values from five measurements are reported.

Electrical Conductivity Test

The *in-plane* conductivity of the samples was measured at 25 °C and relative humidity (RH) of 60 % using a BekkTech (BT-512) four-point probe conductivity test system. Sample dimensions were 4.2 mm in length and of 5.4 mm in width with thickness of 1 mm.

CHAPTER III

DEVELOPMENT OF CONTINUOUS REACTOR FOR THERMOPLASTIC MODIFIED EPOXY-AMINE PREPOLYMERS

Abstract

This chapter described a new continuous reactor method to prepare thermoplastic modified epoxy prepolymers for aerospace prepregs with the aim of replacing traditional batch reactors. Compared to batch reactors, the continuous reactor is capable of producing epoxy prepolymers through simultaneous dissolution of polyethersulfone (PES) and 4, 4' - diaminodiphenylsulfone (44DDS) in tetraglycidyl - 4, 4' - diaminodiphenylmethane (TGDDM). In addition, concurrent chain extension reactions advance prepolymer molecular weights to desired viscosities in less than 2 minutes of mean residence time. Optical micrographs were used to define how process temperature influences PES dissolution in TGDDM in a continuous reactor. Kinetic studies confirmed the chain extension reaction in a continuous reactor is similar to the batch reactor, and the molecular weights and viscosities of prepolymers were readily controlled through reaction kinetics. Atomic force microscopy was used to confirm similar cured network morphologies for formulations prepared from batch and continuous reactors. Additionally tensile strength, tensile modulus and fracture toughness analyses concluded mechanical properties of cured epoxy matrices produced from both reactors were equivalent.

Results and Discussion

The preparation of TGDDM/44DDS/PES prepolymers and cured networks creates a complex physical and chemical environment including dissolution of PES and 44DDS in TGDDM, chain extension reactions or cure reactions of TGDDM/44DDS/PES, and ultimately the reaction induced phase separation of PES in TGDDM/44DDS matrix

during cure. This chapter provided a direct comparison of these processes for batch and continuous reactors to determine the utility of continuous reactors for preparing aerospace prepreg epoxy prepolymers.

PES Modified Epoxy Prepolymer Batch Reaction

Thermoplastic modified epoxy-amine prepolymers are prepared in batch reactors in two steps. First, thermoplastics are dissolved into epoxides at 120 °C to 150 °C over a relatively long period of time until fully dissolved. Once dissolved, temperatures are adjusted for amine dissolution and prepolymer is advanced to prescribed viscosities and molecular weights. Herein, we report 120 °C for dissolution of PES and 44DDS to simplify our analysis. Figure 17 shows optical micrographs for PES dissolved in TGDDM at 120 °C for 10 min, 30 min, 50 min, and 70 min from a batch reactor. Percentages of undissolved PES area (P) quantified by image software were used to depict the progression of PES dissolution under these conditions. In this example, undissolved percentage of PES was 22.2 % after 10 min and 0.27 % after 70 min demonstrating how PES dissolves in TGDDM over-time at 120 °C. It was considered that PES is fully dissolved in TGDDM after 70 min in the batch reactor at 120 °C.

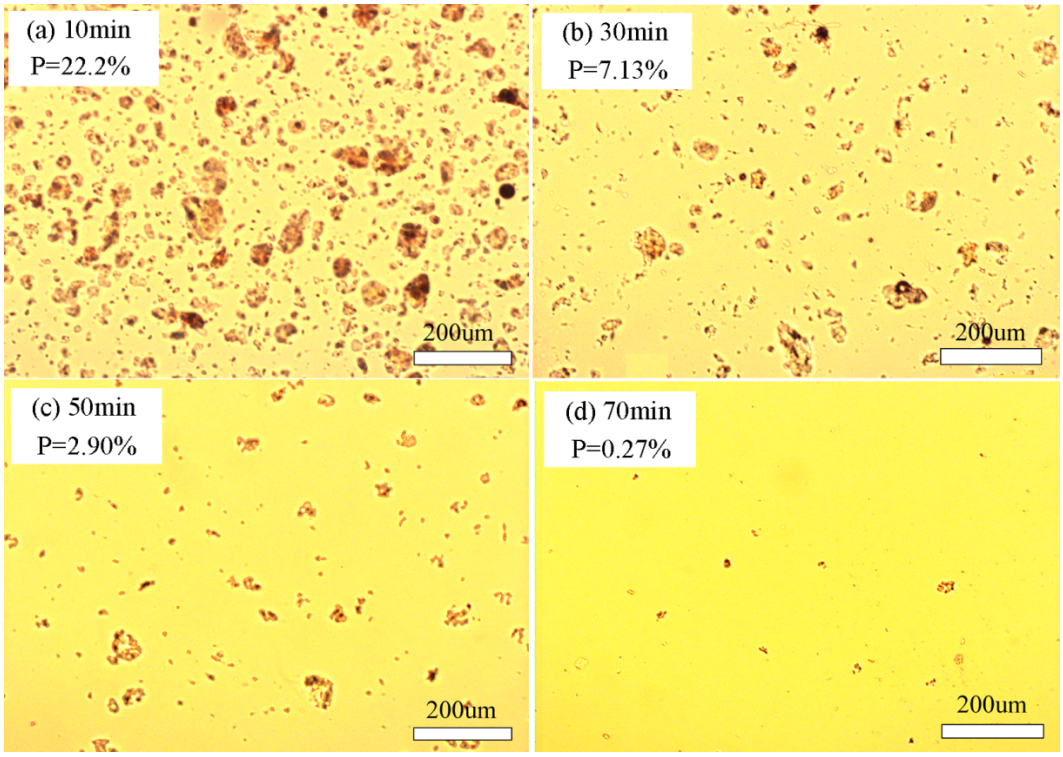

Figure 17. Optical images recorded on batch reactor dissolution states at 120 °C.

Upon PES dissolution in the batch reactor 44DDS was added to the TGDDM/PES mixture and chain extension reactions were started until prescribed molecular weights and viscosities achieved. Reaction kinetics was measured using DSC through a series of isothermal experiments to quantify cure conversions. Figure 18 describes conversion vs. time of TGDDM/44DDS/PES reactions at various temperatures which displaying two distinct regions. The first region in the early stages was kinetically controlled characterized by a rapid rate of reaction. The second region was diffusion controlled described by a slower rate of reaction as the matrix vitrified. To model the progress of cure reaction, diffusion was considered and we employed an autocatalytic expression proposed by Chen and Macosko[72] (Eq. 11 and 12) to describe our reaction behaviors.

$$\frac{d\alpha}{dt} = (k_1 + k_2\alpha^m)(1-\alpha)^{n_1}; \quad \alpha < \alpha_d \text{ (Eq. 11)}$$

$$\frac{d\alpha}{dt} = k_3(\alpha_p - \alpha)^{n_2}; \quad \alpha > \alpha_d \text{ (Eq. 12)}$$

where k_1, k_2, and k_3 are the kinetic rate constants, m, n_1 and n_2 are the kinetic exponents of the cure reactions, α_p is the maximum degree of conversion, and α_d is the maximum of the derivative of the curve from the cure reaction rate as function of conversion describing the onset of the diffusion controlled reaction.

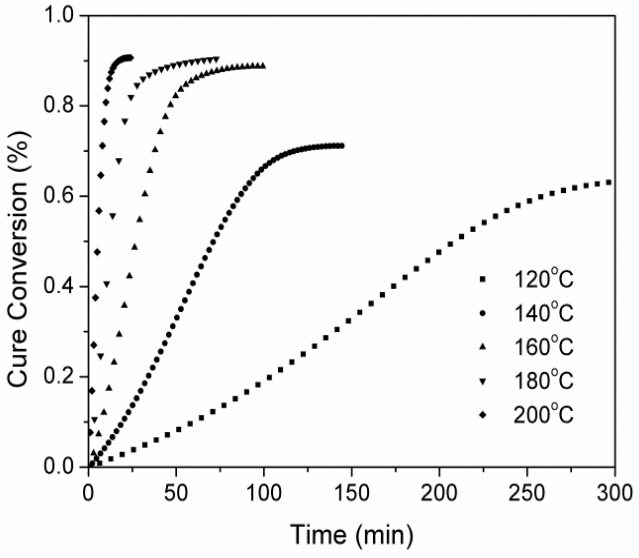

Figure 18. Cure conversions vs. reaction time at different curing temperatures.

The cure model parameters were obtained simultaneously by applying a multiply regression method to calculate the data and provided in Table 5. The overall TGDDM/44DDS/PES reaction order for kinetic controlled reaction, $m+n_1$, was approximately 2.5, while the reaction order for diffusion controlled reaction was approximately 1.0. The rate constants k_1, k_2, and k_3 increased with temperature and k_2 was greater than k_1. The rate constants were temperature dependent and we calculated

Arrhenius relationships between lnk_1, lnk_2, lnk_3, vs. $1/T$ described in Figure 19. The activation energies for E_{a1}, E_{a2}, and E_{a3} were calculated as 74.0 kJ/mol, 63.2 kJ/mol, and 55.0 kJ/mol, respectively. These results agree well with those reported for similar epoxy systems.[73]

Table 5

Kinetic and Diffusion Control Parameters for TGDDM/44DDS/PES Batch Reaction

Temperature (°C)	Kinetic control parameters				Diffusion control parameters	
	m	n_1	k_1	k_2	n_2	k_3
120	1.18	1.51	0.00138	0.0150	0.76	0.0114
140	1.02	1.43	0.00418	0.0324	0.68	0.0244
160	0.96	1.41	0.00995	0.0829	0.91	0.0600
180	1.05	1.45	0.0251	0.186	0.91	0.0900
200	1.01	1.53	0.0653	0.359	1.09	0.211

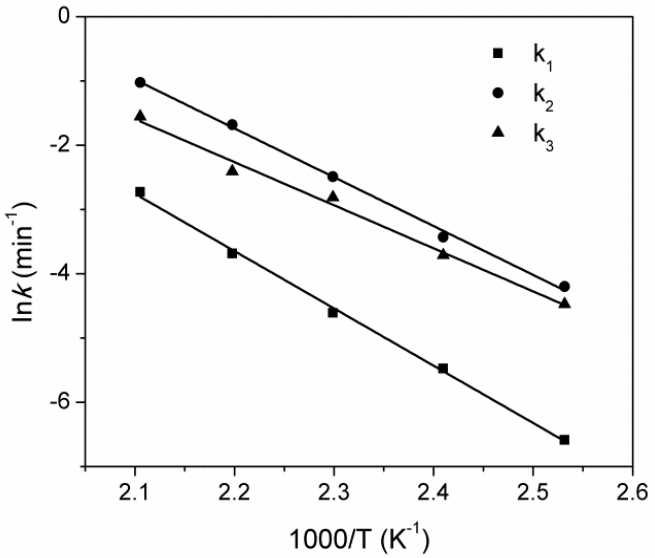

Figure 19. Arrhenius plot of the rate constants for the cure reaction.

Integration of Eq.11 and Eq.12 provides a description of cure conversion as a function of cure time. Figure 20 shows how the experimental values agreed with the model for the batch reaction at 120 °C. The experimental data fit well showing good accuracy of applying the autocatalytic model for TGDDM/44DDS/PES cure reactions in a batch reactor.

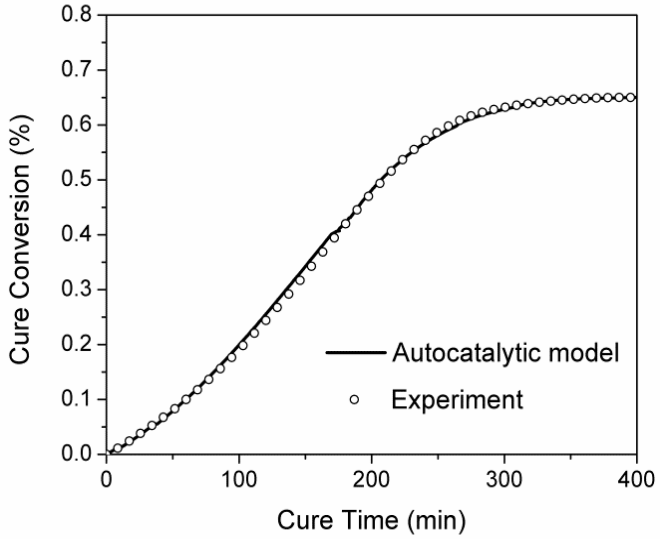

Figure 20. Calculated vs. experimental TGDDM/44DDS/PES conversion at 120 °C.

When developing epoxy prepolymers for prepreg filming, prepolymer viscosity is varied for various impregnation strategies; modeling cure kinetics provides an ability to control prepolymer viscosity with temperature and reaction time. For the purpose of demonstration, a Brookfield viscosity of 20 Pa·s at 80 °C is required for TGDDM/44DDS/PES prepolymers products based on our prepreg manufacturing experience. Figure 21 shows the cure conversion and the corresponding viscosity of TGDDM/44DDS/PES prepolymers as function of reaction time in batch reactor. In this prepolymer reaction example, a Brookfield viscosity of 20 Pa·s at 80 °C is observed at around 16 % of cure conversion and 87 min of reaction time. Quantification of the

relationships between temperature, conversion and viscosity derived through batch reactor experimentation will be critical for understanding epoxy prepolymer continuous reactors.

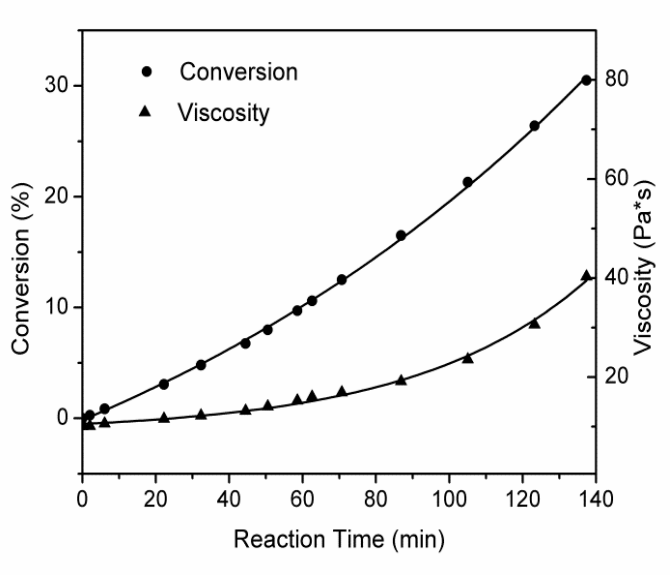

Figure 21. Conversion and 80 °C Brookfield viscosity of TGDDM/44DDS/PES prepolymers.

PES Modified Epoxy Prepolymer Continuous Reaction

The prior discussion is provided to review conventional batch reactor epoxy prepolymer development protocols, highlight critical control variables, and benchmark necessary prepolymer properties for utility in advanced composites prepreg preparation. While batch reactors are generally based upon relatively low-temperature reactions over long periods of time, continuous reactors are designed for higher temperature reactions over short periods of time. Residence time distribution in a continuous reactor is controlled through screw configuration, screw speed, feeding rate and reactor length, and is typically in the range of 1 to 5 min. Since residence time is low, reaction quantities are small and heat transfer efficiencies are high, continuous reactors offer a distinct

advantage over batch reactors for controlling dissolution and cure reactions using elevated temperature.

The residence time distribution (RTD) and mean residence time ($\overline{t_m}$) were first measured to describe the history of materials within the continuous reactor. Figure 22 shows the RTD curve at a fixed operating condition of 300 rpm screw speed and 2.25 kg/h feed rate. The mean residence time was calculated to be approximately 2 min according to Eq.6. Conducting similar experiments over a range of temperatures confirmed mean residence time and distribution to be independent of process temperature for our system.

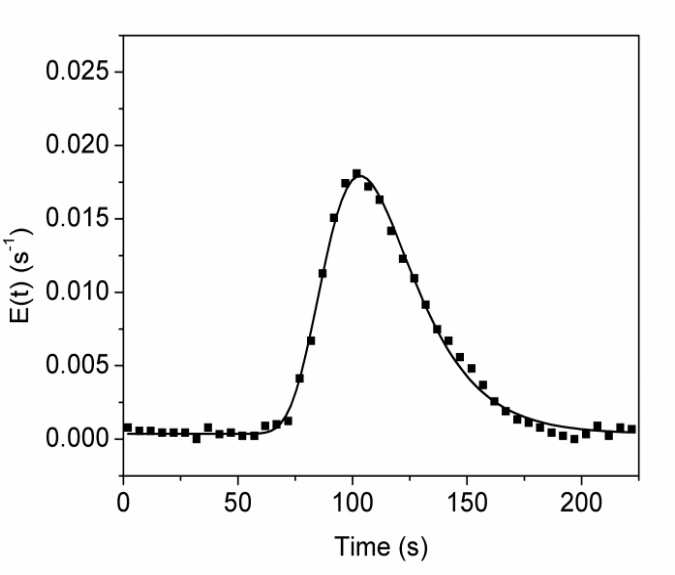

Figure 22. Continuous reactor RTD (solid line is best fit).

Figure 23 shows optical micrographs describing the effect of continuous reactor process temperature (120 °C - 180 °C) on dissolution states of PES in TGDDM. Comparison of 120 °C/2 min continuous reactor dissolution data in Figure 23a with 120 °C/10 min batch reactor data in Figure 17a depicts specific advantages of the continuous

reactor over batch reactor process. This direct comparison highlights the continuous reactor efficiency in mixing and dissolution attributed to the increased shear, improved heat-transfer and reduced volume. Furthermore, the percentage of undissolved PES area in the continuous reactor was readily reduced within the 2 min residence time through increasing reactor temperature. Figure 23d shows the PES is fully dissolved in TGDDM at 180 °C to less than 1 % PES left. When comparing this result to the 120 °C/70 min batch reactor data provided in Figure 17d a marked potential to reduce dissolution time in the continuous reactor by elevated temperature is feasible. From these comparisons, it is obvious that mixing and dissolution through increasing temperature is more efficient in the continuous reactor since similar levels of dissolution states are achieved at significantly less times.

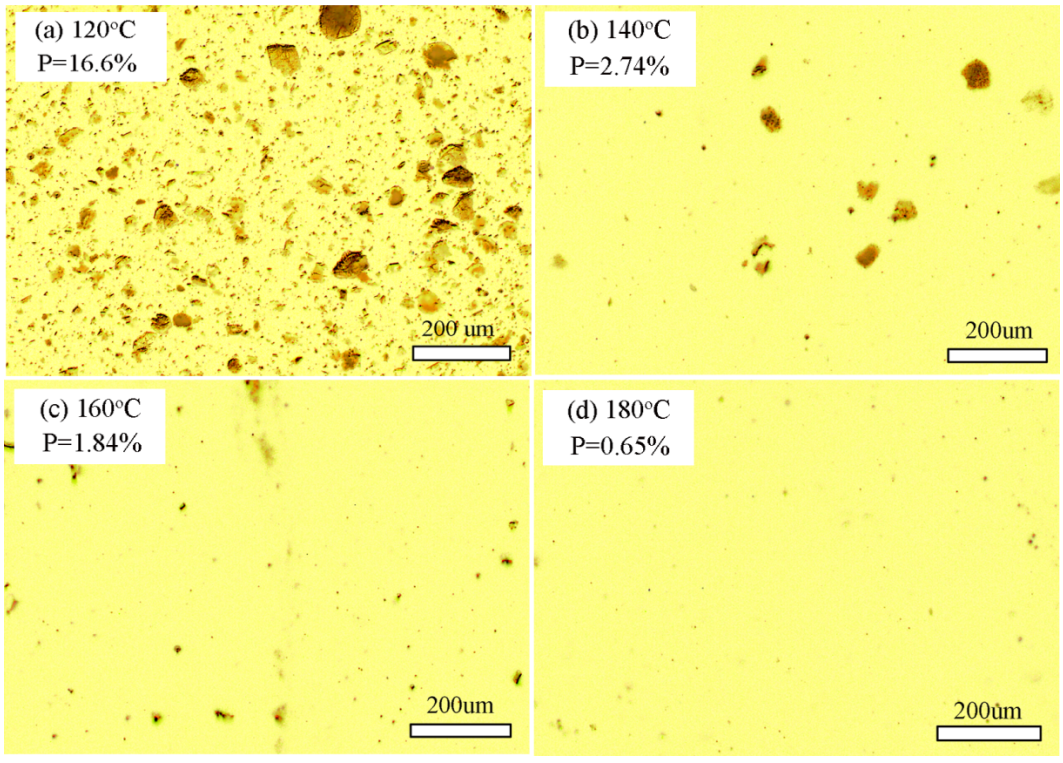

Figure 23. Optical images recorded on continuous reactor dissolution states at various temperatures.

Although temperature can be increased to reduce PES dissolution time in a batch reactor, it is impractical to control 44DDS dissolution and chain extension reaction at high temperatures and avoids gelation considering the large volume of batch reactors. Small reaction volumes and excellent heat transfer in continuous reactors provide pathways for using elevated temperatures to prepare epoxy prepolymers with reduced reaction time. But the challenge for avoiding gelation in a continuous reactor at high temperatures remains a critical problem. We have found predictive modeling of chain extension reactions is necessary for establishing continuous reactor conditions. The Total Segregation Model described by J.H. Ramirez[74] is useful for predicting reaction conversion to avoid gelation in the continuous reactor. This model shown in Eq.13 assumes that at steady state all reactants along the continuous reactor follow the residence time distribution ($E(t)$) and the mean conversion ($\overline{x_m}$) is calculated through a series of discrete conversion states.

$$\overline{x_m} = \sum_{0}^{\infty} x_{batch}(t) \cdot E(t) \cdot \Delta t \quad (\text{Eq. } 13)$$

In the Total Segregation Model, $x_{batch}(t)$ is calculated from the kinetic model described in Eq.11 through the batch reaction analyses. The mean conversion at a given temperature for the continuous reactor was calculated using Eq.11 and Eq.13 and the results are presented in Table 6. It can be seen that the reaction is maintained at a relatively low conversion below 160 °C within our reactor setup. As the temperature is increased to 180°C, conversion increases exponentially with temperature. The predicted conversion is 42.3 % at 220 °C which approaches gelation. For this reason, 200 °C was thus used as the maximum processing temperature for the continuous reaction.

Reaction conversions, viscosities and T_gs of TGDDM/44DDS/PES prepolymers prepared by the continuous reactor at various process temperatures are provided in Table 6. Conversion, viscosity and T_g of TGDDM/44DDS/PES prepolymers increased with increasing process temperatures. 80 °C Brookfield viscosity was 20.3 Pa·s for the 180 °C continuous reaction sample which is excellent for preparing film and impregnating fiber during prepreg processing. Figure 24 compares the experimental conversion data of prepolymer continuous reactions measured by DSC with that calculated from the Total Segregation Model confirming the model fits well. This comparison confirms the nature of TGDDM/44DDS/PES prepolymer follows kinetic control in the continuous reactor leading to predictable levels of conversion which is significant for controlling chain-extension reactions and prepolymer viscosities in continuous reactors.

Table 6

Predicted and Experimental Results for TGDDM/44DDS/PES Prepolymer Continuous Reaction

Temperature (°C)	Predicted Conversion (%)	Experimental Conversion (%)	Experimental Viscosity (Pa·s)	Experimental T_g (°C)
120	0.3	0.35	10.5	6.5
140	1.2	2.1	12.9	8.2
160	2.5	3.9	16.3	9.6
180	6.9	7.8	20.3	12.1
200	18.8	14.4	28.0	16.0
220	42.3	N/A	N/A	N/A

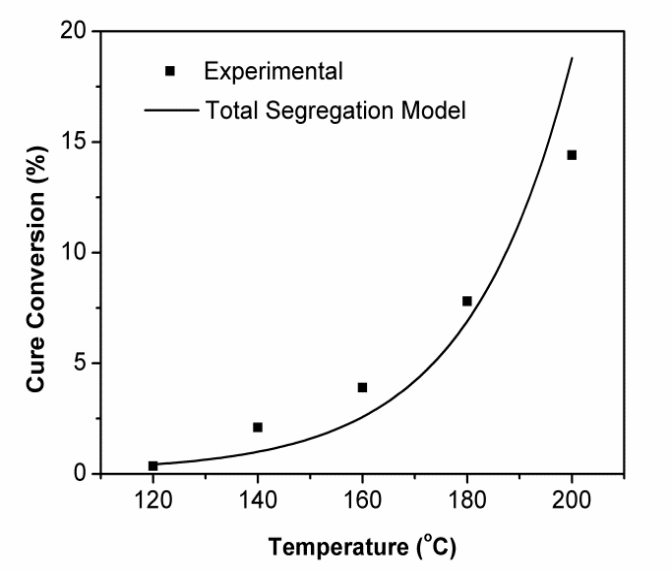

Figure 24. Comparison of simulation vs. experimental cure conversion in continuous reactor.

Influence of Screw Speed and Throughput

In order to gain a better understanding of continuous reaction process and quality control, it is necessary to systematically explore the effects of processing variables on epoxy prepolymers properties. Therefore, samples were prepared with different screw speeds and throughputs, two key process parameters of continuous reactors, at constant process temperature of 160 °C and their cure conversions and viscosities are summarized in Table 7.

As shown in Table 7, epoxy prepolymer viscosities were decreased from 18.4 Pa·s to 14.9 Pa·s as screw speed increased from 200 rpm to 400 rpm. Meanwhile, cure conversions and T_g s of TGDDM/44DDS/PES prepolymers also decreased with the increased screw speeds. Optical micrographs in Figure 25 revealed that 200 rpm prepolymer had a higher percentage of undissolved particles (4.32 %) than 400 rpm prepolymer (1.15 %), suggesting high screw speeds accelerate the dissolution rate. The

influence of screw speeds on prepolymers viscosities and dissolution states can be explained in terms of residence times and shear strengths.[75] On one hand, materials are transported faster towards the die as the screw speed increased, leading to a shorter residence time for cure reactions in continuous reactors. Figure 26 confirms the changes of residence time distributions with respect to screw speeds. It can be seen that the curves shifted toward shorter residence times with a value of 112.6 s, 100.7 s, and 93.6 s for 200, 300, and 400 rpm, respectively. Therefore cure conversions, viscosities, and T_g s of TGDDM/44DDS/PES prepolymers also decreased. On the other hand, increased screw speeds can generate higher shear force applied on the particles during mixing. The total particles surface area exposed to the epoxy matrix were increased and resulted in an improved dissolution state. Although increasing screw speeds tends to reduce the dissolution time during continuous reaction, the shear strengths are more profound for PES and 44DDS dissolution in current process conditions.

Table 7

Process Conditions and Properties of TGDDM/44DDS/PES Prepolymers

Screw Speed (rpm)	Throughput (kg/h)	Conversion (%)	Viscosity (Pa·s)	T_g (°C)
200	2.25	4.5	18.4	11.3
300	2.25	3.9	16.3	9.6
400	2.25	3.1	14.9	8.6
300	1.13	7.7	26.3	14.1
300	3.40	2.6	11.6	7.4

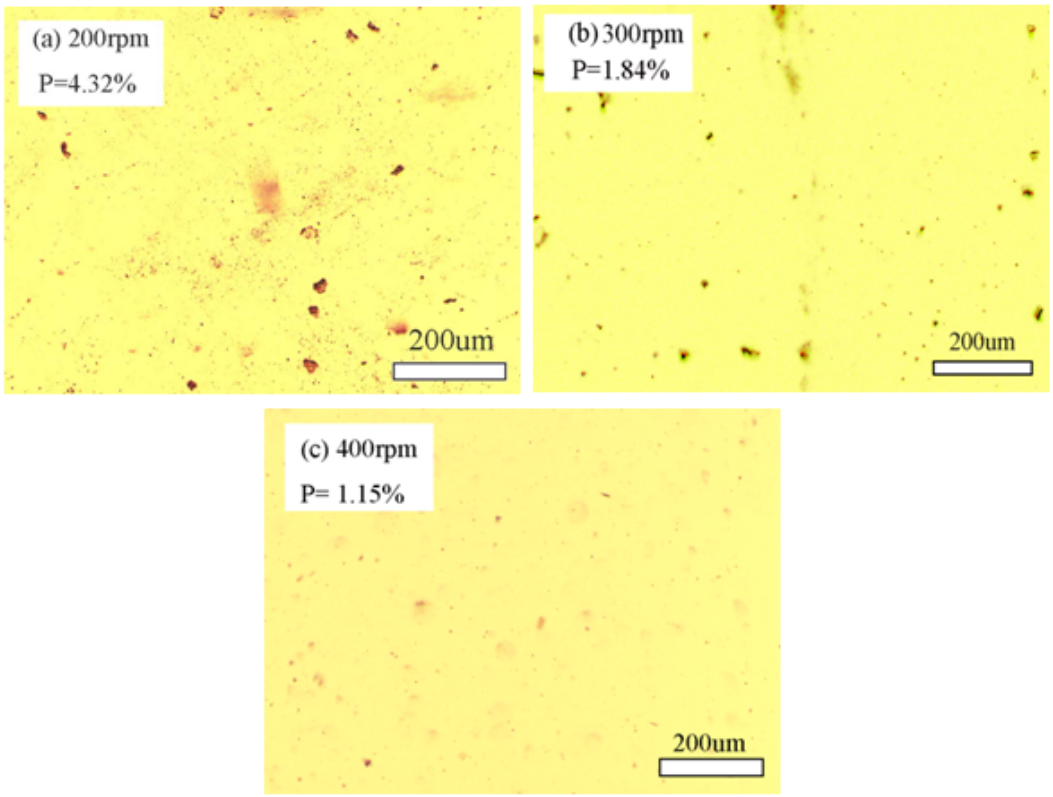

Figure 25. Optical images recorded on continuous reactor dissolution states at various screw speeds.

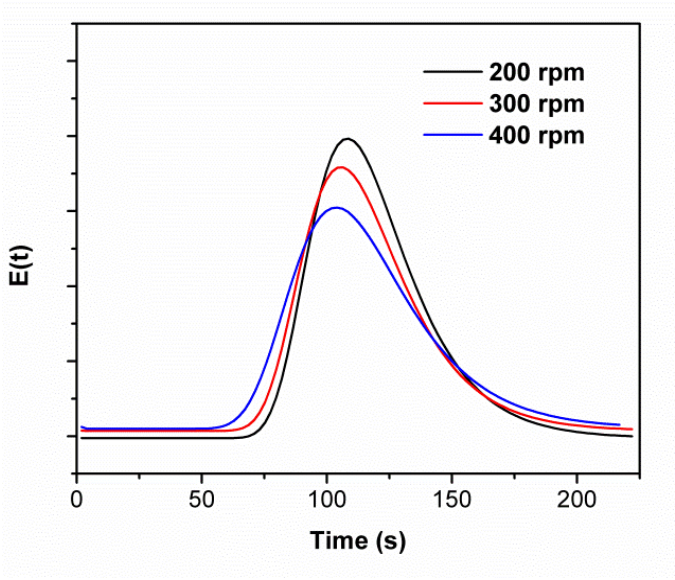

Figure 26. Changes of RTD at different screw speeds of continuous reactor.

Throughputs also exhibited remarkable effects on TGDDM/44DDS/PES prepolymers properties during continuous reaction. As shown in Table 7, prepolymer viscosities increased from 11.6 Pa·s to 26.3 Pa·s and cure conversions increased from 2.6 % to 7.7 % when throughputs decreased from 3.40 kg/h to 1.13 kg/h, respectively. These changes are attributed to the change of residence time distribution showing in Figure 27. The residence time distribution curves shifted to shorter time as the throughput increased. The calculated mean residence times were 160.4 s, 100.7 s, and 75.2 s for the throughput of 1.13 kg/h, 2.25 kg/h, and 3.40 kg/h, respectively. As a consequence, the reduced residence time gave less time for advancing epoxy-amine molecular weight and viscosity during continuous reaction. Furthermore, optical micrographs of TGDDM/44DDS/PES prepolymer samples prepared at different throughputs in Figure 28 indicated that the dissolution states were slightly improved by reducing throughput owing to the longer residence time of mixing. However, the improvement is neglected compared with the influence of screw speeds since shear forces were nearly constant with respect to the throughput.

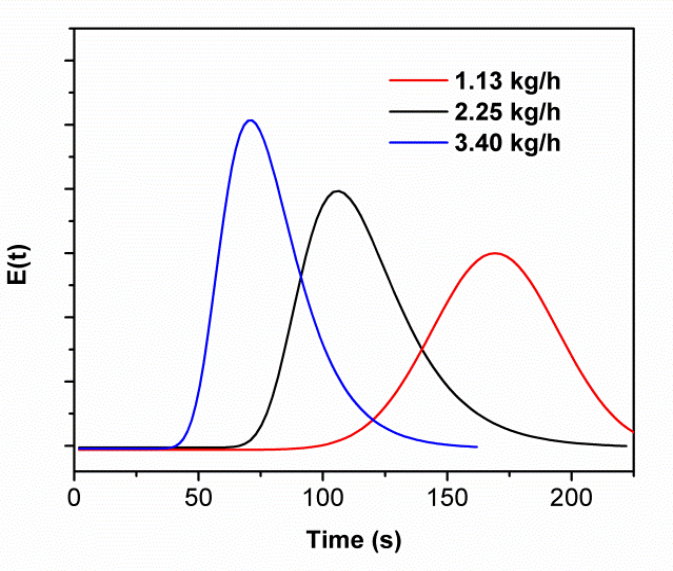

Figure 27. Changes of RTD at various throughputs of continuous reactor.

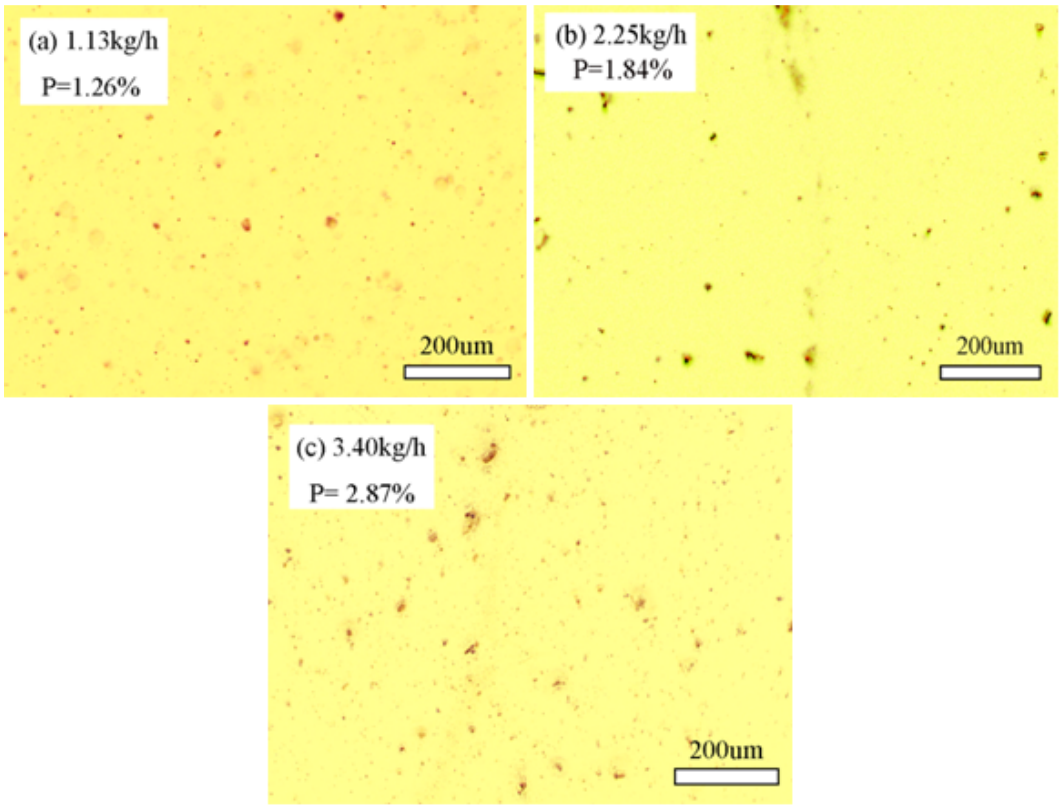

Figure 28. Optical images recorded on continuous reactor dissolution states at various throughputs.

Phase Separated Morphology

Further validation for comparison of continuous reaction prepolymers with batch reaction prepolymers was assessed with cured epoxy morphologies. In particular, the reaction induced phase separation behavior of PES within the epoxy networks upon cure was studied. TGDDM/44DDS/PES prepolymers prepared by batch reaction and 180 °C continuous reaction were fully cured and their phase morphologies were quantified by AFM using nanomechanical mapping (Figure 29). Both polymers displayed similar domain behaviors in the size-scale range of tens of nanometers of PES phase-separated within the cured network morphologies. The dark domains observed in the DMT modulus image Figure 29 (a) and (b) correspond to the lower modulus PES phases for the batch and continuous reactor polymers, respectively. The brighter features in each image are associated with the higher modulus epoxy phases. Both cured polymers are similar in phase separated morphology and typical for what we expect to observe for these polymers. Utilization of imaging software provides an ability to analyze the distribution of size domains and provide a quantitative comparison between samples. A threshold of image color was defined to distinguish between the dark and bright phases shown in Figure 29 (c) and (d) for the batch and continuous reactor polymers, respectively. Again, the general patterns that we observed using this technique suggest similarities in the size and distribution behavior of PES phase separated within the cured TGDDM/44DDS epoxy networks prepared by batch and continuous reaction.

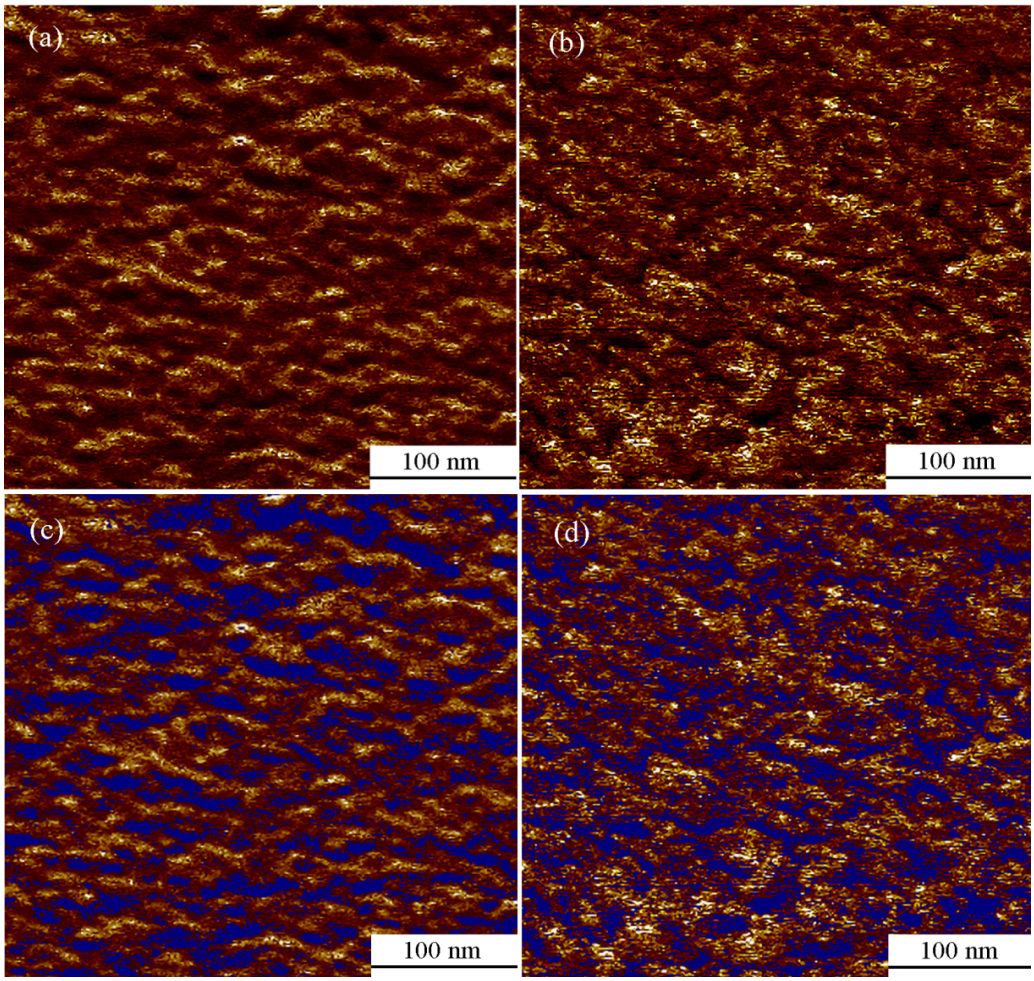

Figure 29. Peak-Force Tapping images of cured TGDDM/44DDS/PES systems: (a) batch reaction (b) continuous reaction (c) batch imaging (d) continuous imaging.

The calculated histograms of PES domains were shown in Figure 30(a) and (b). Similarities were observed for the average PES domain size diameters calculated at 6.85 nm and 6.12 nm for cured samples prepared by batch and continuous reaction, respectively. Although the average domain size for the continuous reactor material is slightly smaller as evidenced by the calculated average diameter and histogram count observed in Figure 30, these domain size variances are well-within expected ranges for the example TGDDM/44DDS/PES formulations. We conclude the cured morphologies of TGDDM/44DDS/PES polymers from the batch and continuous reactors are the same.

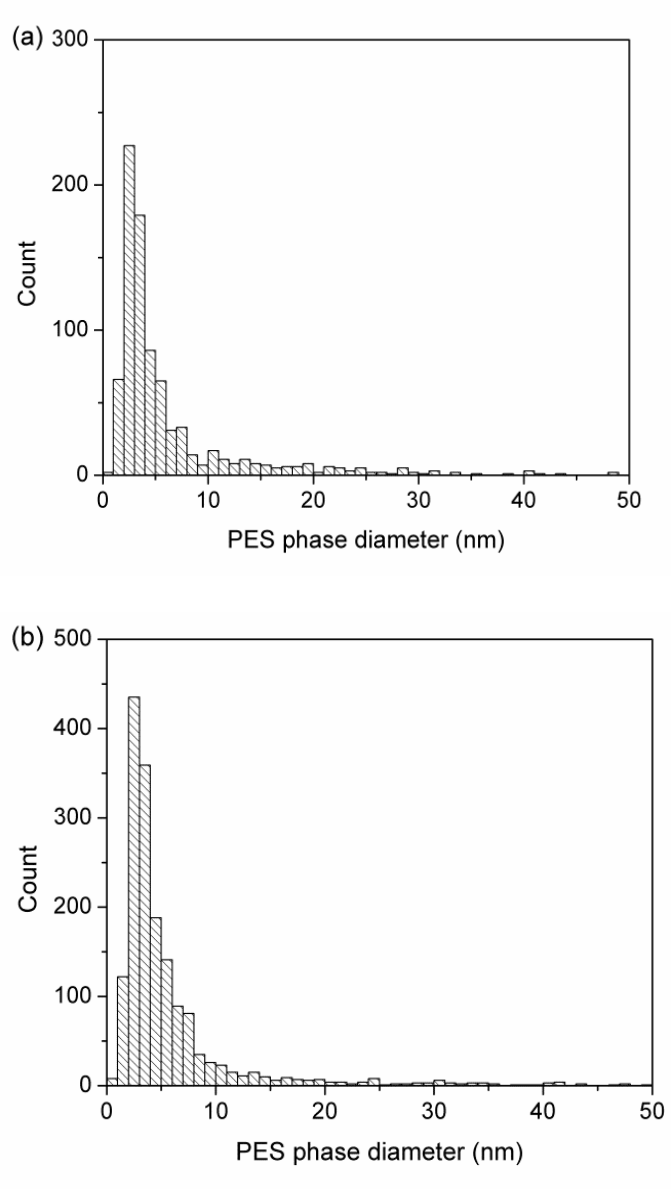

Figure 30. PES phase diameter histograms of (a) batch reaction and (b) continuous reaction.

Mechanical Properties

Mechanical properties of cured TGDDM/44DDS/PES polymers produced by batch reaction and 180 °C continuous reaction were measured to compare tensile strength, tensile modulus, tensile elongation, and fracture toughness shown in Table 8. In

all cases, mechanical properties are statistically similar for both cured polymers and well-within in property values and standard deviations for these glassy polymer networks.

Table 8

Mechanical Properties of Cured TGDDM/44DDS/PES Matrices

Samples	Tensile Modulus (MPa)	Tensile Stress (MPa)	Elongation at Break (%)	K_{IC} (MPa $m^{1/2}$)
Batch Reaction	3040 ± 1 %	60.9 ± 5 %	4.3 ± 4 %	0.709 ± 10 %
Continuous Reaction	3032 ± 6 %	65.4 ± 10 %	5.1 ± 12 %	0.757 ± 8 %

Conclusion

A continuous reactor for preparing glassy polymer network epoxy prepolymers employed within advanced composite materials offers potential advantages over traditional batch reactors. Optical photographs demonstrated similar dissolution states can be achieved in substantially reduced times since higher temperatures can be used due to excellent heat transfer and temperature control compared to large batches. Kinetic studies showed that conversion in continuous reaction is kinetically controlled leading to high degrees of regulation over chain extension reactions, prepolymer viscosity and tack. Reaction conversion and viscosity of TGDDM/44DDS/PES prepolymers was well-controlled by adjusting reaction temperatures and reducing residence times which are impractical for use in batch reactors. AFM with nanomechanical mapping of PES phase-separated morphologies combined with mechanical testing suggests cured network morphologies and properties of cured materials prepared from both reactor processes were similar. The advancement of continuous reactors in this field will lead to new avenues for mixing and blending a broad array of co-reactants, blends, nanoparticles and

etc. due to better control over rheology, shear states and reactor design advantages. We envision continuous reactor sized to directly feed prepreg film lines thus eliminating multiple heating and cold-storage steps currently employed which offers substantial overall energy reduction in prepreg processing.

CHAPTER IV

EFFECTS OF MULTIFUNCTIONAL EPOXY COMPOSITION ON MORPHOLOGIES AND MECHANICAL PROPERTIES OF PES MODIFIED EPOXY BLENDS

Abstract

Thermoplastic polyethersulfone (PES) modified multifunctional tetraglycidyl-4,4'- diaminodiphenylmethane (TGDDM) and triglycidyl para-aminophenol (TGAP) epoxy prepolymers cured with 4,4'-diaminodiphenylsulfone (44DDS) were prepared using a continuous reactor method and their reaction induced phase separated morphologies and resulting mechanical properties were correlated with chemical compositions. Atomic force microscopy (AFM) with nanomechanical mapping was employed to resolve the nanoscale phase-separated morphologies. The extent of phase separation in cured networks and resultant domain sizes were determined to be controllable depending upon the multifunctional epoxy compositions. Final network morphologies were governed through competing PES-epoxy chain extension reactions and epoxy-amine cure kinetics. ^{1}H nuclear magnetic resonance (^{1}H NMR), near-infrared spectroscopy (NIR), and differential scanning calorimetry (DSC) were used to quantify polymer kinetics. Tensile properties and fracture toughness of networks were explained in view of the corresponding phase separated morphologies.

Results and Discussion

In aerospace application, blends of two or more epoxides are often used to produce an epoxy blend with optimized thermal and mechanical properties with improved processability. For example, liquid trifunctional TGAP is currently used to modify viscosity in epoxy prepolymers with the purpose of enhancing fiber impregnation and controlling prepreg tackiness of high viscosity resins after the addition of

thermoplastic modifiers. In order to control ultimate properties in aerospace epoxy networks, it is imperative to resolve the relationship between epoxide blend composition and its influence upon CRIPS and ultimate cured network morphology. Zhang, et al[76] demonstrated that cured TGAP/TGDDM/PES/DDS blends displayed the finer phase separation morphology as compared to TGAP/PES/DDS blends, but did not provide a clear explanation on how chemical composition led to these variances. Other reported controversially results that phase separation did not occur in similar blended multifunctional formulations and concluded homogenous interpenetrating polymer network (IPN) morphologies were formed.[77,78]

It is our opinion that despite the prevalence of scientific reports which relate to CRIPS of thermoplastic/thermosets blends, the relationship between cross-linked glassy polymer network structures, cured network morphologies and their influence for controlling ultimate mechanical properties remains unresolved. In this manuscript, the effects of multifunctional epoxy compositions on thermoplastics phase-separated morphologies were systematically studied using a combination of AFM with nanomechanical mapping, spectroscopic and rheological techniques to provide new insights to resolve CRIPS in multifunctional epoxy blend networks. Furthermore, the relationships between how resultant crosslinked glassy polymer network phase-separated morphologies correlate with mechanical properties are discussed in detail.

Model Reaction and Network Formation

Phenol-terminated PES initiates the chain extension reaction between PES and epoxides due to the high reactivity of phenolic end-groups.[79,80] The PES-epoxy chain extension reaction may compete with epoxy-amine cure reaction and influence the development of cured network architectures. In order to understand the relationships

between glassy network structures and cured morphologies, it is necessary to quantify the reaction between phenol-terminated thermoplastics and epoxides during cure. Figure 31 shows the ^{1}H NMR spectra of a TGDDM/PES model reaction designed to provide insights to the relative rate of the phenol-epoxide reaction. Data is shown for the solubilized and uncured PES-epoxide blend (Figure 31a) and after 1 h of cure at 125 °C (Figure 31b). The general resonance patterns of both spectra are similar, but close examination of Figure 31a indicates the presences of a broad singlet resonance at 10.70 ppm (shown in the inset) which is assigned to the phenolic protons from PES end group.[81] After 1 h at 125 °C, the phenol resonance shifted downfield to 5.25 ppm which is assigned to the epoxy hydroxyl protons shown in the inset of Figure 31b. It appears from ^{1}H NMR spectra that the PES-phenol is fully converted to epoxy within 1 h at 125 °C. This resonance shift confirms the reaction that occurs between epoxide and PES-phenol and provides evidence to how the ultimate network architecture will begin to form during the early stages of cure prior to gelation.

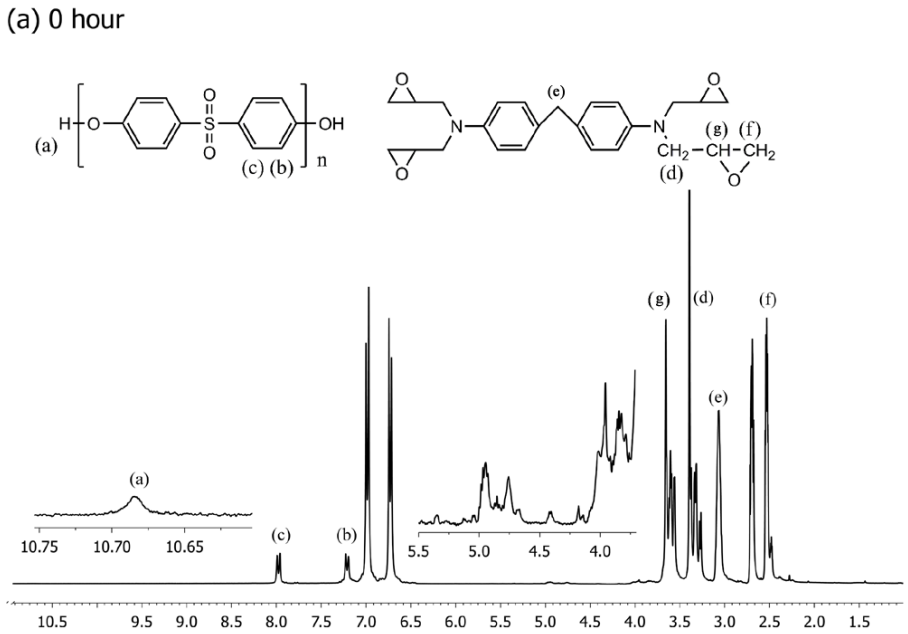

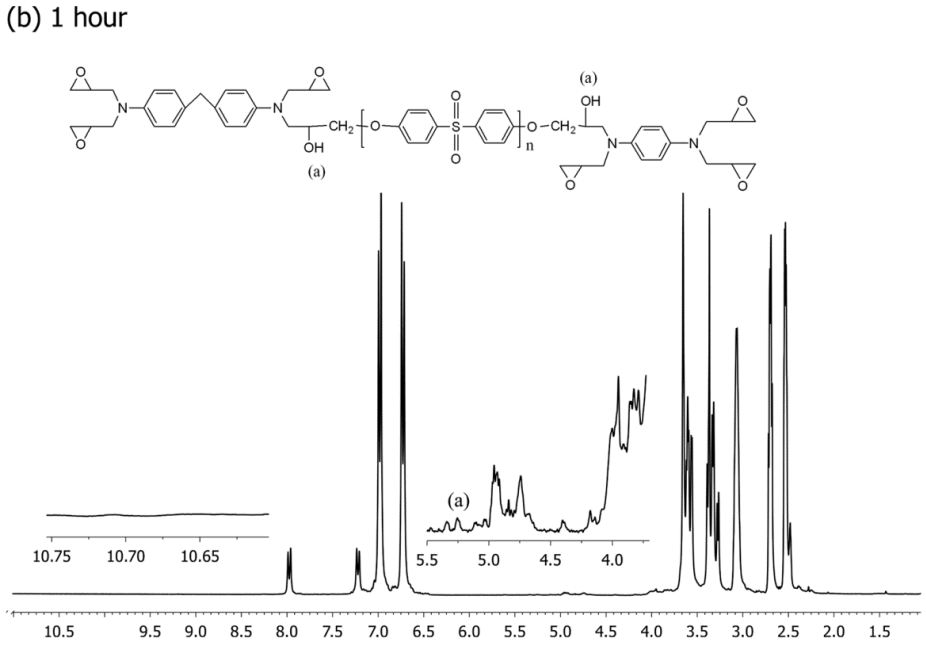

Figure 31. ^{1}H NMR of TGDDM/PES mixtures before (a) and after (b) 1 h at 125 °C.

Assuming the PES-phenol is fully reacted with TGDDM within 1 h at 125 °C, we are able to compare the relative rate of the TGDDM/44DDS reaction in order to gain insight into the PES modified epoxy pre-gel network formation. NIR was employed to track conversion of the TGDDM/44DDS cure in real-time via monitoring the changes in concentration of epoxide and amine functional groups. Figure 32 shows the NIR spectra where epoxide, 1° amine, 2° amine and 3° is tracked for 5 h at 125 °C to provide details for the relative rates of conversion. Absorbances associated with functional groups tracked during the curing reactions include primary amine overtones (4962-5139 cm^{-1}), primary amine-secondary amine combinations (6504-6805 cm^{-1}), and primary amine-epoxy overlaps (4582-4639 cm^{-1}). Functional groups concentrations over time were determined from Beer's Law according to Eq.1.

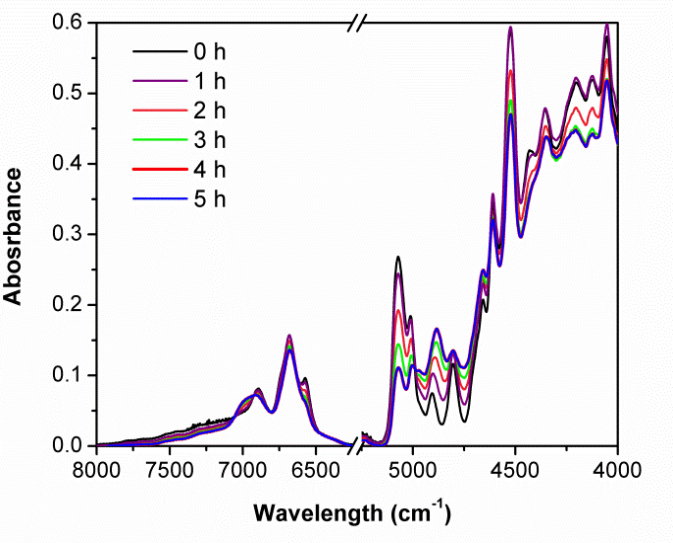

Figure 32. NIR spectra of TGDDM/44DDS cure reaction at 125 °C.

Figure 33 shows the NIR real-time kinetic plots for the TGDDM/44DDS which described the concentration changes of epoxide group, primary amine, secondary amine and tertiary amine, respectively, as a function of reaction time at 125 °C. Primary amine slowly reacted with epoxides with <10 % consumption after 1h. Secondary amine concentration increased with epoxide consumption until end of this pre-cure cycle at 5h suggesting that under this condition, secondary amine did not compete significantly for epoxide reaction. These conditions were established for the TGDDM/44DDS/PES cure reaction in an effort to control the pre-gel network formation and assure complete consumption of PES into the network backbone.

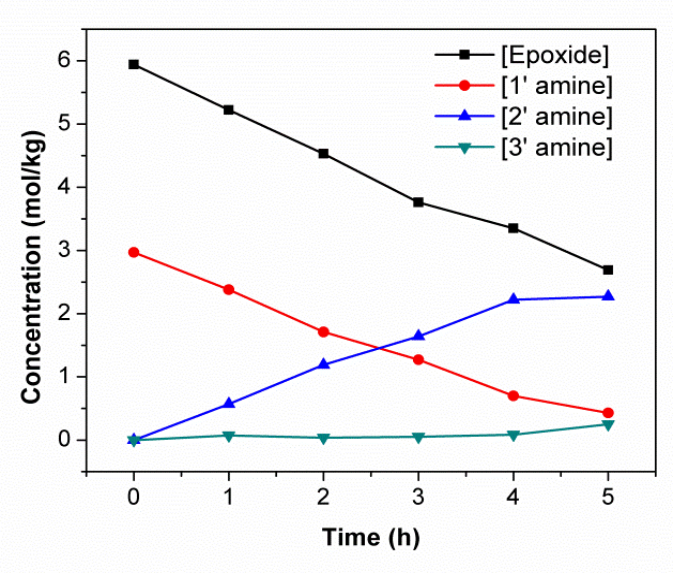

Figure 33. NIR plots tracking conversion for TGDDM/44DDS/PES system.

Similar results were also found in PES modified TGAP/44DDS networks (Figure 34 and Figure 35). The broader singlet peak at 10.70 ppm (Figure 34a) is attributed to the phenol proton from reactive PES chain end. It is shifted downfield to 5.20 ppm and 5.40 ppm after reacting at 125 °C for 1 h (Figure 34b). During this period of reaction, primary amine slowly reacted with epoxides with less than 10 % consumption after 1 h as proved by NIR in Figure 35.

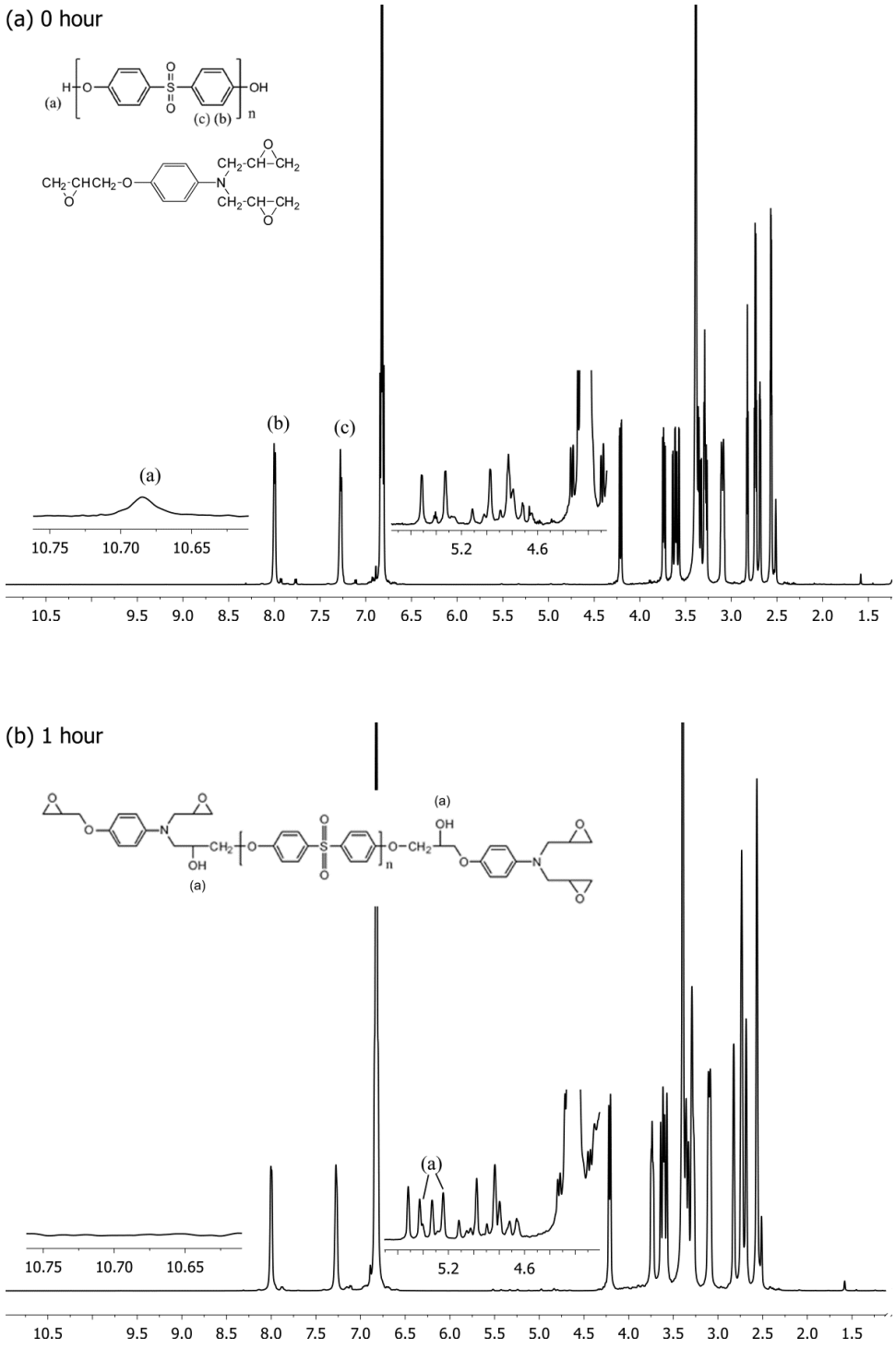

Figure 34. ^{1}H NMR spectra of TGAP/PES mixtures before (a) and after (b) 1 h of curing at 125 °C.

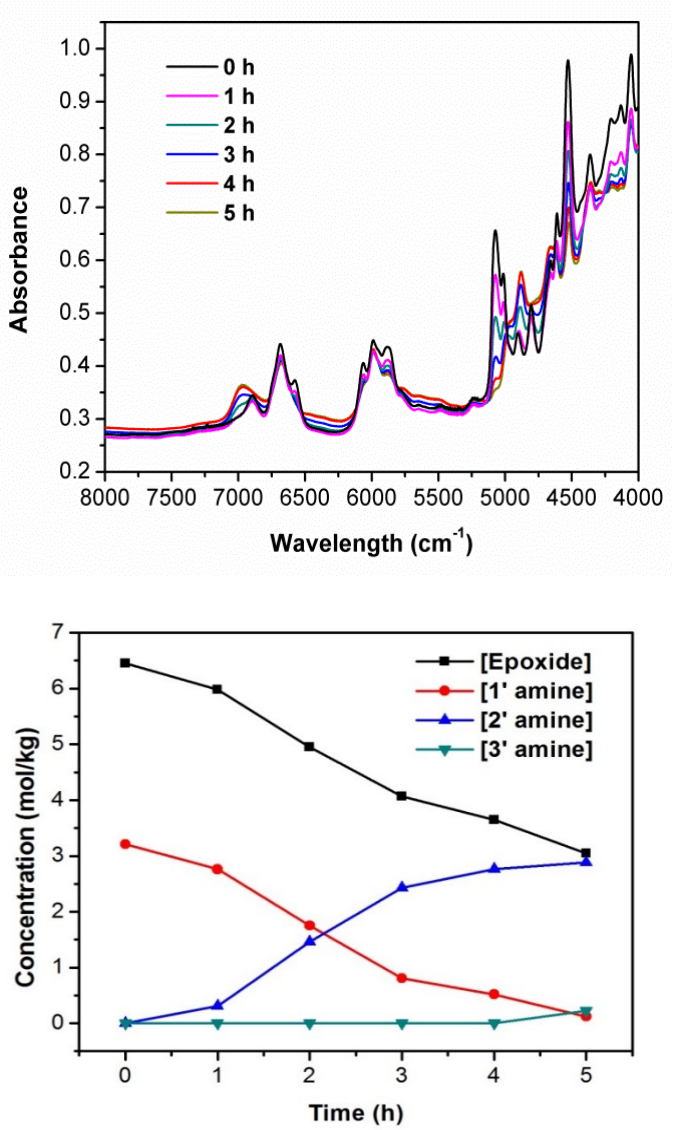

Figure 35. NIR spectra of TGAP/44DDS cure reaction at 125 °C.

Combining the results obtained from ^{1}H NMR and NIR, we can conclude that during the early stages of cure, PES-epoxide and primary amine-epoxide reactions occur simultaneously in TGDDM/44DDS/PES since the PES phenols were depleted within the first hour and amines continued to react over the first 5 h without significant conversion of secondary amine. This approach assured the formation of ultimate architectures with PES fully reacted into the cured networks. After 5 h the reaction temperature was raised

to 200 °C for 2 h which completed the secondary amine-epoxide reaction and formation of the fully crosslinked network. With all above characterization results, we can conclude that epoxy-PES chain extension reaction is finished at the early stage of epoxy-amine cure reaction, forming a block copolymer structure. The schematic depicted in Figure 36 represents the TGDDM/TGAP/44DDS/PES glassy polymer network architecture which we have employed to study cured network morphological variances in this manuscript.

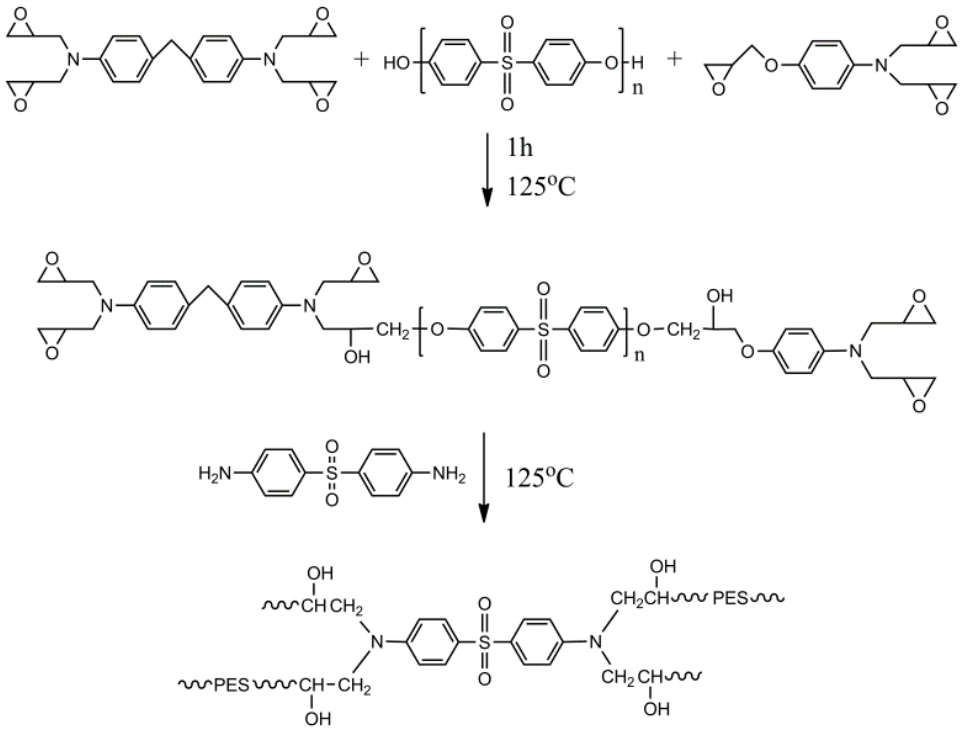

Figure 36. Schematic network formation of PES modified TGDDM/TGAP/44DDS blends.

Cured Network Phase Morphology

The prior discussion was provided to describe our approach for quantifying network formation to study the influence of multifunctional epoxy chemical composition on cured network architectures. Fracture surfaces of all formulations were investigated by

SEM and showed no evidence of reaction induced phase separation. For example, a smooth and homogenous feature was observed for 0TM/100TP as illustrated in Figure 37. Solvent etching by dichloromethane shows no effects on morphology, indicating PES phases might not form during cure. Similar morphologies have been reported in recent studies of phenol terminated PES modified multifunctional epoxy networks and described as non-phase separated homogenous IPN networks.[82] In their works they claimed that PES is reacted with epoxy through chain extension reaction and phase separation process is suppressed leading to the formation of a homogenous IPN network. This conclusion is quantitatively confirmed by ^{1}H NMR and NIR results in the present research. PES-epoxy chain extension reaction and primary amine-epoxy cure reaction will take place simultaneously producing a block copolymer which will be more soluble than PES in the resins. The increased solubility will slow down phase separation rate and suppress the degree of demixing, resulting simultaneous interpenetrating network (SIN) with homogenous morphology. The size of the phase domains of IPN was discovered to be smaller than expected, often in the order of tens of nanometer. In this case, commonly used techniques such as SEM, optical microscopy, dynamic rheological analysis, and small angle lighter scattering are not able to monitor phase morphologies and produce a recognizable features.

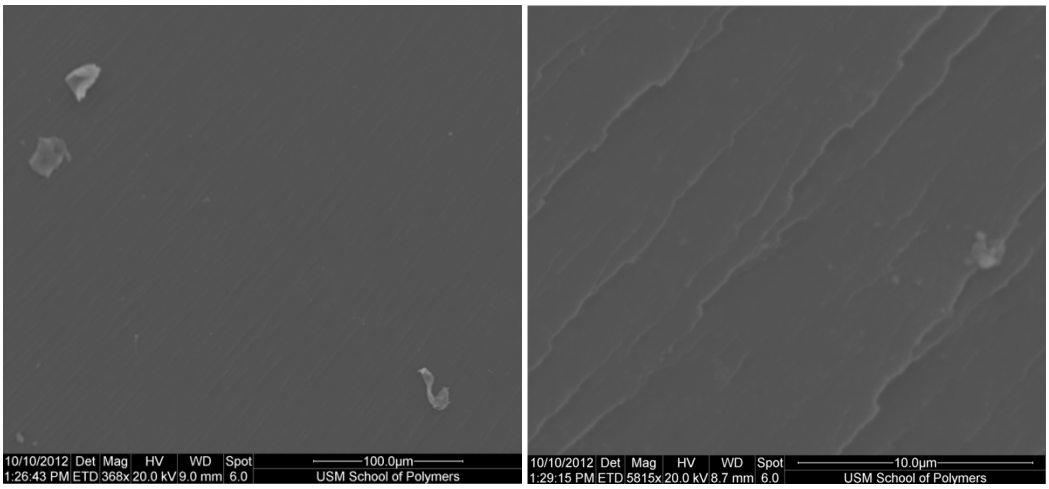

Figure 37. SEM micrographs of the fracture surface for 0TM/100TP.

Further investigations of same fractured surfaces were conducted by AFM with nanomechanical mapping and their DMT modulus images are shown in Figure 38. The dark regions are corresponding to the lower modulus PES-rich phase while the bright features are associated with higher modulus epoxy-rich phase.[83] The differences in elastic modulus on sample surfaces reveal a heterogeneous morphology existing at nanostructure level for all formulations. The formed nanophases are finely divided with a diameter around 50 nm. These results clearly indicate the morphologies of phenol terminated PES modified TGDDM/TGAP/44DDS blends are only homogenous at microstructure level but phase-separated at nanostructure level.

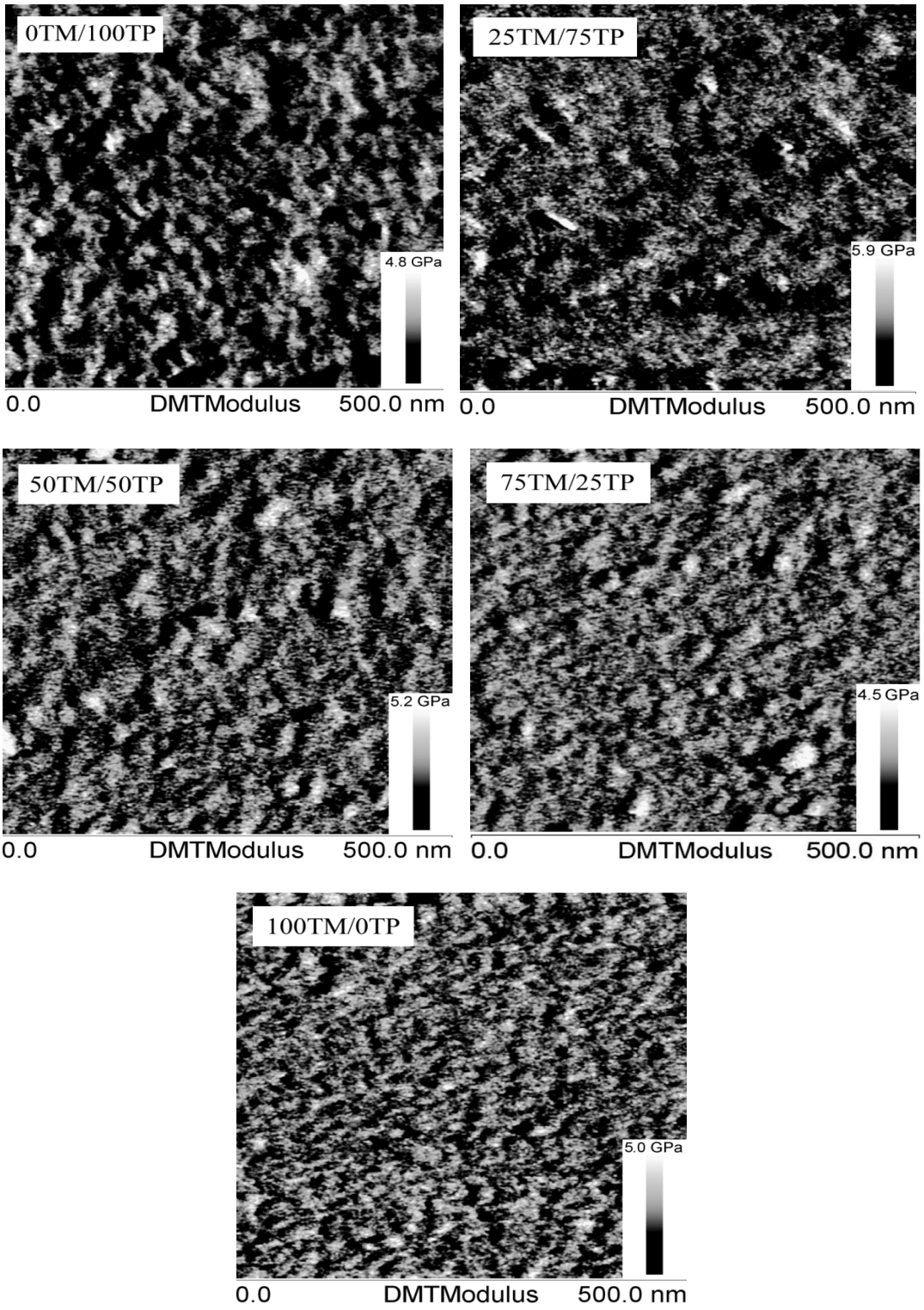

Figure 38. Peak-Force Tapping images of PES modified TGDDM/TGAP/44DDS blends.

Utilization of imaging software provides an ability to analyze the averaged phase domain sizes and provide a quantitative comparison between samples. A threshold of image color was defined to distinguish between dark and bright phases and the calculated results were summarized in Table 9. It can be seen that area percentages occupied by PES-rich phase and epoxy-rich phase are relatively constant and independent of multifunctional epoxy compositions. However, mean diameters of both phases are decreased with the increased TGDDM contents. The domain size of 0TM/100TP is almost twice as large as 100TM/0TP. These results experimentally demonstrated the dependence of phase-separated domain sizes on multifunctional epoxy compositions in PES modified TGDDM/TGAP/44DDS blends. It has been reported earlier by B.S Kim[84] using transmission electron microscopy that reactive PES modified TGAP/44DDS system exhibited a co-continuous phase-separated morphology with the domain size of 100 nm. This result is in good agreement with what we found by AFM with nanomechanical mapping technique.

Table 9

Imaging Analysis of PES Modified TGDDM/TGAP/44DDS Blends

Sample	Epoxy-rich phase		PES-rich phase	
	Area (%)	Mean diameter (nm)	Area (%)	Mean diameter (nm)
100TM/0TP	44.65	54.75	55.35	43.44
75TM/25TP	43.97	71.55	56.03	62.69
50TM/50TP	48.10	79.43	51.90	68.72
25TM/75TP	45.03	89.93	54.97	79.63
0TM/100TP	45.01	96.47	54.99	88.74

The relationship between phase separated domain sizes and multifunctional epoxy compositions can be further proved by DMA as shown in Figure 39. Two peaks appeared at around 220 °C and 270 °C in tan δ curves which can be associated with the glass transition temperatures of PES-rich phase and epoxy-rich phase, respectively. As the content of TGDDM increased, the PES-rich phase peak decreased to such an extent that became a shoulder of epoxy-rich phase peak for 50TM/50TP and almost indistinguishable for 75TM/25TP and 100TM/0TP. This change was directly correlated to the phase structure variation as we observed from AFM-QNM. To explain the epoxy composition-dependent phase domain sizes, time evolution of the phase separation is discussed in the following section.

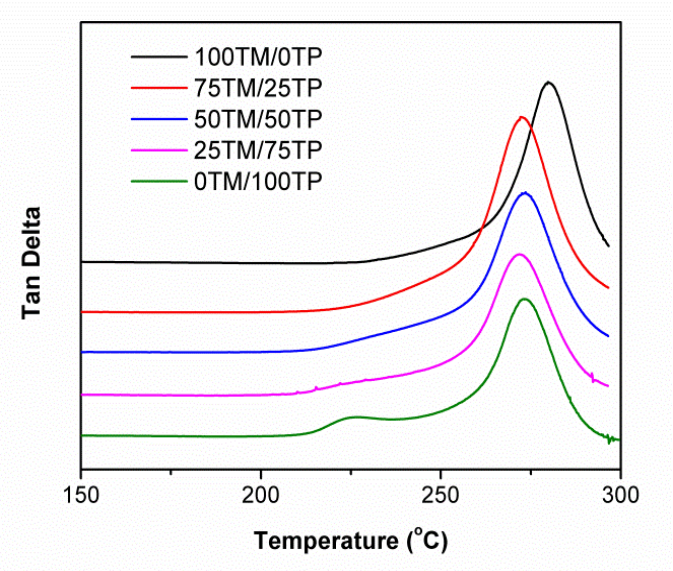

Figure 39. DMA of PES modified TGDDM/TGAP/44DDS blends.

In general, reaction induced phase separation occurs due to the change of mixing enthalpy and entropy which arise from the increased molecular weight of thermosets upon curing. Since phase separation is a kinetic process which is highly viscosity-

dependent, the increased matrix viscosity upon curing can slow down the phase separation and completely suppress it when system vitrified. As a consequence, final phase morphologies of an initially miscible thermoplastic-thermosetting system are controlled by the competition between phase separation rate and crosslinked reaction kinetics, which could be adjusted by curing conditions, resin compositions, thermoplastic structures and molecular weights. In this work, use of reactive thermoplastic and multifunctional epoxies created a unique chemical environment for CRIPS to occur. The accelerated PES-epoxy chain extension reaction rate caused by high polar tertiary amines of TGDDM/TGAP and the relatively slow epoxy-amine cure rate owing to electron withdrawing sulfone groups of 44DDS ensure the completion of PES-epoxy chain extension reaction prior to the phase separation and gelation. The block copolymer produced by the chain extension reaction retards the onset of phase separation. In this case, phase separation still can take place but is hindered by the chemical gel network formation in its early stage of separation. The spinodal coarsening are suppressed and the phase separation domain tends to be smaller within the nanoscale region. Altering the time sequence of PES-epoxy chain extension reaction, phase separation, and gelation could result in phase-separated morphologies that can be observed at microstructure level.[85, 86, 87]

The period between the onset of phase separation and chemical network gelation determine the time during which phase domain can grow. Since theoretically gel point conversion is inversely proportional to the epoxide functionality, it is reasonable to expect the gel time increases from 100TM/0TP to 0TM/100TP. Rheological measurement was then performed to confirm this hypothesis. However, a reverse trend is observed in Figure 40. The gel time is decreased from 305 min for 100TM/0TP to 175

min for 0TM/100TP at 125 °C of cure. Similar trends were also observed by Ratna[88] and explained by epoxy resins viscosity. An increase in matrix viscosity reduced the chemical reaction attributed to the restricted molecular mobility. This result indicated the epoxy composition-dependent domain sizes cannot be explained only by the time to allow phase separation. The viscosity differences should also be taken into consideration. If we compare the complex viscosity traces during cure (Figure 41) we can observe an increase in viscosity in the case of formulation with higher TGDDM content. Although it is difficult to directly observe the onset of nanoscaled phase separation in this study, we can expect that system with higher viscosity should have a delayed onset of phase separation with reduced phase separating rate due to the restricted molecular chain mobility. The changes of onset of phase separation offset the influence of chemical gelation time on phase separation sizes. The reduced phase separation rates further inhibit the growth of phase separation before gelation occurs, resulted in the gradually increased phase separated domain size with respect to multifunction epoxy compositions.

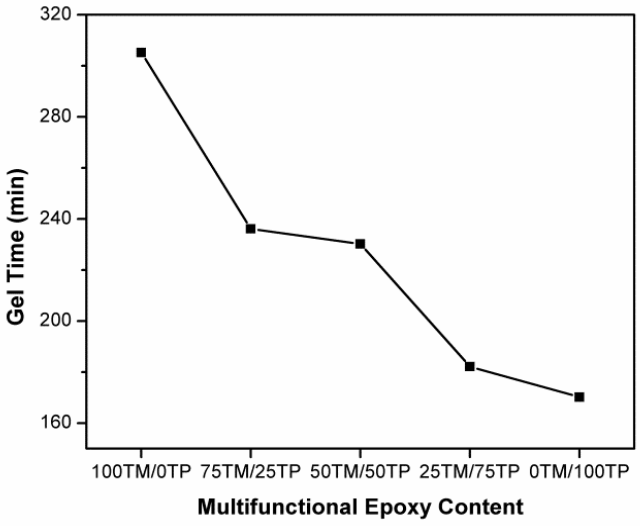

Figure 40. Gel times of PES modified TGDDM/TGAP/44DDS blends.

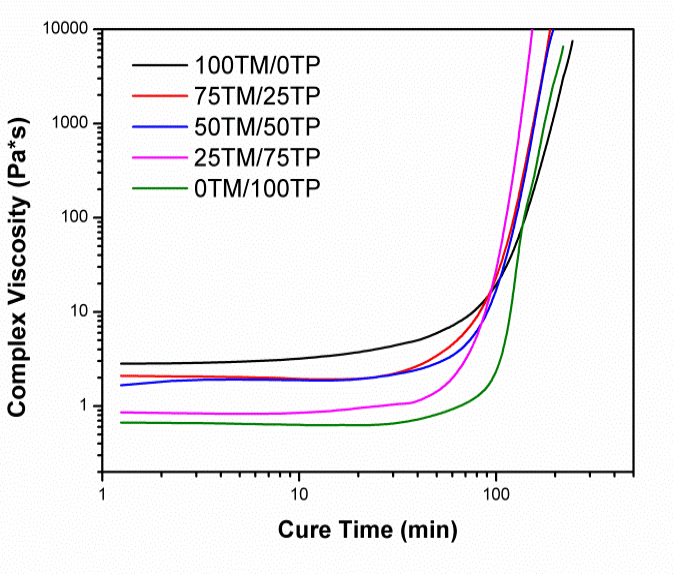

Figure 41. Complex viscosity traces of PES modified TGDDM/TGAP/44DDS blends.

Mechanical Properties

The tunable phase-separated domain sizes by altering multifunctional epoxy compositions provide an opportunity to examine the effects of nanosized thermoplastic-rich domains on mechanical properties of epoxy matrices. Tensile modulus and fracture toughness of cured samples were measured and the results are displayed in Figure 42 and Figure 43, respectively. For the purpose of comparison, mechanical properties of neat multifunctional epoxy blends without PES are also reported.

It can be seen that the tensile moduli are approximately constant for all PES toughened TGDDM/TGAP/44DDS blends. No obvious correlation between tensile modulus and multifunctional epoxy compositions were observed, implying tensile modulus is independent of phase-separated domain sizes in current study. But it is hard to draw conclusion since tensile samples showed relatively high standard error bars which may overlap the difference caused by epoxy composition. Moreover, tensile modulus is

slightly decreased upon the addition of PES in epoxy matrices. This is because the modulus of neat PES is slightly lower than that of neat epoxy matrices.

On the other hand, fracture toughness K_{1C} tends to increase with decreasing TGDDM contents as described in Figure 43 and the highest improvement of fracture toughness is obtained for 0TM/100TP system with the largest phase separation domain size. Since multifunctional epoxy compositions had little effect on the fracture toughness of neat epoxy matrices, it implies that the increased fracture toughness is caused by the growth of phase-separated domain sizes from 100TM/0TP to 0TM/100TP. The increased PES-rich phase created longer path length to stabilize the fracture process. This conclusion is supported by D.J. Hourston[89] who studied the effects of epoxy composition on facture toughness of PEI modified epoxy systems. The author reported better improvement in toughness was achieved in system with lower epoxy functionality.

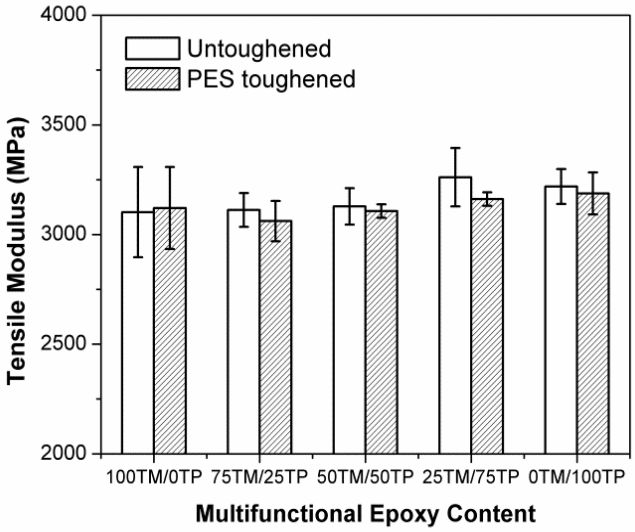

Figure 42. Tensile modulus of TGDDM/TGAP/44DDS blends.

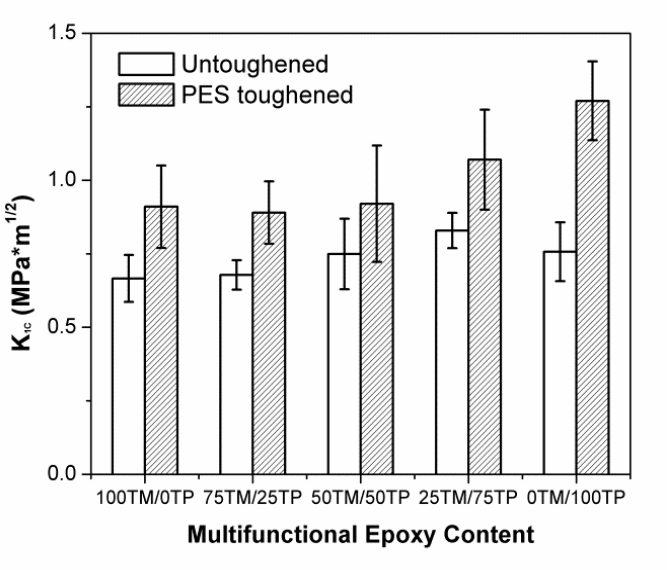

Figure 43. Fracture toughness of TGDDM/TGAP/44DDS blends.

Tunable Morphologies of Epoxy/Thermoplastic Binary Systems

Above discussion explained the phase-separated morphologies in multifunctional epoxy and hydroxyl terminated PES systems. The domain size can be tailored in the nanosized range of 50 nm to 100 nm by controlling multifunctional epoxy compositions. Further increasing domain sizes into microsized or macrosized region requires altering the time sequence of epoxy/thermoplastic chain extension reaction, phase separation and gelation through changes of parameters such as epoxy-amine cure rates, thermoplastic end groups and molecular weights. For the purpose of demonstration, parameters were selectively varied with a constant thermoplastic loading level of 15 wt% of total polymer blends and their cured morphologies are illustrated in Figure 44. In addition, experimental limitations of techniques used for detecting phase separations were also summarized.

As showed in Figure 44, replacing multifunctional epoxy with difunctional epoxy such as DGEBA, the co-continuous morphology size increased to the range between 100

nm and 1 um. On one hand, the relatively slow cure reactivity and low resin viscosity of DGEBA compared to multifunctional epoxies, giving enough time for phase separation to occur and collapse. On the other hand, the epoxy-PES chain extension reaction rate is also reduced by use of DGEBA compared TGDDM and TGAP, as evidenced by viscosity changes in Figure 45. TGDDM/PES mixture viscosity was increased in the first 1 h of reaction at 125 °C indicating the occurrence of chain extension reaction between phenol group and epoxide group. This is in a good agreement with ^{1}H NMR results reported earlier. However, DGEBA/DDS mixture viscosity was relatively constant in the first 1 h of reaction. As a result, phase separation may occur in an early stage prior the formation of epoxy-PES block copolymer.

Replacing hydroxyl terminated PES with non-reactive PES yielded microsized phase-separated morphologies within the region between 1 μm to 10 μm. The non-reactive PES could prevent chain extension reaction between PES and epoxies. PES became less soluble in epoxies and the thermodynamic unstable state reached earlier. Additionally, macrosized phase morphologies (10 μm to 1 mm) can be prepared by incorporating thermoplastics with higher molecular weight such as polyetherimide (PEI) or diamine with higher cure reactivity and lower viscosity such as 4, 4'-methylenedianiline (MDA). Both facilitated the onset of phase separation and increased the phase separation kinetics.

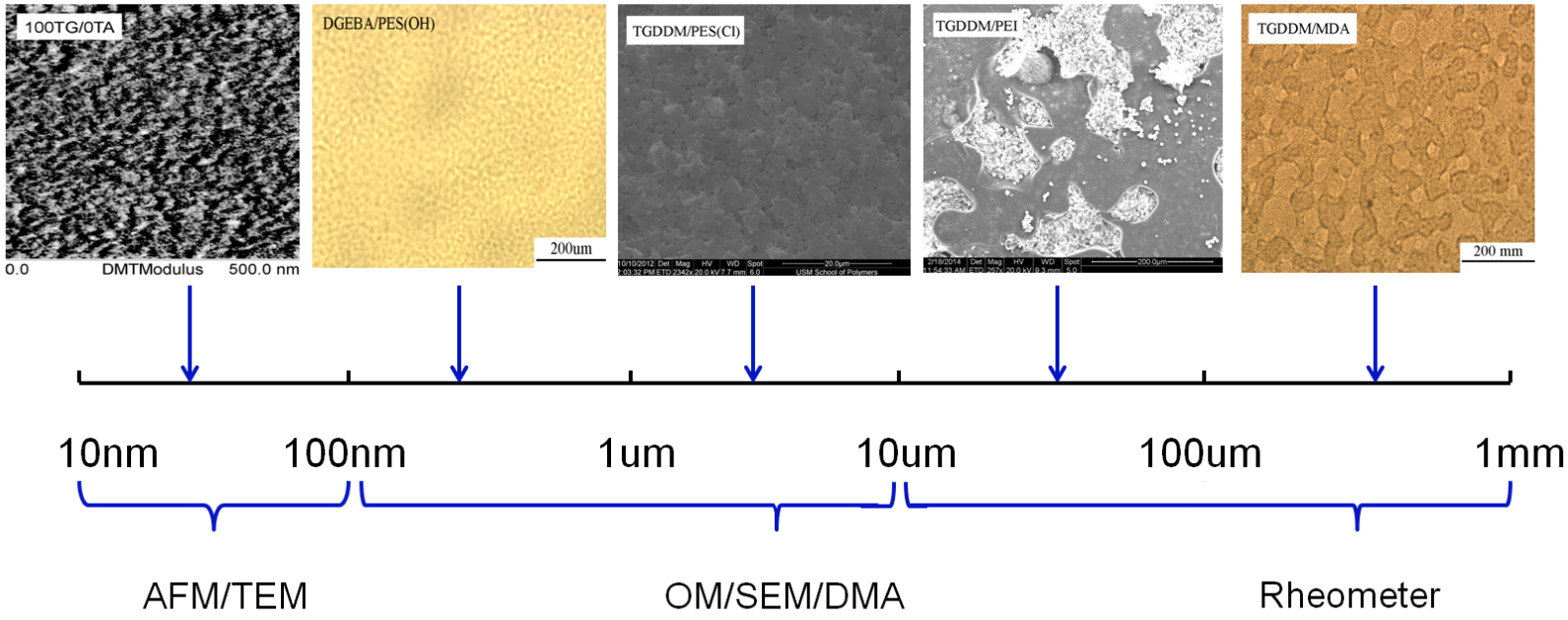

Figure 44. Schematic phase-separated domain sizes of epoxy/thermoplastics blends and techniques limitations.

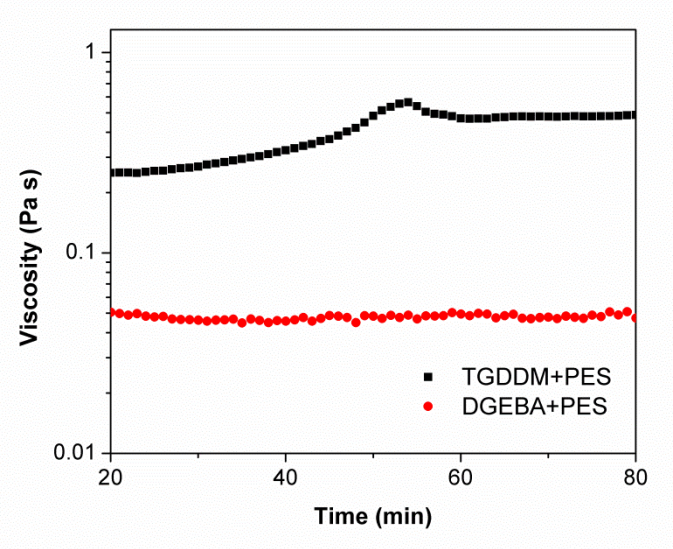

Figure 45. Viscosity changes of TGDDM/PES and DGEBA/PES mixtures at 125 °C.

Due to the substantial selection of epoxy-amine chemistry and thermoplastic categories, only representative examples were provided to highlight that the domain size can be changed in a wide range in current study. Various parameters can influence the phase separation morphology and domain growth alone or together. Cure reaction induced phase separation have some common points or significant differences which are all related to the competition between the cure reaction kinetic and phase separation rate which are summarized as following:

1. Phase separation process is dominated by the competition between phase separation and cure kinetics. Thermoplastic molecular weight and dynamic asymmetric difference (T_g) alter the onset of phase separation thermodynamically. Cure temperature, epoxy-amine stoichiometry, and reactivity control the cure reaction kinetic and the onset of gelation at which point primary phase separation is believed to stop. The time interval between the onset of phase separation and gelation decide phase-separated domain growth and development.

2. When reactive thermoplastic is used, the epoxy-thermoplastic chain extension reaction and epoxy-amine cure reaction occurs simultaneously. Completion of epoxy-thermoplastic chain extension before gelation will suppress phase separation and lead to a smaller phase domain sizes. However, if cure reaction is fast enough to initiate phase separation before chain extension complete, the phase domain size tends to be bigger.

3. Viscosity plays an important role during cure reaction induced phase separation process. It reduces the rate of phase separation and suppresses the phase collapse process by restricting chain mobility. As a consequence, system with a higher viscosity tends to have a smaller phase-separated domain size.

4. Among those commonly used techniques for monitoring phase separation, TEM and AFM are capable of observing phase separation happened in nanosized region. OM, DMA, and SEM can be used to investigate microsized phase separation morphologies. Rheological analysis is only feasible for systems with phase separation domain sizes larger than 10 μm. Understanding limitation of applied techniques will help understanding morphology-property relationship in thermoplastic modified epoxy systems and final composites.

Conclusion

In this chapter, phenol-terminated PES modified TGDDM/TGAP/DDS blends were prepared using a continuous reactor and their crosslinked network structures, phase-separated morphologies and mechanical properties were studied by varying multifunctional epoxy content. ^{1}H NMR and NIR quantitatively demonstrated the concurrent PES-epoxy chain extension reaction and primary amine-epoxy cure reaction in PES modified TGDDM/TGAP/DDS blends led to a more soluble block copolymer structure. AFM with nanomechanical mapping revealed the phase-separated

morphologies of PES modified TGDDM/TGAP/DDS blends at nanostructure level although SEM micrographs showed homogeneous morphologies at microstructure level. In addition, the phase-separated domain sizes were found to depend on multifunctional epoxy compositions. Tensile properties and fracture toughness of PES modified TGDDM/TGAP/DDS blends were also examined in terms of multifunctional epoxy compositions. No obvious correlation between tensile modulus and multifunctional epoxy compositions were observed. Fracture toughness however tend to decrease with increase of TGDDM contents. These findings presented herein could be used to better understand the structure-processing-properties relationships of thermoplastic toughened multifunctional epoxy blends in order to produce novel toughened epoxy composites.

CHAPTER V

DISPERSION AND STABILIZATION OF MWCNT IN EPOXY PREPOLYMER MATRIX USING CONTINUOUS REACTOR

Abstract

This chapter described the application of continuous reactor method on preparing multiwall carbon nanotube (MWCNT)/tetraglycidyl-4, 4'-diaminodiphenylmethane (TGDDM) prepolymers at industrial scale. Our intention through this chapter combined the successful strategies for advancing epoxy chemistries with our approaches achieving good levels of nanotubes dispersion using a twin screw continuous reactor. The continuous reactor consists of two sections, one of which set at 180 °C for partial curing epoxy and advancing viscosity to avoid MWCNT re-agglomeration, and the other maintained at near room temperature for improving MWCNT dispersion in epoxy prepolymer matrix. Optical microscopy and scanning electron microscopy were used to quantify the MWCNT dispersion states and stability in epoxy matrix after continuous process and during curing cycles. Prepolymer matrices with viscosity higher than 3.0 Pa·s were proven to stabilize MWCNT dispersion in our systems. Additionally, electrical conductivities and mechanical properties of final cured MWCNT/TGDDM composites were measured and discussed in view of the corresponding MWCNT dispersion states.

Results and Discussion

In previous chapters, we reported the non-conventional method for preparing thermoplastic modified epoxy prepolymers based on twin screw extruder technology. The advancement of epoxy prepolymer molecular weights and viscosities were controlled by epoxy-amine chemistry, process designs, and processing conditions. Barrel temperature of 180 °C has been proven to be an ideal temperature for fully dissolving 44DDS in

TGDDM and advancing viscosity without concerns of gelation in current used continuous reaction. Therefore in this chapter the pre-cure temperatures were set constantly at 180 °C to simplify our analysis. Focus will be on improving MWCNT dispersion and stability in epoxy prepolymer matrices during processing.

Influence of Process Conditions on MWCNT Dispersion

Several key processing parameters are discussed to highlight critical control variables and benchmark necessary properties in continuous reaction. MWCNT/TGDDM prepolymers were firstly prepared at different dispersing temperatures and their dispersing states were examined using OM. Minimum dispersing temperature was set at 40 °C to avoid any transporting issue which may lead by ultra-high matrix viscosity (>1.0 E+4). Figure 46 illustrated the overall MWCNT dispersion states in epoxy prepolymer matrices after continuous reaction. A distinct size reduction of nanotubes was observed from millimeters to micrometers. For samples prepared at temperatures of 40 °C and 60 °C (EMT01 and EMT02), MWCNT were evenly distributed in matrix resins with few isolated bundles larger than 20 μm which only covering small portion of the total observed area. With the increase of dispersing temperature up to 100 °C, both the number and size of MWCNT agglomerates increased as presented by EMT03 and EMT04 in Figure 46. Besides the changes of particle size and number, unevenly MWCNT distribution in EMT03 and EMT04 also indicated by the transparent epoxy regions which qualitatively illustrated the worse dispersion states at high dispersing temperatures comparing to EMT01 and EMT02 at lower dispersing temperatures.

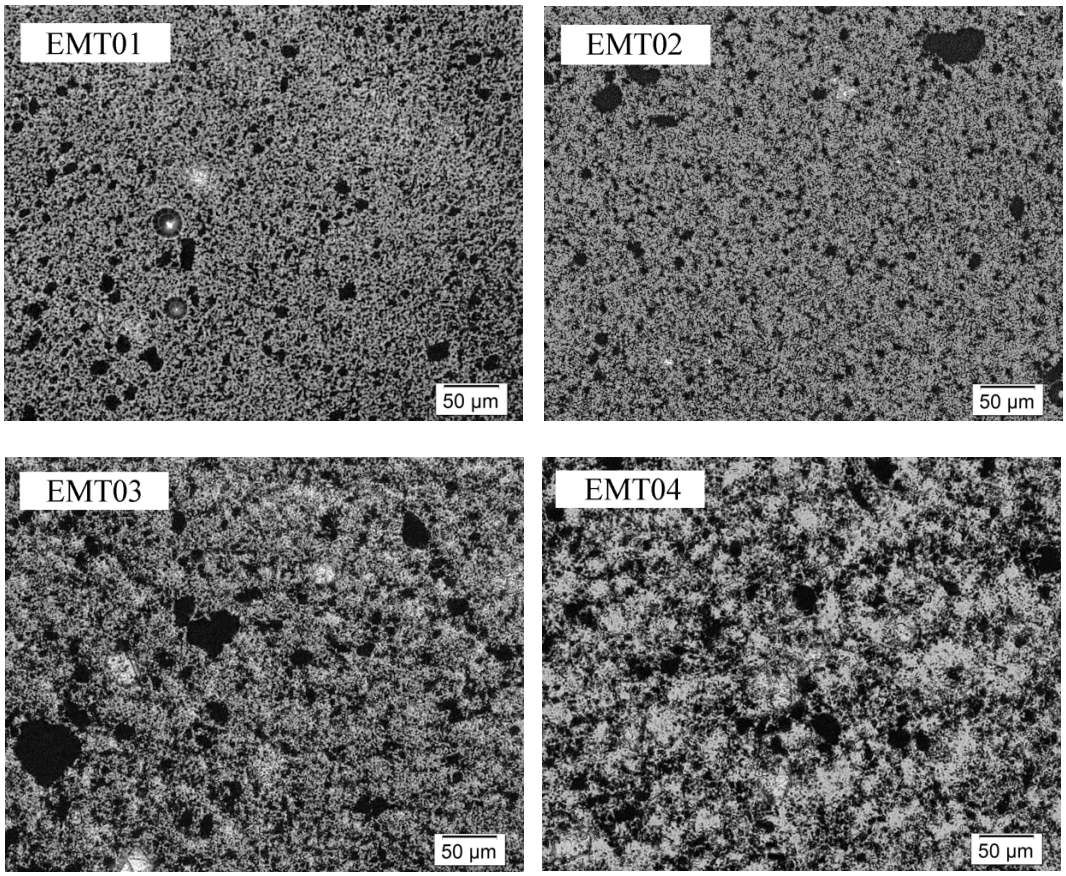

Figure 46. Optical micrographs of MWCNT dispersion states in TGDDM/MWCNT prepolymers at different dispersing temperatures.

By quantitatively measuring dispersion, systematic studies of processing conditions, particles size, and agglomeration become possible. The average dispersion indices *D* calculated based on optical micrographs are plotted as a function of dispersing temperatures in Figure 47. The value of *D* decreased from 97.2 % for EMT01 to 91.7 % for EMT04 as the dispersing temperature increased from 40 °C to 100 °C, respectively. Interestingly, when temperature is higher than 80 °C, difference between dispersion indices became narrower. Only a small level of decrease in *D* is observed for sample of EMT03 and EMT04, indicating the influence of dispersing temperatures on MWCNT dispersion states become less important. Although the unevenly distributed MWCNT and

existence of single large MWCNT agglomerate (> 50 μm) in the selected optical observing area can lead to relatively large variation in the calculated *D* values, this statistical evaluation method still revealed the general trend of MWCNT dispersion with respect to the dispersing temperature in continuous reaction process.

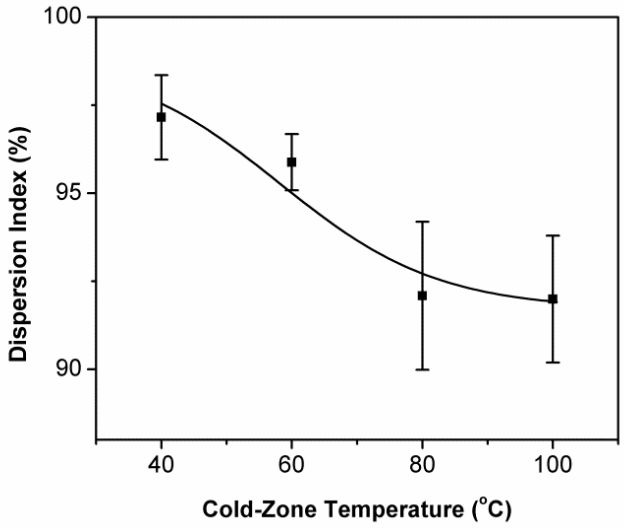

Figure 47. Dispersion index changes of TGDDM/MWCNT prepolymers vs. dispersing zone temperatures.

As dispersing temperature reduced from 100 °C to 40 °C, matrix viscosity increased several orders of magnitude with decreased dispersing temperature. Table 10 shows the TGDDM matrix viscosities at their corresponding dispersing temperatures. The best dispersion state was obtained for EMT01 prepared at 40 °C with the highest matrix viscosity of 1.7 E+3 Pa·s. Shear stress generated by the continuous reactor can be used to explain MWCNT dispersion state changes with respect to dispersing temperatures.[90] The increased viscosity helps the low viscous epoxy resins filling up the space between twin screws, building up pressure, and generating shear stress that can be applied on MWCNT bundles.[91] With a constant shear rate, the matrix with higher

viscosity can produce higher shear stress. As a consequence, MWCNT dispersion can be improved by reducing dispersing temperature.

Table 10

Dispersion Indices and Processing Viscosities of TGDDM/MWCNT Prepolymers at Different Dispersing Temperatures

Samples	Dispersing temperature (°C)	*D* (%)	Viscosity (Pa·s)*
EMT01	40	97.2 ± 1.2	1.7 E+3
EMT02	60	95.8 ± 0.8	1.6 E+2
EMT03	80	92.1 ± 2.1	1.1 E+1
EMT04	100	91.7 ± 1.8	3.4 E+0

* Complex viscosities were measured at the corresponding dispersing temperature immediately after samples were collected.

Effects of screw speeds on MWCNT dispersion in epoxy prepolymer matrices were also investigated. As shown in Figure 48, MWCNT dispersion state is greatly improved from EMS01 to EMS04 as screw speeds increased from 200 to 800 rpm, respectively. Their dispersion indices were plotted against screw speeds in Figure 49. EMS01 prepared at the lowest screw speed showed the worst dispersion state among all the samples with a D value of 85.5 %. Increasing screw speeds led to an improved dispersion index until 600 rpm whereas further increase to 800 rpm showed little effects. Similar trends were also observed by several authors within thermoplastic fields and explained in terms of counterbalance between shear stress and residence time during continuous reaction.[92, 93] Higher screw speed generates higher shear stress during

continuous reaction process, facilitating MWCNT bundles breakup and enhancing their dispersion in polymer matrices. However at the same time, materials experienced shorter residence time at higher screw speed within the continuous reactor as we proved in *Chapter III*. The counteracting balance between shear stress and residence time is observed at around 600 rpm in this study. Further improvement of MWCNT dispersion states requires prolonging the residence time through modifying continuous reactor design and screw profiles which will continue to be explored in our future research.

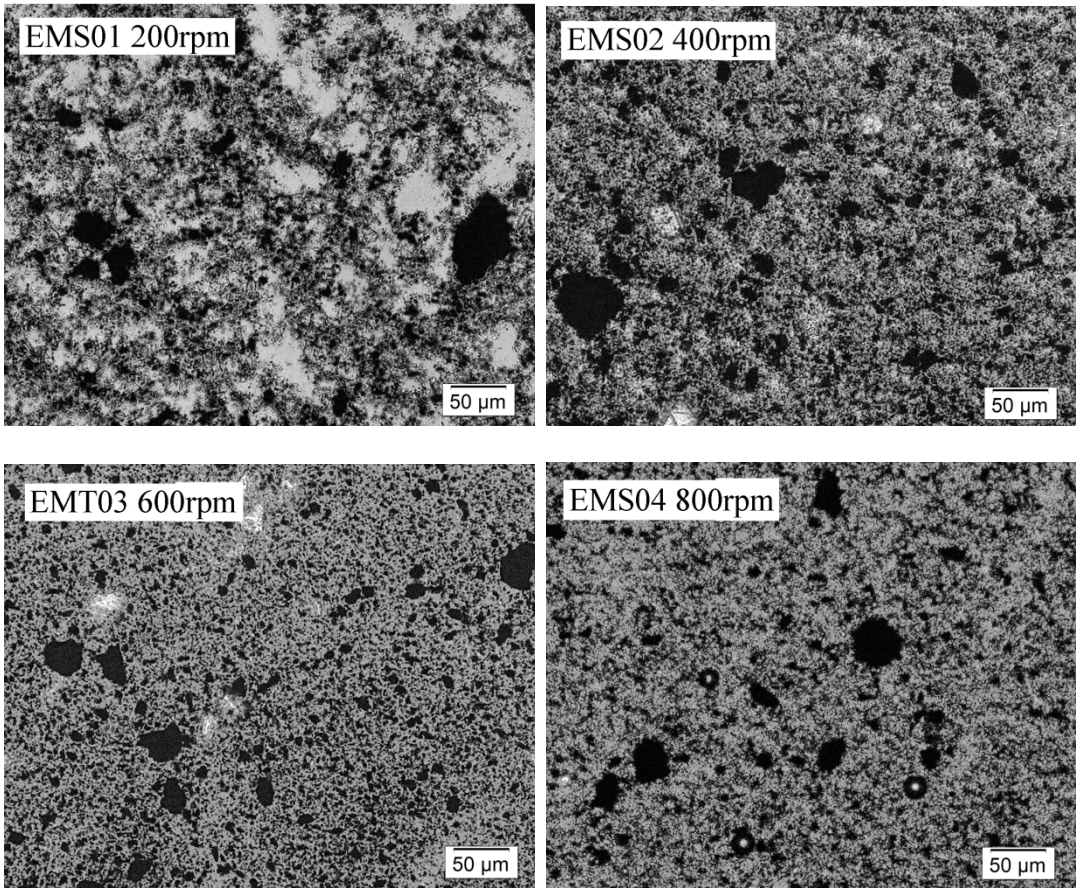

Figure 48. Optical micrographs of MWCNT dispersion states in TGDDM/MWCNT prepolymers at different screw speeds.

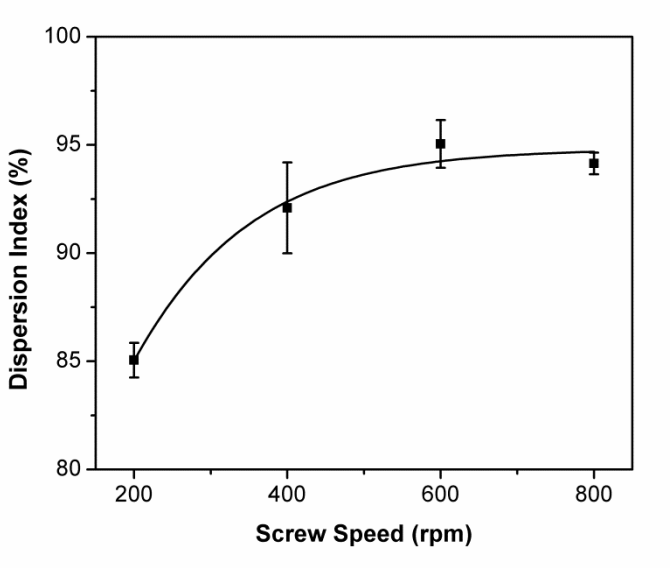

Figure 49. Dispersion indices of TGDDM/MWCNT prepolymers vs. screw speeds.

The above results demonstrated that low viscous epoxy prepolymers can be processed as thermoplastic by applying dispersing zones with a reduced barrel temperature and increased screw speed. Within current continuous reactor design, the MWCNT sizes were able to reduce from 1 mm to 50 μm in diameter in epoxy prepolymer matrices. Dispersing nanoparticles in epoxy matrix at low temperature is neither feasible nor efficient using traditional batch reactor owing to the highly viscous matrices. We believe this idea can serve as the general guideline for preparing MWCNT/epoxy nanocomposites for epoxy prepreg industries.

Influence of Cure Procedures on MWCNT Stability

Dispersion of MWCNT in epoxy resin matrices is difficult so far. The dispersion is further complicated considering the differences between epoxy resin and common thermoplastic polymers since epoxy resin requires curing prior to any use. When temperature is raised above room temperature for curing, especially most epoxy resins

require high temperature, the viscosity of resin matrices can reduce significantly which may affect MWCNT dispersion stability and favor re-agglomeration.[94, 95]

For the purpose of demonstration, TGDDM prepolymers containing 0.5 wt% MWCNT were selected and isothermally cured at different elevated temperatures and their MWCNT dispersion state changes were recorded in real time by optical microscopy. MWCNT at higher loading are too close to each other causing very dark optical images that it is impossible to differentiate the nanotube dispersion as a function of various influencing factors. Figure 50 presented the MWCNT re-agglomeration evolution at 120°C of cure and provided direct evidence of MWCNT re-agglomeration in epoxy matrix upon curing. Nanotubes were well dispersed in TGDDM prepolymer matrix at the initial stage of cure reaction with average particle size less than 20 μm. As cure progressed, particles start to collapse and grow until an interconnected network structure formed at around 200 min of cure. No obvious morphology change was observed with longer curing time. Similar trends were also seen in the same sample cured at 140 °C (Figure 51), 160 °C (Figure 52), and 180 °C (Figure 53).

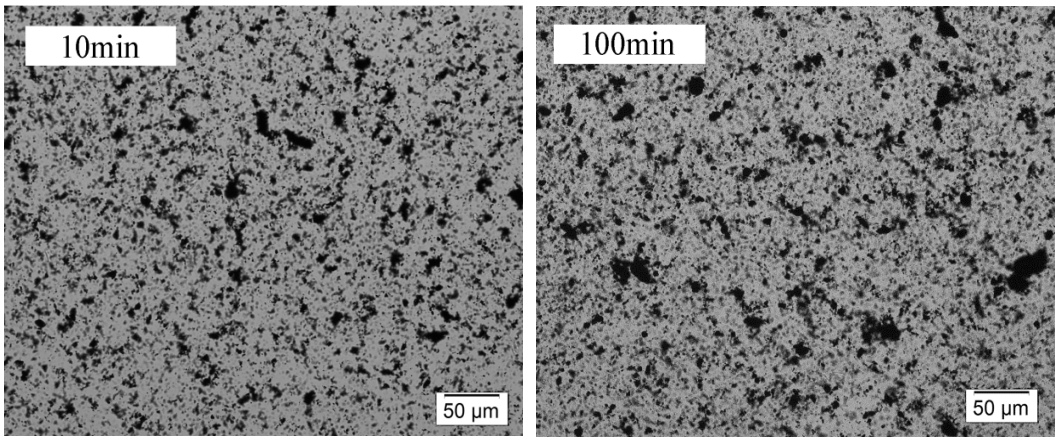

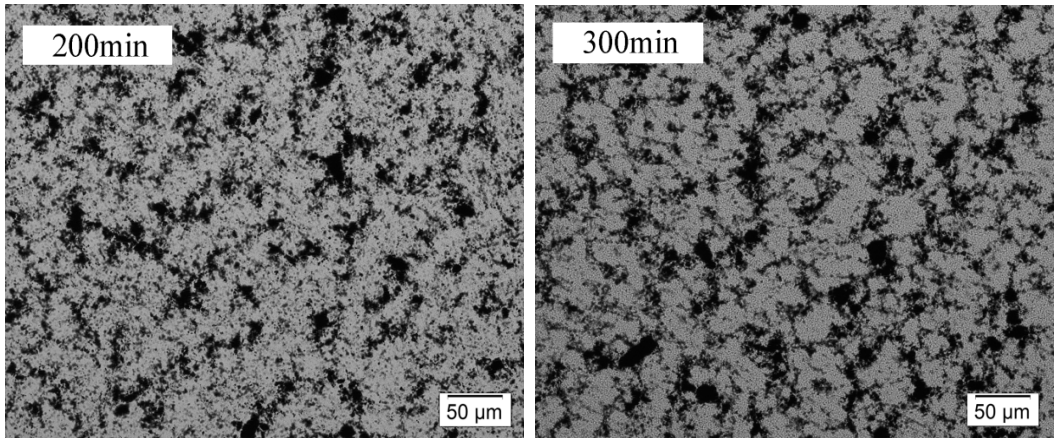

Figure 50. Optical micrographs of MWCNT/TGDDM prepolymers curing at 120 °C.

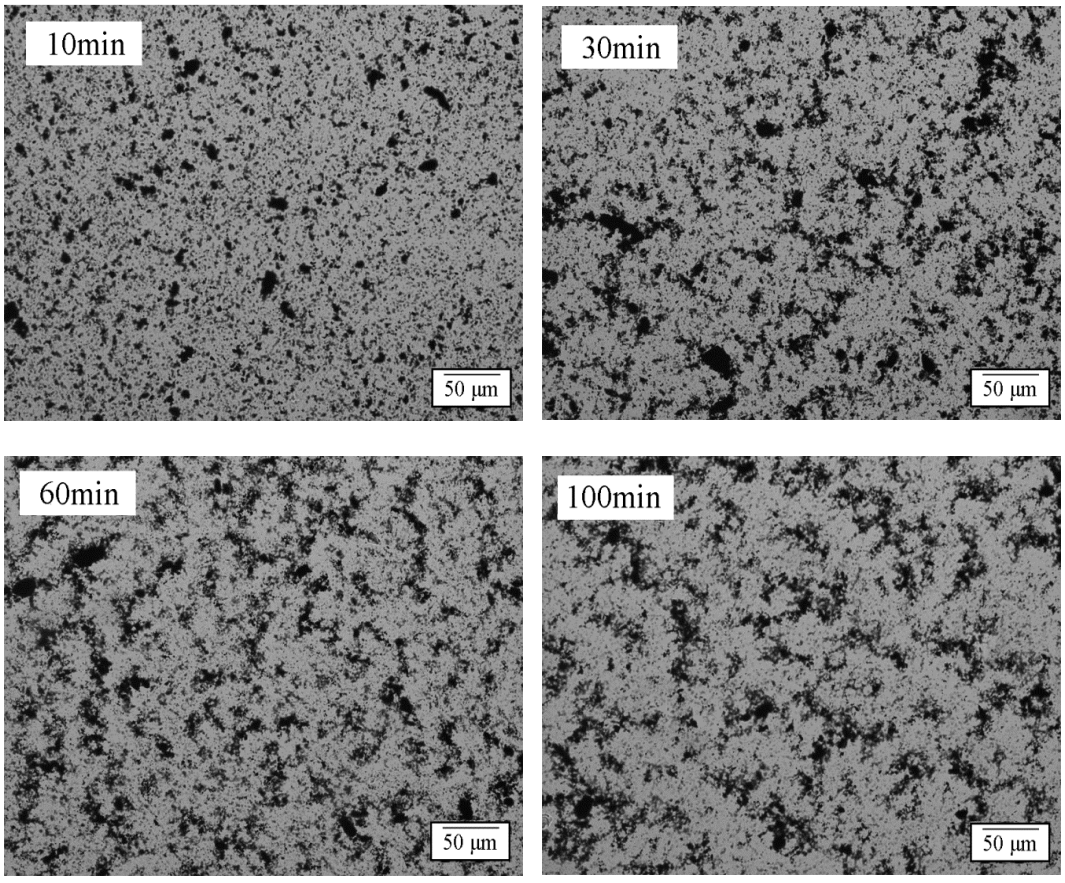

Figure 51. Optical micrographs of MWCNT/TGDDM prepolymers curing at 140 °C.

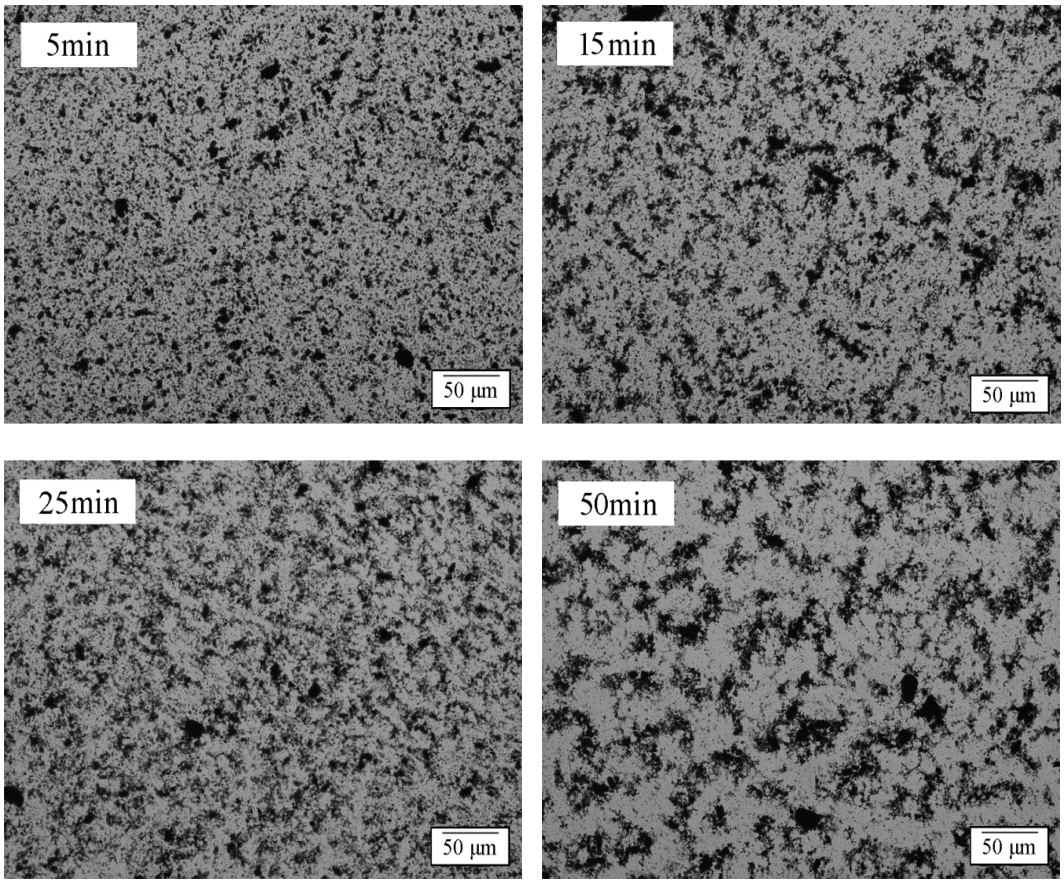

Figure 52. Optical micrographs of MWCNT/TGDDM prepolymers curing at 160 °C.

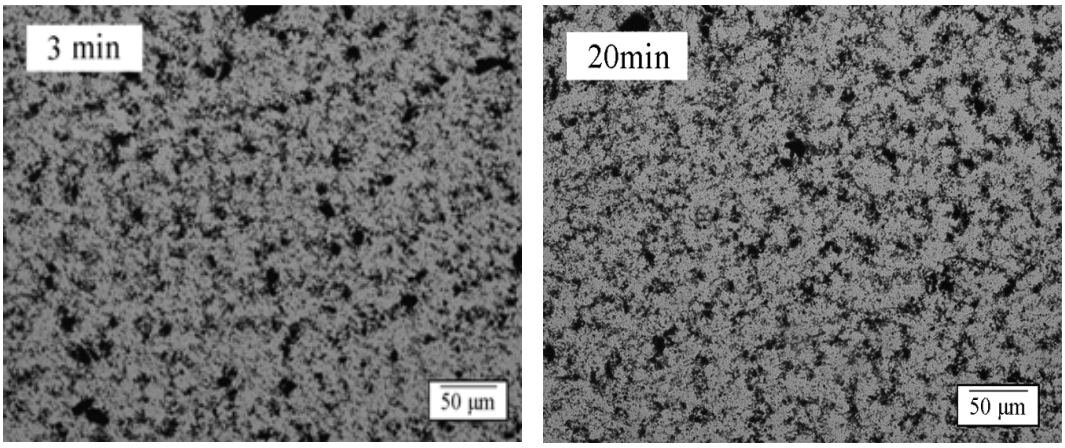

Figure 53. Optical micrographs of MWCNT/TGDDM prepolymers curing at 180 °C.

Cured morphologies of TGDDM/MWCNT composites were also studied by SEM to confirm above observation. Samples were isothermal cured at 120 °C for 300 min and

post-cured at 200 °C for 1 h. Their fractured surfaces are shown in Figure 54 where the bright spots are assigned to MWCNT agglomerates.[96] Figure 51(a) revealed an interconnected nanotube network with increased agglomerates sizes in the final cured composites. This is in good agreement with results obtained from optical microcopy observation. In addition, MWCNT particles concentrated from edges into the interior of epoxy matrices as indicated in Figure 50(b), suggesting the unstable nature of MWCNT in epoxy matrices during cure reaction.

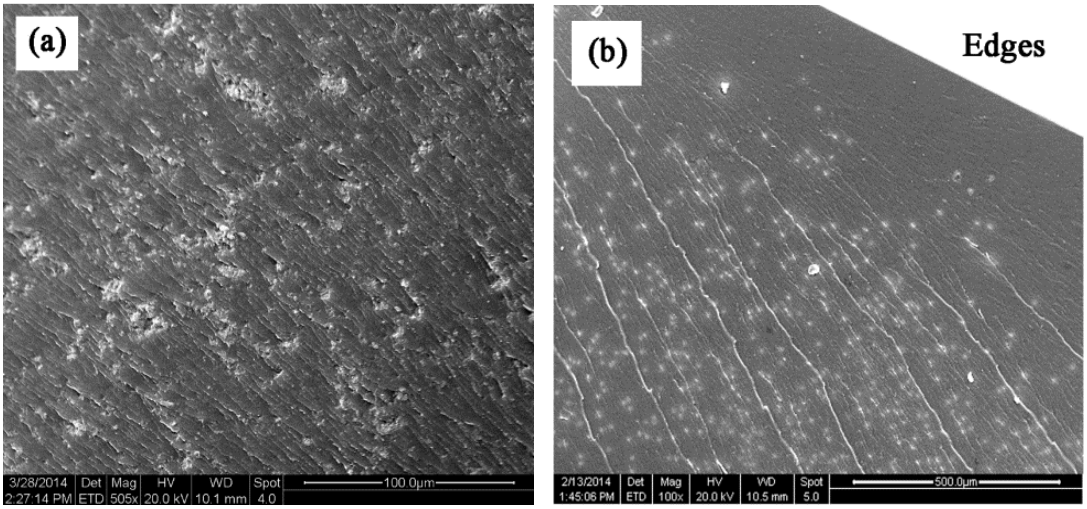

Figure 54. SEM images of fully cured MWCNT/TGDDM nanocomposites.

Although many researchers have been directly observed similar MWCNT re-agglomeration phenomena in epoxy matrices and claimed it was caused by the reduced matrices viscosity during curing,[97, 98] to our best knowledge, the relationship between nanotubes stability and matrices viscosity has not been fully understood yet. In order to quantify the relationship between MWCNT stability and epoxy matrix viscosity, dispersion indices *D* were calculated based on the real-time optical micrographs and plotted as function of curing time listed in Figure 55. For sample cured at 120 °C (Figure

55a), *D* is decreased at the early stage of cure reaction indicating the MWCNT was unstable in epoxy prepolymer matrix and re-agglomerated rapidly. After around 200 min, the decrease of dispersion index became less pronounced. Further curing at the same temperature caused very little change on the morphology and dispersion index. Similar trends were also observed for the same sample cured at 140 °C (Figure 55b) and 160 °C (Figure 55c). In contrast, the 180 °C cured sample (Figure 55d) showed no tendency to decrease indicating MWCNT is nearly stable upon cure. But the dispersion index at the onset of 180 °C cure reaction is much lower and the final index is higher compared to others. Here we defined the time at which dispersion index does not significantly change with cure time as the critical time (t_c). Critical times for 120 °C, 140 °C, 160 °C, and 180 °C cured samples were estimated from Figure 55 as 250 min, 100 min, 40 min, and 3 min, respectively. After critical time, MWCNT dispersion states were considered as stable in epoxy networks.

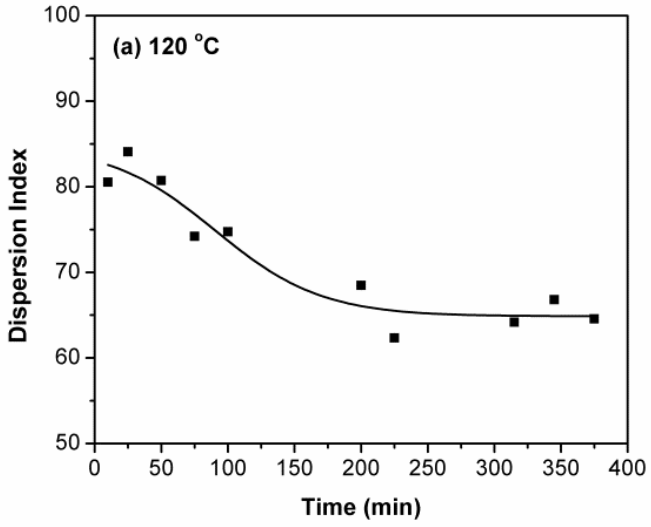

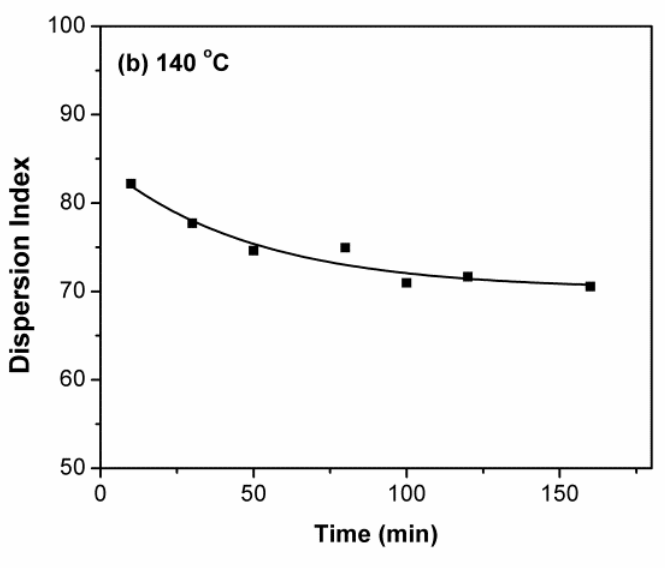
(b) 140 °C
Dispersion Index
Time (min)
100
90
80
70
60
50
0
50
100
150

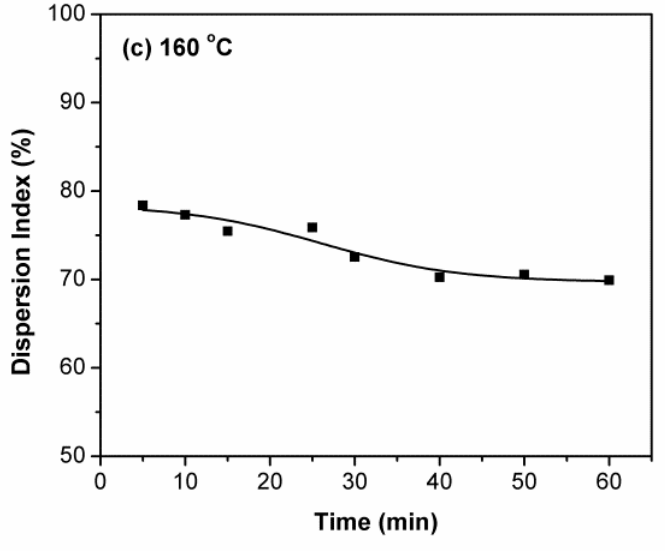
(c) 160 °C
Dispersion Index (%)
Time (min)
100
90
80
70
60
50
0
10
20
30
40
50
60

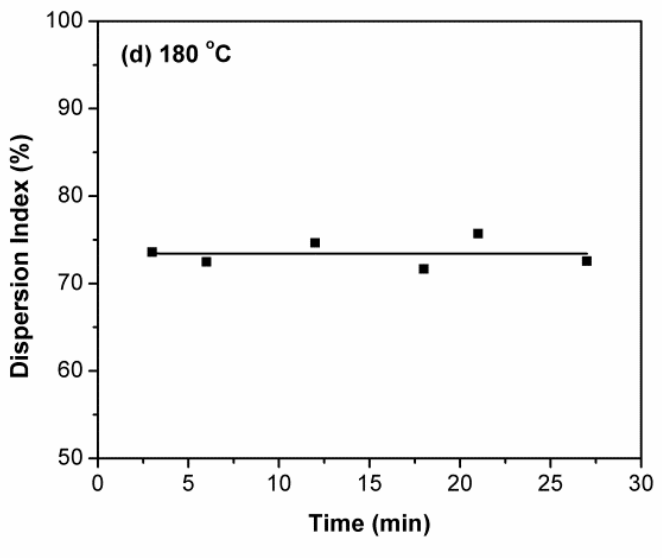

Figure 55. Dispersion index vs. curing time at different isothermal temperatures.

Quantifying MWCNT dispersion states using dispersion indices provides an opportunity to investigate the correlation between MWCNT dispersion states and epoxy matrix viscosities during cure cycles. Complex viscosity (η^*) changes during cure reaction were measured by dynamic rheological analysis and presented in Figure 56. With having this viscosity information, the initial viscosity (η_0) at the onset of curing reaction, the critical viscosity (η_c) at the critical time, and gelation time (t_{gel}) can be obtained simultaneously as listed in Table 11. It can be seen that η_0 are relatively low for all samples except the one cured at 180 °C. The reduced matrix viscosity by elevating temperature increased nanotube mobility. Van der Waals interaction became the dominated driving factor for nanotubes dispersion and led to the rapidly decrease in dispersion indices at the early stage of curing at 120 °C, 140 °C, and 160 °C. 180 °C sample showing a higher η_0 with a lower initial dispersion index is due to both the cure reaction and MWCNT re-agglomeration were accelerated by the higher temperature used.

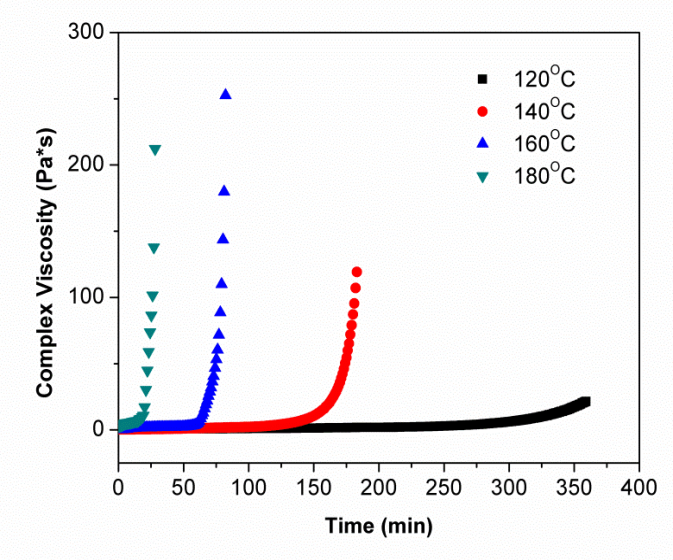

Figure 56. Viscosity profiles of MWCNT/TGDDM prepolymers at various cure temperatures.

Table 11

Critical Time and Viscosities of MWCNT Re-agglomeration in TGDDM Prepolymer Matrix at Various Cure Temperatures

Cure Temperature (°C)	η_0 (Pa·s)*	t_c (min)	η_c (Pa·s)	t_{gel} (min)
120	0.52	250	2.80	410
140	0.30	100	2.23	220
160	0.16	40	2.05	85
180	3.40	3	3.40	25

*5 min equilibration time prior to measurement.

As cure reaction progressed, MWCNT re-agglomerations were inhibited by the increased matrix viscosity and nanotubes gradually lost their mobility. Eventually they were locked into the chemical crosslinked glassy networks when system gelled and

vitrified. Since elevated temperature leads to faster viscosity increasing rate of epoxy matrices, sample cured at higher temperature gave a shorter t_c as evidenced in Table 11. It is also very interesting to notice that the η_c at their corresponding t_c are almost identical (~ 3.0 Pa·s) for all samples. At the critical time, systems were only partially cured and far beyond the gel point ($t_c < t_{gel}$). All these findings clearly suggested that MWCNT stability is strongly viscosity-dependent in epoxy matrices and their mobility can be greatly reduced once systems reached certain level of cure conversion prior to gelation occurred. In other word, it is reasonable to expect that MWCNT re-agglomeration can be minimized by controlling TGDDM prepolymer matrix viscosity higher than η_c at a given temperature.

To prove this hypothesis, TGDDM/MWCNT prepolymer was cured at a lower temperature with longer cure time (80 °C for 24 h and 120 °C for another 5 h) and its morphological changes were monitored by OM. As shown in Figure 57(a), MWCNT remained fairly uniform during the cure cycle compared to the dispersion states showed in Figure 50-Figure 53. No severe re-agglomerated MWCNT bundles or interconnected networks were formed during the cure cycle and in the final epoxy matrix, confirming that increased viscosity indeed stabilize MWCNT dispersion states. The dispersion states were also compared by examining fractured surface of cured composites on SEM, as shown in Figure 57(b). Compared to Figure 54, no nanotube agglomerates larger than 50 μm was observed. Viscosity evolution during the cure cycle was recorded in Figure 58 and revealed the viscosity-dependent nature. It can be seen that matrix viscosity was maintained above the determined critical viscosity (~ 3.0 Pa·s) throughout the curing cycle. Raising temperature from 80° C to 120 °C led to a viscosity drop but still above the defined re-agglomeration regions.

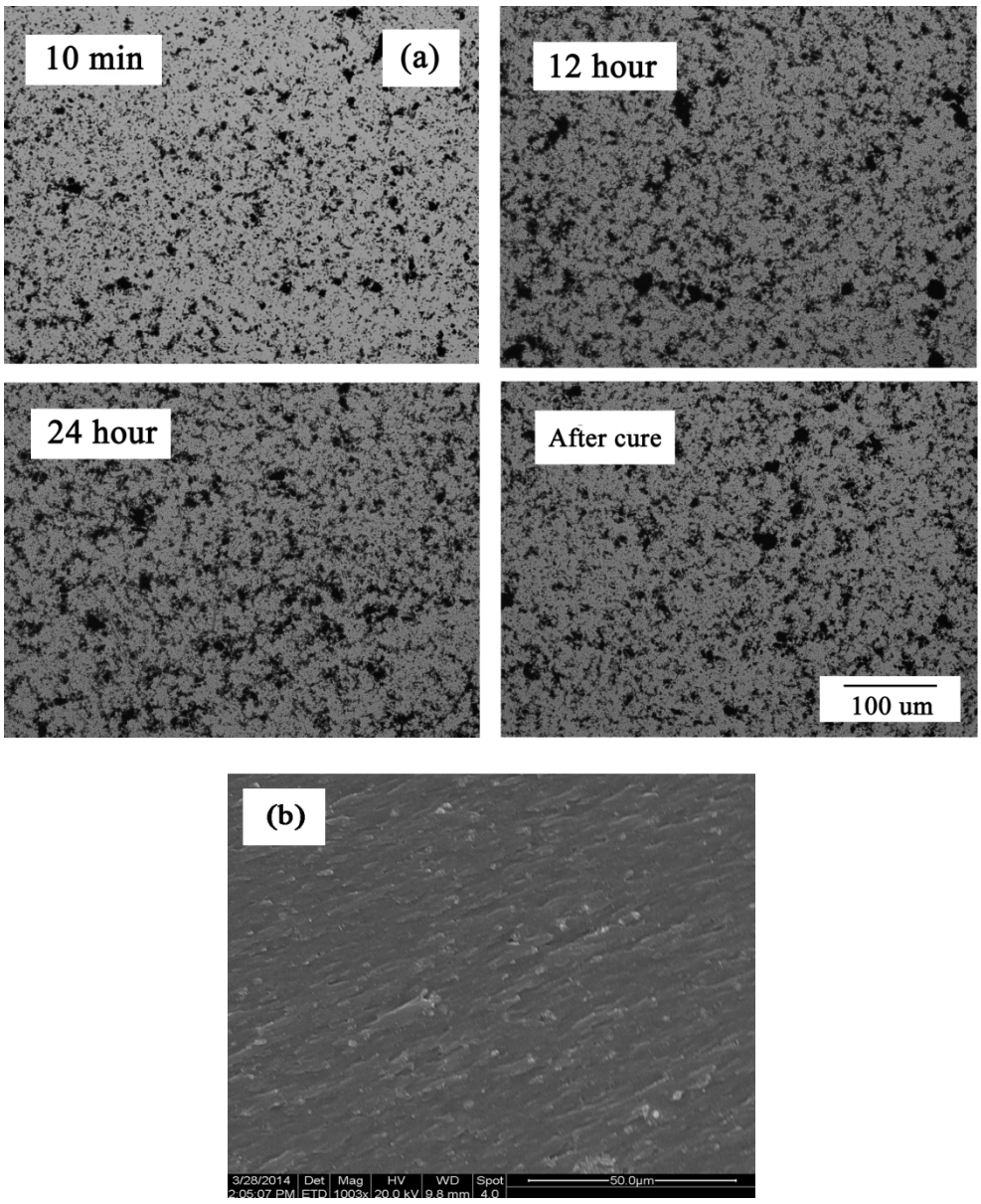

Figure 57. OM (a) and SEM (b) images of TGDDM containing 0.5 wt% MWCNT during and after cured at 80 °C for 24 h and 120 °C for 5 h.

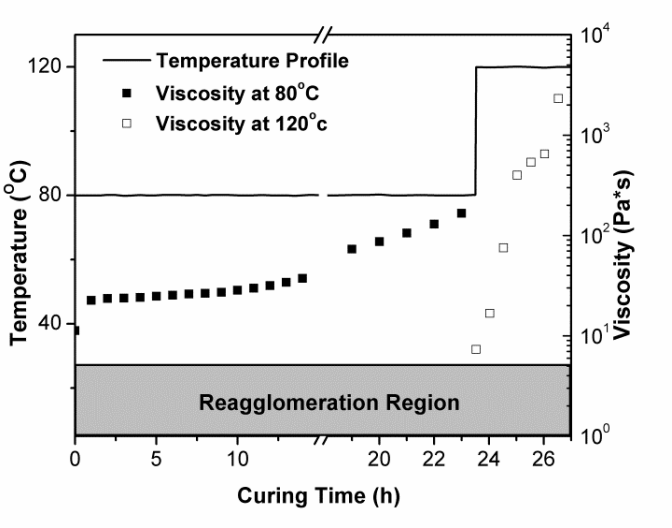

Figure 58. Viscosity profiles during cured at 80 °C for 24 h and 120 °C for 5 h.

It is worth to note that TGDDM/MWCNT prepolymers were partially cured after continuous reaction with an advanced molecular weight and viscosity. Compared to batch reactor method of which MWCNT is dispersed in neat resin followed by adding cure agents, continuous reactor allows dissolving cure agents, advancing molecular weight and viscosity, and dispersing MWCNT in pre-reacted resin matrix simultaneously. The concurrent dispersion and cure reaction eliminated the re-agglomeration caused by adding hardeners. At the meantime, the advanced prepolymer viscosity enhances MWCNT dispersion during continuous reaction and suppresses re-agglomeration during cure reaction.

Mechanical and Electrical Properties of TGDDM/MWCNT Nanocomposites

Above discussion highlighted the unique advantages of using continues reactor to prepare epoxy/MWCNT prepolymers and described the viscosity-dependent MWCNT re-agglomeration process. The use of continuous reactor combined with pre-curing zones and dispersing zones can reduce MWCNT agglomerate size from millimeter to micrometer and stabilize the dispersion in their final cured composites by adjusting

process conditions. Changes of MWCNT dispersion and stability may result in different mechanical and electrical properties in the cured composites. Understanding these technical information and fundamental knowledge is critical for exploring epoxy/MWCNT nanocomposites with good mechanical and electrical properties. In this section, a series of TGDMM/MWCNT prepolymers with MWCNT loading levels were prepared and their mechanical and electrical properties were examined accordingly. Since continuous reactor is able to handle materials with a broad viscosity range, epoxy prepolymer samples with a very high MWCNT content up to 10 wt% were successfully prepared. For the purpose of comparison, samples were prepared followed two different cure cycles: 180 °C for 3 h; 80 °C for 24 h, 120 °C for 5 h and 200 °C for 1 h.

In-plane electrical conductivities of TGDDM/MWCNT composites are shown in Figure 59. Samples prepared by both cure procedures exhibited an exponentially increased electrical conductivity as MWCNT content increased. Percolation thresholds were achieved with less than 0.5 wt% of MWCNT content. The electrical conductivity of composites based on 10 wt% MWCNT content is above 0.1 S/cm, which is higher than those reported in the literature prepared via other techniques.[99]

Differences are noticed when compared samples with the same MWCNT content. 180 °C cured sample's electrical conductivity is approximately one order of magnitude higher than the 80 °C pre-cured samples. A qualitative correlation between electrical conductivity and the observable microstructures was found. The electrical conductivity differences are attributed to the MWCNT dispersion state changes caused by different cure cycles as we discussed earlier on. In the composites cured at 180 °C, interconnected MWCNT network was formed, providing a continuous conducting path for efficient charge transport. While for the 80 °C cured samples, MWCNT re-agglomeration is

suppressed by the raised matrix viscosity. A relatively well-dispersed MWCNT morphology with few nanotube agglomerates was formed with a less efficient conducting pathway. From this comparison, it is obvious that re-agglomeration of nanotubes after dispersing is favorable during curing process when electrical conductivity is the major property of concern for application.

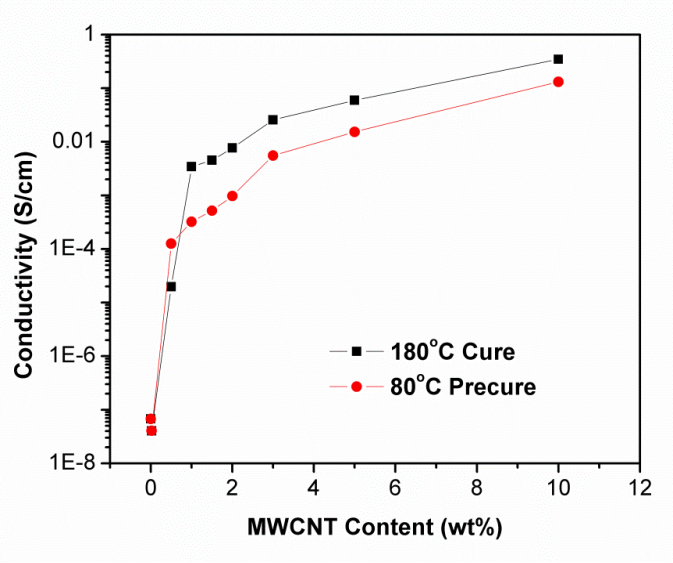

Figure 59. Electrical conductivities vs. MWCNT contents of TGDDM/MWCNT nanocomposites.

DMA was further used to investigate the dynamic mechanical property differences between samples prepared by two cure procedures. Figure 60 presents the storage modulus and tan delta plots as function of temperature for TGDDM/MWCNT nanocomposites containing 0.5 wt% MWCNT. The storage modulus, *G'* of 80 °C cured sample is higher than 180 °C cured sample. This increase in storage modulus is attributed to the reinforced effect of the well-dispersed MWCNT in 80 °C cured sample. In addition, 80 °C cured sample showed a single glass transition temperature (T_g) peak at 280 °C whereas 180 °C cured sample presented a reduced T_g at 270 °C with a shoulder at

230 °C. The shoulder is likely caused by heterogeneity in MWCNT dispersion. The formed interconnected MWCNT networks may disrupt the local resin stoichiometry and affect the way that crosslink network forms. The high concentration of aggregates can also cause physical gelation. Regions around nanotubes could therefore vitrify in earlier cure reaction. These issues are currently being investigated and will be further discussed in *Chapter VI*. Based on DMA results, we can conclude that increased prepolymer matrix viscosity with lower cure temperature is preferred to obtain TGDDM/MWCNT nanocomposites with better mechanical property.

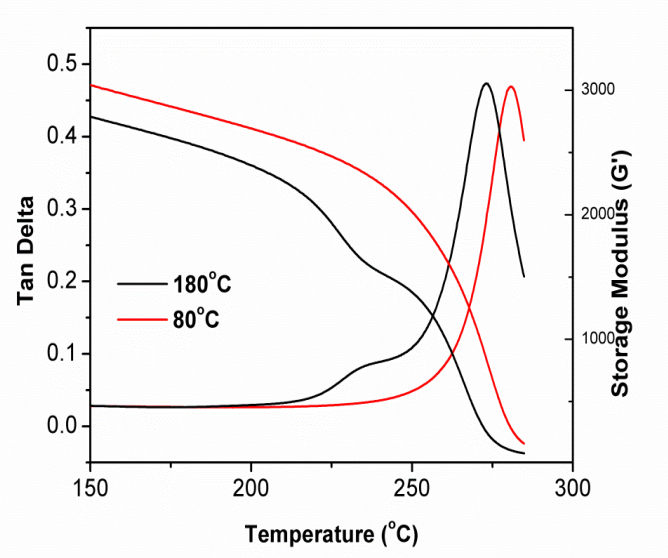

Figure 60. Storage modulus and tan δ of MWCNT/TGDDM composites containing 0.5 wt% MWCNT.

Figure 61 shows the young's modulus changes as a function of MWCNT contents for TGDDM/MWCNT composites cured at 80 °C. The modulus was slightly enhanced before the percolation threshold reached at 0.5 wt%. After passing the percolation threshold, the modulus rapidly decreased with increasing MWCNT content. Unfortunately, we are unable to compare tensile properties between different cure

procedures since the measured differences being within the range of errors due to sample preparation difficulties. But it is reasonable to expect samples cured at 180 °C should have a reduced modulus due to the interconnect MWCNT networks.

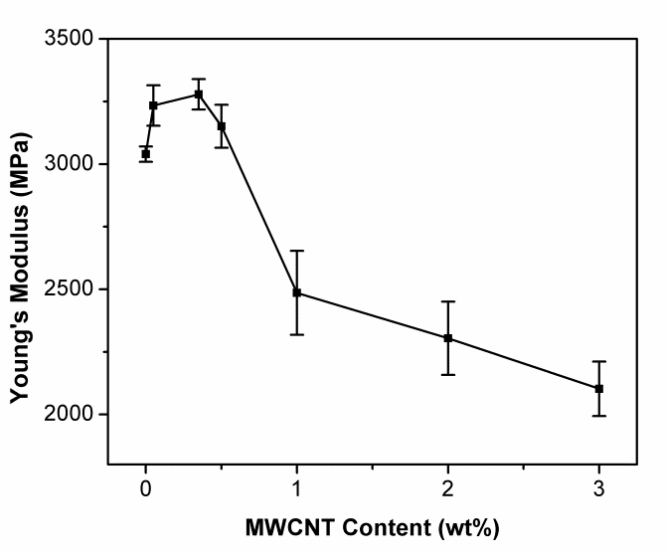

Figure 61. Tensile modulus vs. MWCNT contents of MWCNT/TGDDM composites.

Conclusion

TGDDM/MWCNT prepolymers have been prepared by a continuous reactor in an industrial scale. The continuous reactor consists of two sections, one of which is responsible for the partial curing at high temperature to avoid re-agglomeration of MWCNT, and the other for dispersing MWCNT in epoxy matrix at low temperature.

MWCNT dispersion in TGDDM matrix has been systematically studied by varying process parameters. Optical microscopy and SEM analysis demonstrated that the applied shear strength acting on the MWCNT agglomerates is critical for the MWCNT dispersion. Thereby, reducing dispersing process temperatures and increasing screw speeds facilitated a better dispersion state. Additionally, the relationship between

MWCNT stability and epoxy matrix viscosities was established during curing cycle. Epoxy matrix viscosity can be used to tune the re-agglomeration process and thus dispersion states of MWCNT in their final cured composites. In this work, a matrix viscosity higher than ~3.0 Pa·s was determined to stabilize MWCNT dispersion, forming a well-dispersed MWCNT morphologies. Both electrical property and mechanical properties were found to strongly depend on the MWCNT dispersion states in cured composites. Interconnected MWCNT network led to an increased electrical conductivity with reduced T_g.

As it was the aim of this work, we were able to establish a guideline for the processing of epoxy/MWCNT prepolymers and composites using the continuous reaction process. The advancement of continuous reactors in this field would lead to new avenues for mixing and blending a broad array of co-reactants, blends, and nanoparticles, due to better control over rheology, shear states and reactor design advantages.

CHAPTER VI

EFFECTS OF MWCNT ON REACTION INDUCED PHASE SEPERATION AND PROPERTIES OF EPOXY/PEI BLENDS

Abstract

In this chapter, ternary systems of MWCNT reinforced polyetherimide (PEI)/epoxy prepolymers were prepared through simultaneously dispersing MWCNT, dissolving PEI and 44DDS, and advancing TGDDM/TGAP chemistry using the continuous reactor methods. Influence of MWCNT on CRIPS mechanism and final cured morphologies were systematically investigated using SEM and rheological analysis. Results showed that incorporation of MWCNT can lead to a morphological transformation from phase inverted, to co-continuous, and to droplet dispersed morphology due to CRIPS process was frozen at an earlier stage of cure by increased viscosity. In additional, physical properties of produced ternary blends were explored by DMA. A third peak in tan delta curves was exhibited and assigned to the heterogeneity of MWCNT dispersion in thermoplastic/thermosets systems.

Results and Discussion

Recently, many types of organic or inorganic fillers have been introduced into thermoplastic/thermosets binary systems to control CRIPS, such as silica particles[100], aluminum nitride[101], and clay.[102] Incorporation of fillers inevitably modifies the viscosity of the matrix in which the particles are dispersed, therefore inducing morphological variations. In our previous work, thermoplastic toughened epoxy prepolymers have been prepared and their phase-separated morphologies have been systematically studied. Meanwhile, MWCNT have been successfully dispersed and stabilized into epoxy prepolymer matrix using continuous reactor method. The present work thus aspires to

simultaneously introduce MWCNT and thermoplastic phase into epoxy resin in order to benefit from effects of both additives on the system properties. PEI was selected to provide better resolution in phase morphology domain size. In particular, the influence of MWCNT nanoparticles on phase separation mechanism, morphologies and physical properties of cured composites were discussed in details.

TGDDM/TGAP/PEI Blends

TGDDM/TGAP/PEI prepolymers without MWCNT were firstly prepared via continuous reaction to benchmark the morphological and mechanical properties. Samples were isothermally cured at 180 °C for 3 h and fractured after immersing in liquid nitrogen. Fractured surface was etched by dichloromethane to dissolve PEI-rich phase for SEM observation, as shown in Figure 62. In all images presented here, the dark regions correspond to the epoxy-rich phase, whereas the bright etched regions correspond to the PEI-rich phase. All samples presented microsized morphologies and changed from PEI dispersed droplet, to co-continuous, and to phase-inverted structures upon PEI weight content increases. Many fine PEI-rich globules with a size of 1 μm can be observed in the sample of 3.2 PEI. The size of PEI globules increased to around 5 μm in diameter for 6.4 PEI. Further increasing PEI content led to a morphological transition from PEI dispersed droplet to co-continuous structure with domain size around 100 μm, as evidenced by 9.6 PEI. Eventually phase inversion occurred and epoxy-rich globules can be observed on the surface of 12.8 PEI. Thermoplastic/thermosets binary system showed very different morphology upon changing PEI content. The formed different morphologies resulted from different phase separation mechanisms. In current cases, 3.2 PEI and 6.4 PEI with droplet dispersed morphologies followed the nucleation and growth mechanism while 9.6 EPI and 12.8 PEI with co-continuous and phase-inverted structures underwent spinodal

decomposition mechanism. Therefore by observing the morphological structure on sample surface we can preliminarily decide the CRIPS mechanism for a particular formulation. The different phase separation mechanism will lead to interesting phase morphology changes with respect to MWCNT which will be discussed later on.

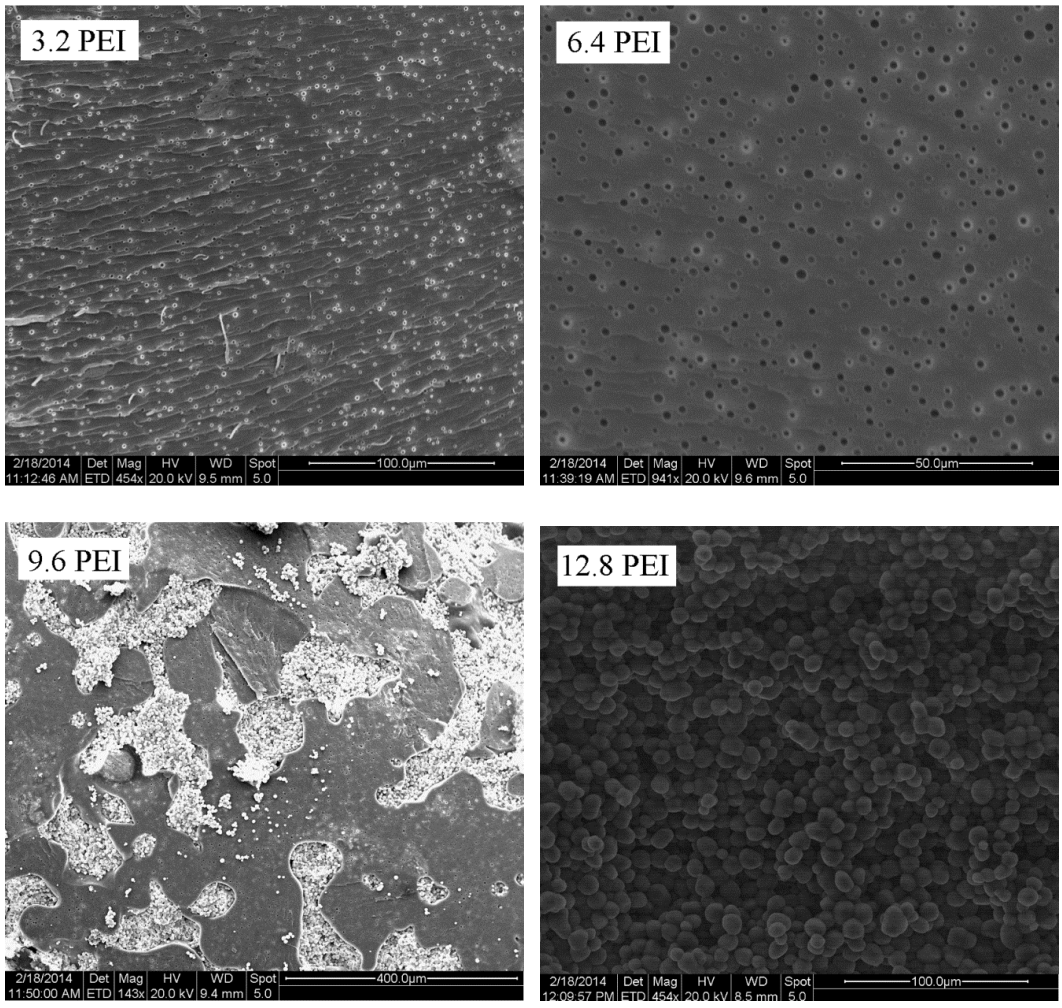

Figure 62. SEM images of TGDDM/TGAP/PEI phase morphologies cured at 180 °C.

Since phase separation occurred at a microstructure level in TGDDM/TGAP/PEI systems, dynamic rheological analysis becomes a suitable technique to monitor the phase separation process and provides insights for phase separation mechanism. Complex viscosity changes of TGDDM/TGAP/PEI prepolymers cured at 180 °C are shown in

Figure 63. Viscosities for all the samples increased with curing time caused by the increased epoxy molecular weight. A rapid increase in viscosity appeared at approximate 35 min of cure for 9.6 PEI and 12.8 PEI, corresponding to the onset of phase separation. The abrupt viscosity increase was attributed to the formation of high viscous continuous PEI-rich phase following the SD mechanism.[103] No obvious signal of phase separation was observed for 3.2 PEI and 6.4 PEI. It should be noted that a decreased viscosity at the onset of phase separation is expected for 3.2 PEI and 6.4 PEI owing to the demixing of highly viscous PEI from the initial homogeneous solution through nucleation mechanism. However, in our study a cure temperature of 180 °C for isothermal rheological analysis was used. The increased viscosity caused by epoxy-amine cure reaction at this temperature is fast enough to compensate the decreased viscosity caused by thermoplastic demixing. In fact, as further confirmed by rheological analysis which is not shown in this dissertation, a decrease in viscosity appeared for PEI 3.2 and PEI 6.4 cured at 160 °C or below.

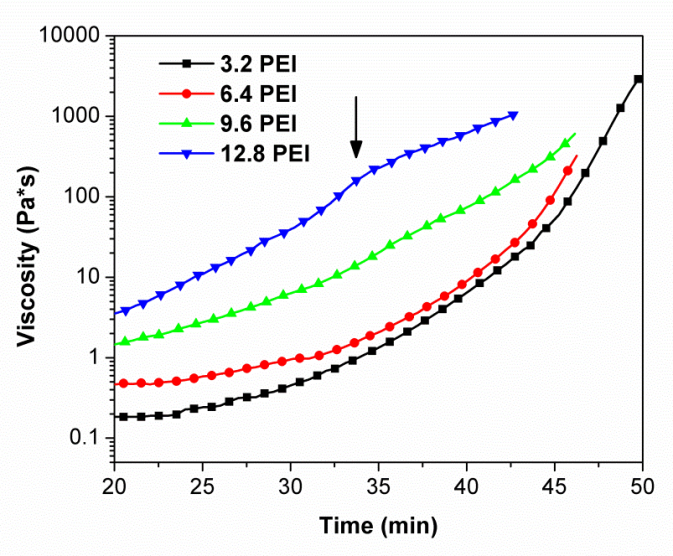

Figure 63. Complex viscosities of TGDDM/TGAP/PEI prepolymers cured at 180 °C.

DMA also confirmed the phase separated morphologies in TGDDM/TGAP/PEI blends. Two peaks appeared at the loss factor curves as shown in Figure 64.The one at the temperature of 270 °C is corresponding to the glass transition temperature of epoxy-rich phase whereas the other one at around 190 °C is associated with the glass transition temperature of PEI-rich phase. PEI-rich phase peaks increased with PEI content, indicating the growth of PEI-rich domains from separated globules to continuous matrix.

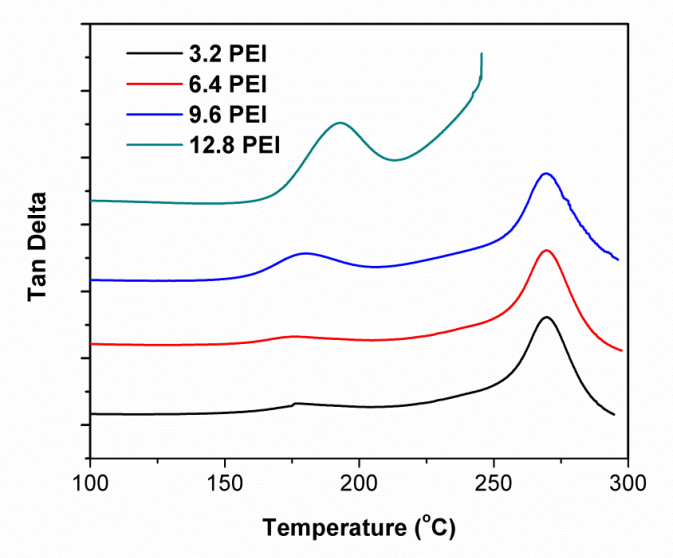

Figure 64. Tan delta curves of TGDDM/TGAP/PEI blends cured at 180 °C.

TGDDM/TGAP/PEI/MWCNT Blends

Ternary blends based on thermoplastic/thermosets with nanoparticles additives have been rarely studied in literatures. A fundamental understanding of the effects of nanoparticles on the reaction induced phase separation mechanism is still lacking in aerospace epoxy matrices. Since resin viscosity increases dramatically after dispersing nanoparticles, it brings difficulties in dissolving amine and thermoplastic during batch reactors. The continuous reactor method described in this dissertation provides a unique

one-step procedure for dispersing both nanoparticles and thermoplastics in epoxide resins, dissolving hardeners, and advancing molecular weight and viscosity. This provides us an opportunity to investigate the effect of MWCNT on reaction induced phase separation of thermoplastic/thermosets binary blends.

6.4 PEI prepolymers with different MWCNT contents were firstly prepared by continuous reactor method. After curing at 180 °C for 3 h, samples were fractured in liquid nitrogen, and etched in dichloromethane to ensure that all the PEI-rich phase had been dissolved. Their fractured morphologies were observed using SEM as described in Figure 65. Adding MWCNT up to 1.0 wt% did not significantly change the phase morphological structures in 6.4 PEI blends. PEI-rich droplets uniformly dispersed in epoxy-rich phase in all cases. However, it can be visually observed that both the number and size of PEI-rich droplets decreased with increasing the amount of MWCNT. This is attributed to the incorporation of MWCNT causing a less-complete phase separation process.[104] We have shown that the phase separation in 6.4 PEI followed the NG mechanism before. New PEI nuclei phase is generated from the epoxy phase at the onset of phase separation and can grow spherically and may coalesce with each other. Since phase separation is a kinetic process and predominantly determined by system viscosity, the extent of PEI-rich sphere growth is retarded by adding nanotubes and the final phase-separated morphology is thereafter varied in spherical sizes.

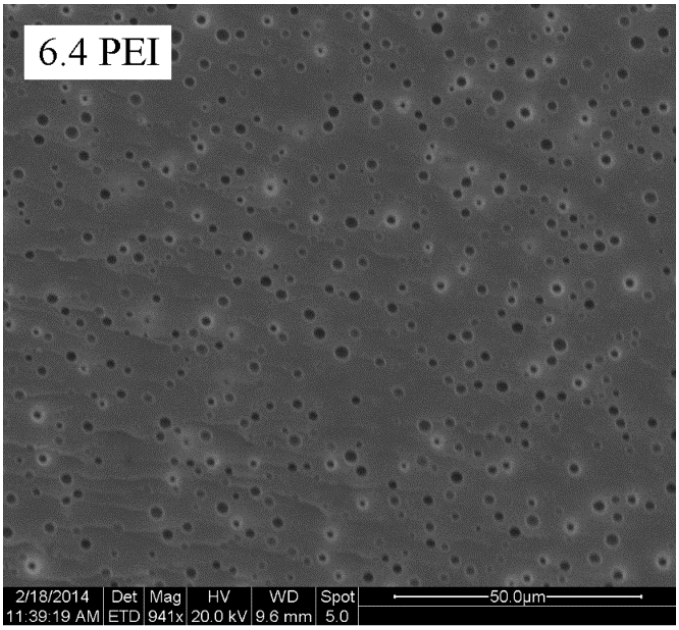
6.4 PEI
2/18/2014 11:39:19 AM
Det ETD
Mag 941x
HV 20.0 kV
WD 9.6 mm
Spot 5.0
50.0µm

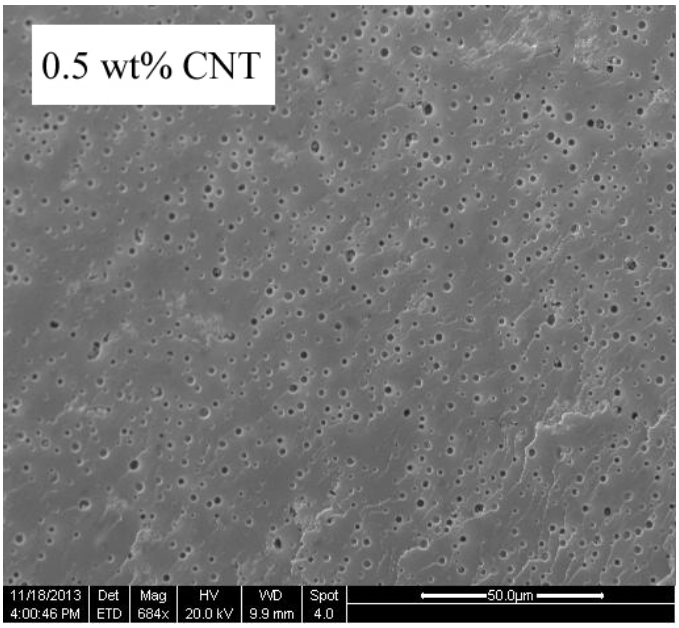
0.5 wt% CNT
11/18/2013 4:00:46 PM
Det ETD
Mag 684x
HV 20.0 kV
WD 9.9 mm
Spot 4.0
50.0µm

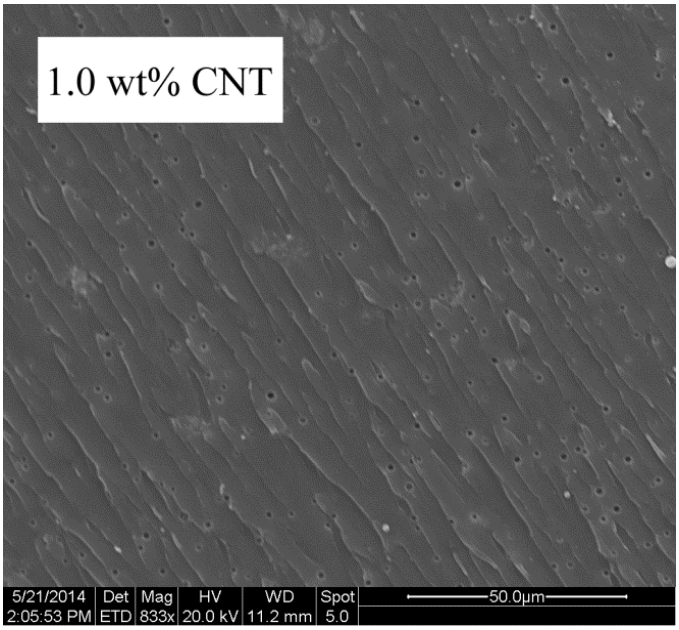

Figure 65. SEM images of 6.4 PEI morphologies with different MWCNT weight contents.

The influence of MWCNT in 9.6 PEI samples is remarkably different compared to 6.4 PEI. Phase morphologies of 9.6 PEI with 0.5, 1.0, and 1.5 wt% MWCNT are shown in Figure 66. For 0.5 wt% MWCNT, SEM image confirmed the co-continuous structure but the domain sizes of both phases were dramatically reduced (~ 20 μm) compared with the one without MWCNT (~200 μm). Then as the MWCNT content increased up to 1.0 wt%, the co-continuous phase structure transformed to a PEI droplets structure. Further increasing MWCNT content to 1.5 wt% diminished the PEI droplets and led to a nearly uniform morphology with only nanotubes can be seen on the surface. Followed with the spinodal decomposition mechanism, the 9.6 PEI sample formed an interconnected co-continuous structure throughout entire matrix at the onset of phase separation but their domain growth was inhibited by the increased matrix viscosity. 0.5 wt% MWCNT is sufficient to reduce domain size from 200 μm to 20 μm in current study. The co-continuous PEI-rich phase was further refined by adding greater amount of

MWCNT. Phase separation only took place locally following the NG mechanism in 1.0 wt% MWCNT and completely suppressed by 1.5 wt% MWCNT.

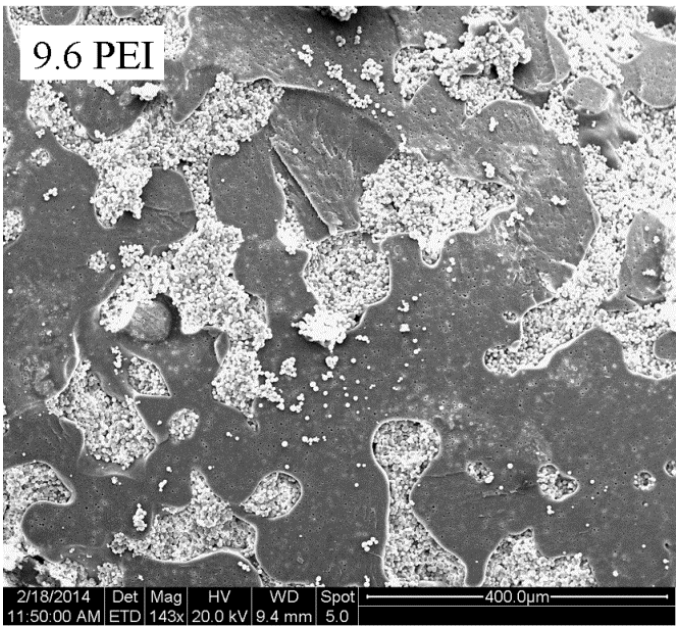

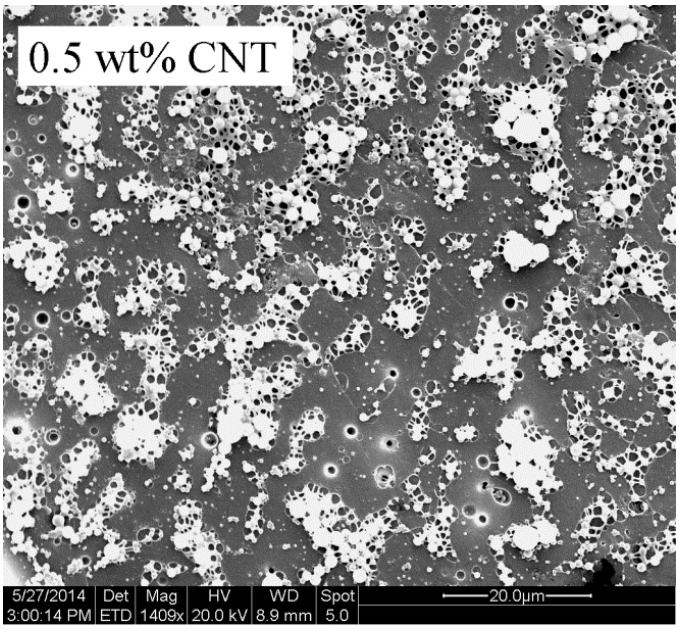

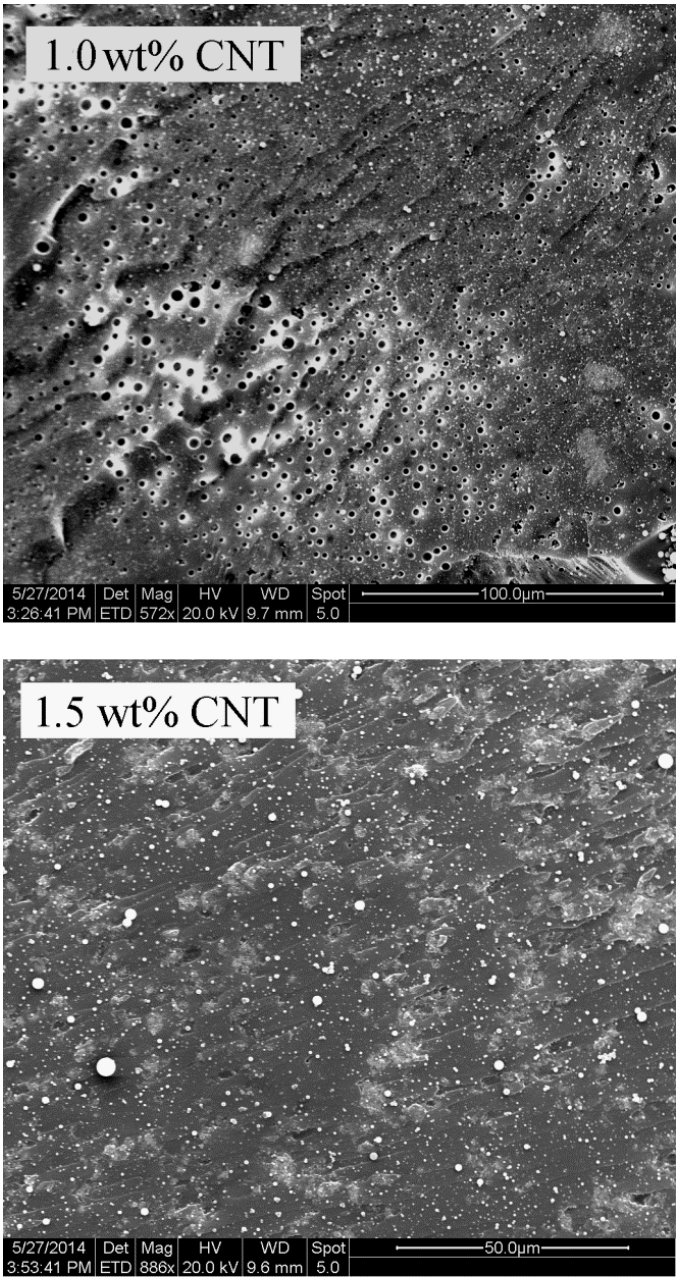

Figure 66. SEM images of 9.6 PEI morphologies with different MWCNT weight contents.

The effects of MWCNT on CRIPS and phase-separated morphologies are also striking for 12.8 PEI systems as indicated by Figure 67. The 12.8 PEI with an epoxy globules dispersed in continuous PEI-rich phase was gradually transformed to a co-continuous structure with the increase of MWCNT content. Those interconnected epoxy

globules are merged together suggesting an incomplete phase separation process. The morphological evolution provided the evidence that CRIPS in 12.8 PEI indeed follows the SD mechanism. If the viscosity is sufficiently low, density differences of both phases can cause co-continuous structure to collapse toward spherical structure with a lower interfacial tension. However, incorporation of MWCNT led to a significant increase in matrix viscosity so that phase collapse is dominated by diffusion rather than interfacial tension, giving the incompletely spherical growth.

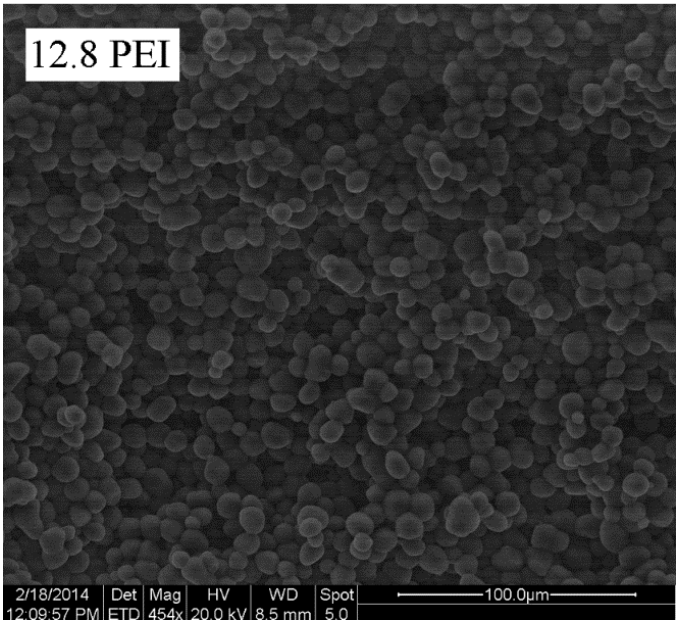

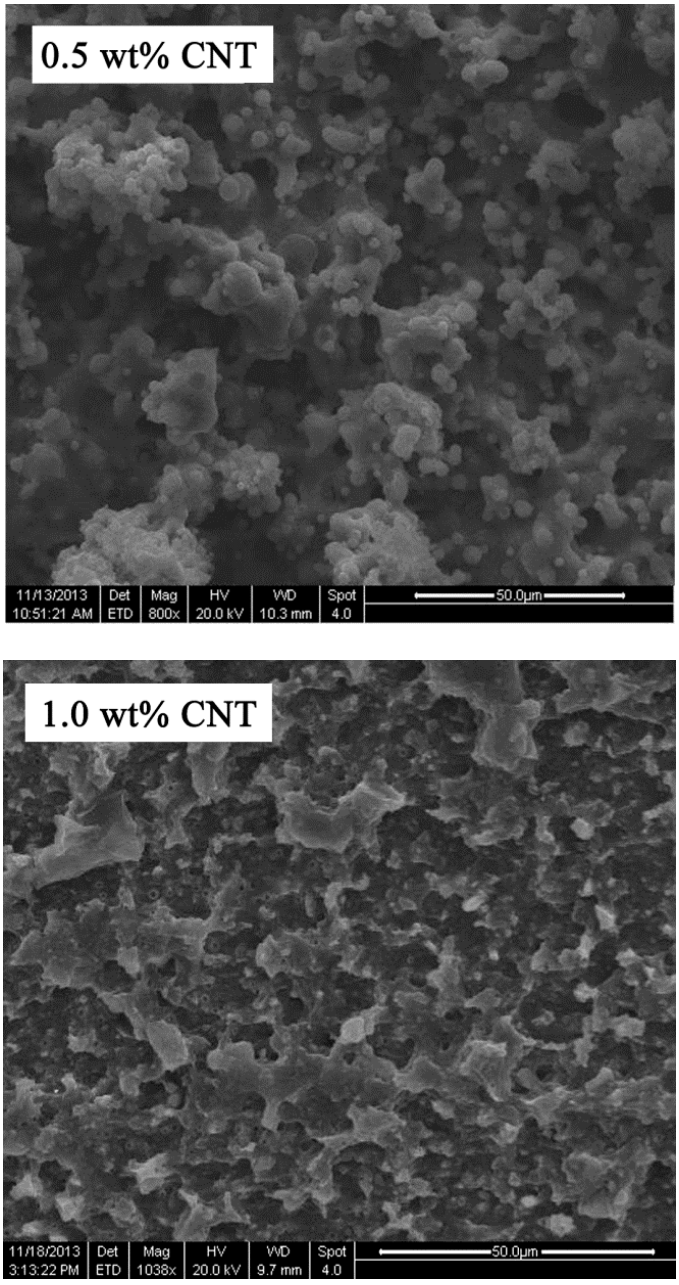

Figure 67. SEM images of 12.8 PEI morphologies with different MWCNT weight contents.

To confirm the effects of MWCNT on CRIPS observed by SEM, 9.6 PEI was selected and further analyzed by rheological measurement. The complex viscosity changes (η^*) were plotted as a function of curing time and displayed in Figure 68. An abrupt increase stages in η^* can be observed from samples with 0.5 wt% and 1.0 wt%

MWCNT. The viscosity increase began at around 45 min of cure for 0.5 wt% CNT and 60 min for 1.0 wt% CNT, corresponding to the onset of PEI-rich continuous phase formation. Compared to the neat 9.6 PEI showing viscosity increase at 35 min, the onset of phase separation was delayed by MWCNT dispersion. For 1.5 wt% CNT, the viscosity increasing stage is not obvious to see, indicating no microsized phase separation occurred. In this case, phase separation still may occur at a small length scale but is able to detect by rheological analysis.

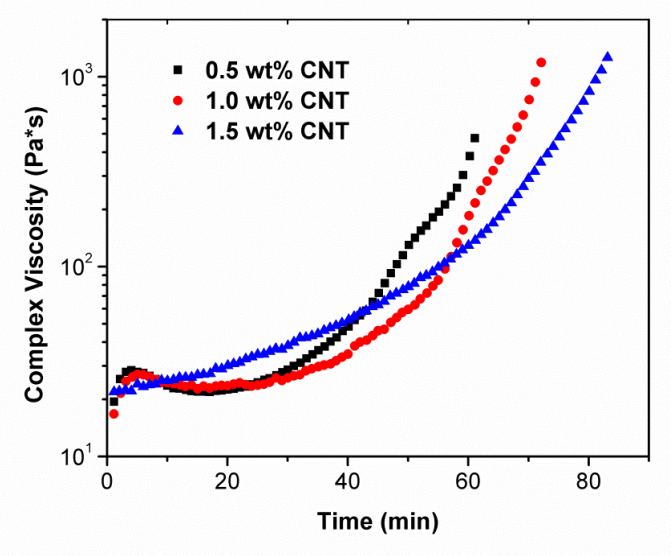

Figure 68. Complex viscosity of 9.6 PEI with different MWCNT weight contents cured at 180 °C.

The dynamic mechanical properties were also studied to provide more insights to the ternary blends. Tan delta curves of 9.6 PEI with different MWCNT contents are shown in Figure 69. It can be found that introducing MWCNT resulted in a third T_g peak at around 230 °C and its peak area increased with MWCNT loading level. Similar trend was also observed in TGDDM/MWCNT nanocomposites as found in *Chapter V*. These remarkable changes in T_g compared are likely caused by heterogeneity of the MWCNT

dispersion.[105] The high viscous area around aggregated nanotubes may disrupt the local resin stoichiometry and affect the way that crosslink network forms. It can also cause system vitrifying in earlier cure conversion, resulting in incompletely cured glassy network with reduced glass transition temperature. The peak at 270 °C is corresponding to the glass transition temperature of epoxy-rich phase and the peak at 190 °C is assigned to the glass transition temperature of PEI-rich phase. Both peaks decreased in area with the increase of MWCNT content, indicating the phase separation domain sizes decreased. These results agreed well with SEM and rheological data and confirmed the phase separation process is suppressed by nanotubes.

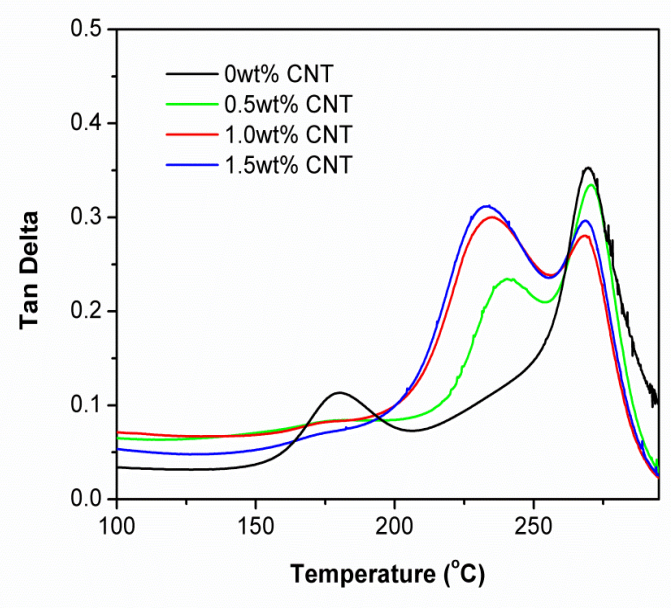

Figure 69. Tan delta curves of 9.6 PEI blends with different MWCNT contents cured at 180 °C.

The above results clearly showed that the influence of MWCNT on CRIPS mechanism and the morphologies of TGDDM/TGAP/PEI blend. When phase separation follows the nucleation and growth mechanism, PEI droplets dispersed phase morphology

is maintained but droplets size is reduced by MWCNT. On the other hand, when the PEI content exceeded the critical concentration and phase separated following spinodal decomposition mechanism, the morphological structures are significantly affected by MWCNT content and may result in phase transformation. It is also worth to note that a non-uniformed morphology is often seen in samples with high MWCNT weight content owing to local viscosity differences caused by the heterogeneity of MWCNT dispersion in epoxy matrices.

Conclusion

Influence of MWCNT on reaction induced phase separation of TGDDM/TGAP/PEI blends has been studied in this chapter. The CRIPS behavior of TGDDM/TGAP/PEI without MWCNT followed the NG mechanism to form PEI droplets morphology and the SD mechanism to generate co-continuous structure and phase inversion, which was proven by SEM and rheological measurements.

By adding MWCNT into the thermoplastic/thermosets binary systems, the complex viscosity of the matrix increased. As a result, the CRIPS behavior was suppressed and the final morphology was frozen at an earlier stage of phase separation. For system followed the NG mechanism, the droplets size became smaller and finally disappeared as the content of MWCNT increased from 0.5 wt% to 1.5 wt%. While for system followed the SD mechanism the co-continuous and phase inverted structure were refined by the addition of greater MWCNT contents and eventually led to an incomplete phase separation.

As for the properties of the final cured composites, the dynamic mechanical analysis indicated that the glass transition temperature of epoxy-rich phase did not change

[106]much but a third peak appeared at around 230 °C and increased with MWCNT loading levels. This peak is likely caused by heterogeneity in the MWCNT dispersion.

The results obtained in this chapter indicate the potential of using MWCNT to tailor the structure and properties of CRIPS systems. While further investigation is still required in order to provide systematically understanding of the process-structure-property relationship.

REFERENCES

1. Mohanty A.K.; Misra M.; Hinrichsen G. *Macromol. Mater. Eng.* **2000**, 276-277, 1-24.

2. Puskas J.E.; Seo K.S.; Sen M.Y. *Euro. Polym. J.* **2011**, 47, 524-534.

3. Roller M.B. *Polym. Eng. Sci.* **1975**, 15, 406-414.

4. Kim J.; Moon M.J.; Howel J.R. *J. Comp. Mater.* **2002**, 36, 2479-2497.

5. Bakis C.; Bank L.; Brown V.; Cosenza E. *J. Compos. Constr.* **2002**, 6, 73-87.

6. Mimura K.; Fujioka I.H. *Polymer* **2000**, 41, 4451-4459.

7. Hodgkin J.H.; Simon G.P.; Varley R.J. *Polym. Advan. Technol.* **1998**, 9, 3-10.

8. Heinz S.R.; Wiggins J.S. *Polym. Test.* **2010**, 29, 925-932.

9. Arias M.L.; Frontini P.M.; Williams R.J.J. *Polymer*, **2003**, 44, 1537-1546.

10. McGarry F.J.; Sultan J.N. *J. Polym. Sci*. **1973**, 13, 29-34.

11. Butta E.; Levita G.; Marchetti A.; Lazeri A. *Polym. Eng. Sci.* **1986**, 26, 63-73.

12. Kim H.C.; Char K.H. *Ind. Eng. Chem. Res.* **2000**, 39, 955-959.

13. Park S.J.; Kim H.C. *J. Polym. Sci. Part B: Polym. Phys.* **2001**, 39, 121-128.

14. Bucknall C. B.; Partridge I. K. *Br. Polym. J.* **1983**, 15, 71-75.

15. Bucknall C. B.; Partridge I. K. *Polymer* **1983***,* 24, 639-644.

16. Kim B.S.; Chiba T.; Inoue T. *Polymer* **1995**, 1, 43-47.

17. Hourston D.J.; Lane J.M. *Polymer* **1992**, 33, 1379-1383.

18. Bennett G.S.; Farris R.J.; Thompson S.A. *Polymer* **1991**, 32, 1633-1641.

19. Hiemenz P.C.; Lodge T.P. *Polymer Chemistry*, 2ed Ed. Dekker: New York, 1984.

20. Yu G.; Wu P. *Polym. Chem.* **2014**, 5, 96-104.

21. Yang G.; Zheng B.; Yang J.P.; Fu S.Y. *J. Polym. Sci. Part A: Polym. Chem.* **2008**, 46, 612-624.

22. Yu Y.; Wang M.; Foix D.; Li S. *Ind Eng Chem Res* **2008**, 47, 9361-9369.

23. Ma Z.; Stanford J.L.; Dutta B.K. J. *Appl. Polym. Sci.* **2009**, 112, 2391-2400.

24. Girard-Reydet E.; Vicard V.; Pascault J.P.; Sautereau H. *J. Appl. Polym. Sci.* **1997**, 65, 2433-2445.

25. Mimura K.; Ito H.; Fujioka H. *Polymer* **2000**, 41, 4451-4459.

26. Poncet S.; Boiteux G.; Pascault J.P.; Sautereau H.; Pogozinski G.; Kranbuehl D. *Polymer* **1999**, 40, 6811-6820.

27. Zhang X.J.; Yi X.S.; Xu Y.Z. *J. App. Polym. Sci.* **2008**, 109, 2195-2206.

28. Zhang X.J.; Yi X.S.; Xu Y.Z. *Acta Polymeric Sinica* **2007**, 8, 715-720.

29. Derjaguin B.V.; Muller V.M.; Toporov Y.P. *J. Colloid. Interface Sci.* **1975**, 53, 314-326.

30. Haba D.; Kaufmann J.; Brunner A. J.; Resch K.; Teichert C. *Polymer* **2014**, 55, 4032-4040.

31. Koo J.H. *Polymer nanocomposites: processing, characterization, and applications.* McGraw-Hill: New York, 2006.

32. Ajayan P.M.; Schadler L.S.; Braun P.V. *Nanocomposite science and technology*, Wiley-VCH: Weinheim, 2003.

33. Cho J.; Daniel I.M.; Dikin D.A. *Compos. Part A-Appl. S.* **2008**, 39, 1844-1850.

34. Zheng Y.; Zhang A.; Chen Q.; Zhang J.; Ning R. *Mater. Sci. Eng. A.* **2006**, 435-436, 145-149.

35. Bryning M.B.; Islam M.F.; Kikkawa J.M.; Yodh A.G. *Adv. Mater.* **2005**, 17, 1186-1191.

36. Ma P.C.; Kim J.K.; Tang B.Z. *Comp. Sci. Tech.* **2007**, 67, 2965-2972.

37. Li Q.; Zaiser M.; Koutsos V. *Phys. Status Solidi A.* **2004**, 201, 89-91.

38. Geng Y.; Liu M.Y.; Shi X.M.; Kim J.K. *Composites Part A* **2008**, 39, 1876-1883.

39. Sandler J., Shaffer M.S.P.; Prasse T.; Bauhofer W.; Schulte K.; Windle A.H. *Polymer* **1999**, 40, 5967-5971.

40. Zaragoza-Contreras E.A.; Lozano-Rodríguez E.D.; Román-Aguirre M.; Antunez-Flores W.; Hernández-Escobar C.A.; Flores-Gallardo S.G.; Aguilar-Elguezabal A. *Micron* **2009**, *40*, 621-627.

41. Chang L.; Friedrich K.; Ye L.; Toro P. *J. Mater. Sci.* **2009**, 44, 4003-4012.

.42 Gojny F.H.; Wichmann M.H.G.; Köpke U.; Fiedler B.; Schulte K. *Comp. Sci. Tech.* **2004**, 64, 2363-2371.

43. Wichmann M.; Sumfleth J.; Fiedler B.; Gojny F.; Schulte K. *Mech. Compos. Mater.* **2006**, 42, 395-406.

44. Karippal J.J.; Murthy H.N.N.; Rai K.S.; Krishna M.; Sreejith M. *Polym-Plast. Technol.* **2010**, 49, 1207-1213.

45. Karippal J.; Murthy H.N.; Rai K.; Krishna M.; Sreejith M. *J. Mater. Eng. Perform.* **2010**, 19, 1143-1149.

46. Cui S.; Canet R.; Derre A.; Couzi M.; Delhaes P. *Carbon* **2003**, 41, 797-809.

47. Luan J.; Zhang A.; Zheng Y.; Sun L. *Compos. A-Appl. S.* **2012**, 43, 1032-1037.

48. Kim S.H.; Lee W.I.; Park J.M.; *Carbon* **2009**, 47, 2699-2703.

49. Chakraborty A.K.; Plyhm T.; Barbezat M.; Necola A.; Terrasi G.P. *J. Nanopart. Res.* **2011**, 13, 6493-6506.

50. Hollertz R.; Chatterjee S.; Gutmann H.; Geiger T.; Nuesch F.A.; Chu B.T.T. *Nanotechnology*, **2011**, 22, 125702.

51. Wang S.; Liang Z.; Liu T.; Wang B.; Zhang C. *Nanotechnology* **2006**, 17, 1551-1557.

52. Gojny F.H.; Schulte K. *Compos. Sci. Technol.* **2004**, 64, 2303-2308.

53. Gong X.; Liu J.; Baskaran S.; Voise R.D.; Young J.S. *Chem. Mater.* **2000**, 12, 1049-1052.

54. Butta E.; Levita G.; Marchetti A.; Lazeri A. *Polym. Eng. Sci*. **1986**, 26, 63-73.

55. Grossiord N.; Loos J.; Regev O.; Koning C.E. *Chem. Mater.* **2006**, 18, 1089-1099.

56. Prat L.; N'Daiye S.; Rigal L.; Gourdon C. *Chem. Eng. and Processing.* **2004**, 43, 874-881.

57. Finnigan B.; Martin D.; Halley P.; Truss R.; Campbell K. *Polymer* **2004**, 45, 2249-2260.

58. Cai C.; Shi Q.; Li L.; Zhu L.; Yin J. *Rad. Phys. Chem.* **2008**, 77, 370-372.

59. Shokoohi S.; Arefazer A.; Naderi G. *Mater. Design*. **2011**, 32, 1697-1703.

60. Brown S.B.; Orlando C.M. *Encyclopedia of Polymer science and Engineering*, Wiley: New York, 1988.

61. Xanthos M. *Reactive Extrusion: Principles and Practice.* Hanser Publishers: Munich, 1992.

62. Moad G. *Prog. Polym. Sci.* **1999**, 24, 81-142.

63. Rauwendaal C. *Polymer Mixing, a Self-Study Guide*, Carl Hanser Veriag: Munich, 1998.

64. Rauwendaal C. *Polym. Eng. Sci.* **1981**, 21, 1092-1100.

65. Herrmann H.; Burckhardt U. *Kunststoffe* **1978**, 68, 753-760.

66. Liu H.; Wang P.; Gogos C.G. *Inter. J. Pharm.* **2010**, 383, 161-169.

67. Titier C.; Pascault J.P.; Taha M.; Rozenberg B.J. *J. Polym. Sci., Part A* **1995**, 33, 175-184.

68. Titier C.; Pascault J.P.; Taha. M. *J. Polym. Sci. Part A* **1996**, 59, 415-422.

69 Shaffer M.S.P.; Windle A.H. *Advanced Materials* **1999**. 11, 937-941.

70 Tobias V.; Petra P.; Sven P.; Liane H.; Bernd K. *Polymer* **2008**, 49, 3500-3509.

71. Butt H.J.; Cappella B.; Kappl M. *Surface Science Reports* **2005,** 59, 1-152.

72. Chen Y.T.; Macosko C.W. *24th International SAMPE Technical Conference,* Toronto, 1992.

73. Lopez J.; Lopez-Bueno I.; Nogueira P.; Ramirez C.; Abad M.J.; Barral L.; Cano J. *Polymer* **2001**, 42, 1669-1677.

74. Ramirez J.H.; Duarte F.M.; Martins F.G.; Costa C.A.; Madeira L.M. *Chem. Eng. J.* **2009**, 148, 394-404.

75. Jongbloed H.A.; Kiewiet J.A.; Van Dijk J.H. *Polym. Eng. Sci.* **1995**, 35, 1569-1579.

76. Zhang J.; Guo Q.; Fox B.L. *Compos. Sci. Technol.* **2009**, 69, 1172-1179.

77. Fernandez B.; Arbelaiz A.; Diaz E.; Mondragon I. *Polym. Comp.* **2004**, 25, 480-488.

78. Rajasekaran R.; Alagar M.; Chozhan C.K. *eXpress Polymer Letter* **2008**, 2, 339-348.

79. Anton M.K.; Koenig J.L. *J. Polym. Sci.: Polym. Chem.* **1981**, 19, 549-570.

80. Montserrat K.; Flaque C.; Calafell M.; Andreu G.; Malek J. *Thermochim. Acta.* **1995**, 269, 213-229.

81. Li S, Lundquist K. *Nordic. Pulp. Paper. Res. J* **1994**, 9, 191-195.

82. Blanco I.; Cicala G.; Costa M.; Recca A. *J. Appl. Polym. Sci.* **2006**, 100, 4880-4887.

83. Mark J.E. *Polymer Data Handbook,* Oxford University Press, London, 1999.

84. Kim B.S.; Chiba T.; Inoue T. *Polymer* **1995**, 36, 43-47.

85. MacKinnon A.J.; Jenkins S.D.; McGrail P.T.; Pethrik R.A. *Macromolecules* **1992**, 25, 3492-3499.

86. Blance I.; Cicala G.; Motta O.; Recca A. *J. Appl. Polym. Sci.* **2004**, 94, 361-371.

87. Yoon T.H.; Liptak S.C.; Priddy D.B.; McGrath G.E. *J. Adhesion.* **1994**, 45, 191-203.

88. Ratna D.; Varley R.; Simon G.P. *J. Appl. Polym. Sci.* **2004**, 92, 1605-1610.

89. Hourston D.J.; Lane J.M.; Zhang H.X. *Polym. Intl.* **1996**, 42, 349-355.

90. Kasaliwal G.R.; Goldel A; Potschke P.; Heinrich G. *Polymer* **2011**, 52, 1027-1036.

91. Van Der Goot A.J.; Poorter O.; Janssen L.P. *Polym. Eng. Sci.* **1998**, 38, 1193-1198.

92. Gaurav L.; Andreas G.; Petra P. *J. Appl. Polym. Sci.* **2009**, 112, 3494-4509.

93. Petra P.; Tobias V.; Beate K. *Polymer* **2013**, 54, 3071-3078.

94. Ma P.C.; Mo S.Y.; Tang B.D.; Kim J.K. *Carbon* **2010**, 48, 1824-1834.

95. Battisi A.; Skordos A.A.; Partridge I.K. *J. Phys. D: Appl. Phys.* **2009**, 42, 155402.

96. Kovacs J.Z.; Andresen K.; Pauls J.R.; Garcia C.P.; Schossig M.; Schulte K.; Bauhofer W. *Carbon* **2007**, 45, 1279-1288.

97. Chakraborty A.K.; Plyhm T.; Barbezat M.; Necola A.; Terrasi G.P. *J. Nanopart. Res.* **2011**, 13, 6493-6506.

98. Hollertz R.; Chatterjee S.; Gutmann H.; Geiger T.; Nuesch F.A.; Chu B.T. *Nanotechnology* **2011**, 22, 125702-125710.

99. Bauhofer W.; Kovacs J.Z. *Compos. Sci. Technol.* **2009**, 69, 1486-1498.

100. Zhang J.; Xie X.M. *Composites Part B* **2001**, 43, 2163-2169.

101. Duan J.K.; Kim C.N.; Jiang P.K.; Wang G.L. *J. Appl. Polym. Sci.* **2007**, 115, 2734-2746.

102. Peng M.; Li D.S.; Chen Y.; Zheng Q. *J. Appl. Polym. Sci.* **2007**, 104, 1205-1214.

103. Inoue T. *Prog. Polym. Sci.* **1995**, 20, 119-153.

104. Rotrekl J.; Matejka L.; Kapralkova L.; Zhigunov A.; Hromadkova J.; Kelnar I. *eXPRESS Polym. Letter* **2012**, 6, 975-986.

105. Abdalla M.; Dean D.; Adibempe D.; Nyairo E.; Robinson P.; Thompson G. *Polymer* **2007**, 48, 5662-5670.